

AFML-TR-71-160

AD736470

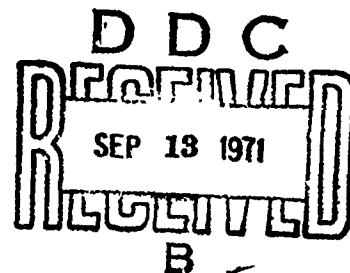
# MULTIAXIAL BEHAVIOR OF ATJ-S GRAPHITE INTERIM REPORT

J. Jortner

McDonnell Douglas Astronautics Company

TECHNICAL REPORT AFML-TR-71-160

July 1971



Approved for Public Release; Distribution Unlimited

Air Force Materials Laboratory  
Air Force Systems Command  
Wright-Patterson Air Force Base, Ohio

Reproduced by  
NATIONAL TECHNICAL  
INFORMATION SERVICE  
Springfield, Va. 22151

Unclassified

Security Classification

## DOCUMENT CONTROL DATA - R &amp; D

(Security classification of title, body of abstract and indexing annotation must be entered when the overall report is classified)

1. ORIGINATING ACTIVITY (Corporate author) McDonnell Douglas Astronautics Company-West Santa Monica, California 90406		2a. REPORT SECURITY CLASSIFICATION Unclassified	
3. REPORT TITLE Multiaxial Behavior of ATJ-S Graphite		2b. GROUP	
4. DESCRIPTIVE NOTES (Type of report and inclusive dates) Interim Report, 1 December 1970 - 15 May 1971			
5. AUTHOR(S) (First name, middle initial, last name) Julius Jortner			
6. REPORT DATE July 1971		7a. TOTAL NO. OF PAGES 118	7b. NO. OF REFS 16
8a. CONTRACT OR GRANT NO. F33615-71-C-1143		9a. ORIGINATOR'S REPORT NUMBER(S) MDC G2078	
b. PROJECT NO. 7381		9b. OTHER REPORT NO(S) (Any other numbers that may be assigned this report) AFML-TR-71-160	
c. Task No. 738102			
d.			
10. DISTRIBUTION STATEMENT Approved for public release, distribution unlimited.			
11. SUPPLEMENTARY NOTES		12. SPONSORING MILITARY ACTIVITY Air Force Materials Laboratory Wright Patterson Air Force Base, Ohio 45433	
13. ABSTRACT A program to explore the behavior of ATJ-S graphite under multiaxial stress states is described. The program includes biaxial tests, off-axis uniaxial tests, and the development of a triaxial test capability.  The first phase of the program is to conduct fracture tests on specimens of ATJ-S graphite under biaxial stress states at room temperature and 2000°F at low strain rates. (approximately $10^{-2}$ /min). The biaxial tests consist of simultaneous axial loading and internal pressurization of hollow cylindrical specimens. The biaxial stress-states investigated include combinations of across-grain tension with with-grain tension, and across-grain compression with with-grain tension. The second phase is to conduct uniaxial tensile and compressive tests on ATJ-S specimens oriented at 0°, 45°, 70° and 90° to the across-grain axis of the material.  The biaxial and off-axis uniaxial tests have been completed. The results are presented in a preliminary manner in this report. The biaxial results suggest that there is a reduction in average tensile strength when a second principal stress is applied to ATJ-S graphite; however, the lower bound of the data conforms quite well to a maximum principal stress criterion. Another significant result is that the strains measured under biaxial tension are greater than would be predicted from uniaxial strains using current constitutive equations. The off-axis results show that the off-axis compressive strength is approximately equal to the with-grain compressive strength, that the off-axis tensile strengths lie between the across-			

DD FORM 1 NOV 65 1473

Unclassified

Security Classification

# NOTICE

When Government drawings, specifications, or other data are used for any purpose other than in connection with a definitely related Government procurement operation, the United States Government thereby incurs no responsibility nor any obligation whatsoever; and the fact that the government may have formulated, furnished, or in any way supplied the said drawings, specifications, or other data, is not to be regarded by implication or otherwise as in any manner licensing the holder or any other person or corporation, or conveying any rights or permission to manufacture, use, or sell any patented invention that may in any way be related thereto.

ACCESSION NO.	
CHSTI	WHITE SECTION <input checked="" type="checkbox"/>
DCC	DIFF SECTION <input type="checkbox"/>
UNANNOUNCED	<input type="checkbox"/>
JUSTIFICATION	
BY	
DISTRIBUTION/AVAILABILITY CODES	
DIST.	AVAIL. and/or SPECIAL
A	

Copies of this report should not be returned unless return is required by security considerations, contractual obligations, or notice on a specific document.

DOCUMENT CONTROL DATA - R&D (Cont'd)

grain and with-grain tensile strengths, and that the off-axis Young's moduli increase monotonically with off-axis angle. The probable shape of the biaxial failure envelope under off-axis loading is deduced from the uniaxial off-axis data; it is concluded that the differences in strength between on-axis and off-axis biaxial loading are likely to be minor in comparison to the scatter observed in on-axis biaxial tests.

14. KEY WORDS	LINK A		LINK B		LINK C	
	ROLE	WT	ROLE	WT	ROLE	WT
<p>Graphite Mechanical Behavior Multiaxial Stress Biaxial Stress Triaxial Stress ATJ-S Graphite Off-Axis Testing</p>						

Unclassified

Security Classification

AFML-TR-71-160

MULTIAXIAL BEHAVIOR OF ATJ-S GRAPHITE  
INTERIM REPORT

J. Jortner  
McDonnell Douglas Astronautics Company

TECHNICAL REPORT AFML-TR-71-160  
July 1971

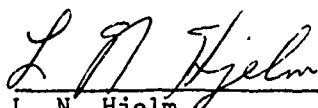
Approved for public release; distribution unlimited

## FOREWORD

This interim report was prepared for the United States Air Force Materials Laboratory (AFML), Wright-Patterson AFB, Ohio under Contract F33615-71-C-1143, Project 7231, Task 738102. Lt. John R. Koenig, LAS, is the AFML Project Engineer. This report describes the results of biaxial testing and off-axis uniaxial testing of ATJ-S graphite which were the first two phases of the program entitled Exploratory Development of Multiaxial Behavior of ATJ-S Graphite. The program was initiated on 1 December 1970; the period of performance is ten months. The work reported here was performed between 1 December 1970 and 15 May 1971.

J. Jortner is program manager and principal investigator at the McDonnell Douglas Astronautics Company-West (MDAC-West). Others who contributed their efforts and knowledge to the program include J. C. Schutzler (deputy principal investigator), B. R. Lyons (stress analysis), W. W. Reinhardt (material screening), and T. T. Sakurai (mechanical testing).

Publication of this report does not constitute Air Force approval of the report's findings or conclusions. It is published only for the exchange and stimulation of ideas.



L. N. Hjelm  
Chief, Space and Missile Systems  
Support Branch  
Materials Support Division  
Air Force Materials Laboratory

This document was prepared as MDAC-West report number MDC G2078.

## ABSTRACT

A program to explore the behavior of ATJ-S graphite under multi-axial stress states is described. The program includes biaxial tests, off-axis uniaxial tests, and the development of a triaxial test capability.

The first phase of the program is to conduct fracture tests on specimens of ATJ-S graphite under biaxial stress states at room temperature and 2000°F at low strain rates (approximately  $10^{-2}$ /min). The biaxial tests consist of simultaneous axial loading and internal pressurization of hollow cylindrical specimens. The biaxial stress-states investigated include combinations of across-grain tension with with-grain tension, and across-grain compression with with-grain tension. The second phase is to conduct uniaxial tensile and compressive tests on ATJ-S specimens oriented at 0°, 45°, 70° and 90° to the across-grain axis of the material.

The biaxial and off-axis uniaxial tests have been completed. The results are presented in a preliminary manner in this report. The biaxial results suggest that there is a reduction in average tensile strength when a second principal stress is applied to ATJ-S graphite; however, the lower bound of the data conforms quite well to a maximum principal stress criterion. Another significant result is that the strains measured under biaxial tension are greater than would be predicted from uniaxial strains using current constitutive equations. The off-axis results show that the off-axis compressive strength is approximately equal to the with-grain compressive strength, that the off-axis tensile strengths lie between the across-grain and with-grain tensile strengths, and that the off-axis Young's moduli increase monotonically with off-axis angle. The probable shape of the biaxial failure envelope under off-axis loading is deduced from the uniaxial off-axis data; it is concluded that the differences in strength between on-axis and off-axis biaxial loading are likely to be minor in comparison to the scatter observed in on-axis biaxial tests.



## TABLE OF CONTENTS

	<u>Page</u>
Section 1 INTRODUCTION . . . . .	1
Section 2 BACKGROUND . . . . .	3
2.1 Material Anisotropy . . . . .	3
2.2 Conditions of Interest . . . . .	5
2.3 Available Test Techniques . . . . .	5
Section 3 SCOPE AND STATUS OF CURRENT PROGRAM . . . . .	9
3.1 Biaxial Tests . . . . .	9
3.2 Off-Axis Tests . . . . .	10
3.3 Triaxial Test Development . . . . .	16
Section 4 BIAXIAL TESTS . . . . .	19
4.1 Material . . . . .	19
4.2 Biaxial Test Methods . . . . .	19
4.3 Biaxial Specimens . . . . .	32
4.4 Fracture Patterns . . . . .	39
4.5 Fracture Data . . . . .	48
4.6 Stress-Strain Behavior . . . . .	60
Section 5 OFF-AXIS TESTS . . . . .	63
5.1 Material and Anisotropy . . . . .	63
5.2 Analysis of Shear Coupling Effects . . . . .	75
5.3 Compressive Test Method . . . . .	84
5.4 Tensile Test Method . . . . .	84
5.5 Results in Compression . . . . .	90
5.6 Results in Tension . . . . .	103
5.7 Comments on Off-Axis Biaxial Strength . . . . .	103
Section 6 CONTINUING EFFORTS . . . . .	115
Section 7 REFERENCES . . . . .	117

# LIST OF ILLUSTRATIONS

<u>Figure</u>		<u>Page</u>
1	Material and Stress Axes . . . . .	4
2	Cylindrical Specimen Orientations. . . . .	6
3	Biaxial Stress States. . . . .	11
4	Off-Axis Biaxial Failure Envelope. . . . .	14
5	Billet Cutting Plans - Schematic . . . . .	21
6	Room Temperature Biaxial Test Set-Up . . . . .	28
7	Elevated Temperature Biaxial Test Set-Up . . . . .	29
8	Biaxial Specimen and Flag Assembly for Strain Measurement at Elevated Temperature. . . . .	30
9	Biaxial Specimen (Current Program) . . . . .	33
10	Short Biaxial Specimen (Reference 1) . . . . .	36
11	Stress Distribution in Short Biaxial Specimen. . . . .	37
12	Stress Distribution in 4-Inch Biaxial Specimen . . . . .	38
13	Specimen After Uniaxial Tension Test at 70°F . . . . .	41
14	Specimen After Hoop Tension Test at 70°F . . . . .	42
15	Specimen After Compression-Tension Test at 70°F. . . . .	43
16	Specimen 24 After Biaxial Tension Test at 70°F . . . . .	44
17	Specimen 1 After Biaxial Tension Test at 70°F. . . . .	45
18	Specimen 13 After Biaxial Tension Test at 70°F . . . . .	46
19	Typical Remains of Biaxial Specimen Tested at 2000°F . . . . .	47
20	Specimen After Uniaxial Tension Test at 2000°F . . . . .	49
21	Specimen and Nickel Bladder After Compression-Tension Test at 2000°F . . . . .	50
22	Specimen and Nickel Bladder After Biaxial Tension Test at 2000°F . . . . .	51
23	Nomenclature for Crack Location and Orientation. . . . .	53
24	Biaxial Failure Stresses at 70°F (ATJ-S) . . . . .	55
25	Biaxial Failure Stresses at 2000°F (ATJ-S) . . . . .	56
26	Biaxial Failure Strains at 70°F (ATJ-S), Measured at Outer Surface of Specimen . . . . .	57

# LIST OF ILLUSTRATIONS (Cont'd)

<u>Figure</u>		<u>Page</u>
27	Biaxial Failure Strains at 2000°F (ATJ-S), Measured at Outer Surface of Specimen . . . . .	58
28	Biaxial Strain Response at 70°F Measured at Outer Surface of Specimens from ATJ-S Billet 1C0-15 at 3500 psi Maximum Principal Stress . . . . .	61
29	Biaxial Strain Response at 2000°F Measured at Outer Surface of Specimens from ATJ-S Billet 1C0-15 at 3500 psi Maximum Principal Stress . . . . .	62
30	Sectioning Plan, Billet 16K9-27. . . . .	64
31	Cutting Plan for 45° and 70° Tensile Specimens . . . . .	65
32	Cutting Plan for 0° and 90° Tensile Specimens. . . . .	66
33	Cutting Plan for Acoustic-Velocity Disks . . . . .	67
34	Cutting Plan for Compression Specimens . . . . .	68
35	Angular Variation of Acoustic Velccity, Disk 2-3 . . . . .	70
36	Angular Variation of Acoustic Velocity, Disk 1-3 . . . . .	71
37	Angular Variation of Acoustic Velocity, Disk 1-2 . . . . .	72
38	Angular Variation of Acoustic Velocity, Tensile and Compressive Specimens. . . . .	74
39	Deformation of Anisotropic Tensile Specimens . . . . .	76
40	Axial Stresses at Mid-Length and Ends of Partially-Restrained Uniform-Section Off-Axis Specimens. . . . .	79
41	Specimen Configurations for Finite-Element Shear-Coupling Analysis. . . . .	81
42	Variation of Axial Stress Across Width of 45° Tensile Specimen . . . . .	82
43	Variation of Axial Stress Across Width of 45° Compression Specimen . . . . .	82
44	Variation of Axial Stress Along Length of 45° Tensile Specimen . . . . .	83
45	Variation of Axial Stress Along Length of 45° Compression Specimen . . . . .	83
46	Compression Specimen for Off-Axis Study. . . . .	85
47	Compression Test Set-Up. . . . .	86

# LIST OF ILLUSTRATIONS (Cont'd)

<u>Figure</u>		<u>Page</u>
48	Tensile Specimen for Off-Axis Study . . . . .	88
49	Tensile Specimen and Jig for Doubler Bonding. . . . .	89
50	Tensile Load Train for Off-Axis Tests . . . . .	91
51	Typical Primary Fracture Planes in Off-Axis Compression Tests . . . . .	94
52	Compressive Fracture Planes in Parent Slab. . . . .	97
53	Compressive Strength and Modulus, Off-Axis Study. . . . .	100
54	Axial Strain Curves in Compression, Off-Axis Study. . . . .	101
55	Axial Strain Response in Compression, Off-Axis Study. . . . .	102
56	0° Tensile Specimens After Test . . . . .	104
57	90° Tensile Specimens After Test. . . . .	105
58	45° Tensile Specimens After Test. . . . .	106
59	70° Tensile Specimens After Test. . . . .	107
60	Fracture Plane Orientation in Off-Axis Tensile Tests. . . . .	108
61	Tensile Strength and Modulus, Off-Axis Study. . . . .	110
62	Axial Strain Curves in Tension, Off-Axis Study. . . . .	111
63	Estimated Effect of Off-Axis Loading on Biaxial Strength. . . . .	113

# LIST OF TABLES

<u>Table</u>		<u>Page</u>
I	Biaxial Test Matrix . . . . .	12
II	Off-Axis Test Matrix. . . . .	15
III	Billet Characteristics. . . . .	20
IV	Characteristics of Biaxial Specimen Cores . . . . .	22
V	Billet Characterization (Specimen Core Data). . . . .	23
VI	Average Characteristics of Billet Regions . . . . .	24
VII	Specimen Allocations. . . . .	25
VIII	Results of Wall Thickness Study . . . . .	34
IX	Summary of Biaxial Failure Results at 70°F. . . . .	52
X	Summary of Biaxial Failure Results at 2000°F. . . . .	54
XI	Characterization of Specimen Blanks (Off-Axis Study). . . . .	69
XII	Elastic Moduli Assumed in Shear Coupling Analysis . . . . .	78
XIII	Strain Gages Used in Off-Axis Compression Tests . . . . .	87
XIV	Strain Gages Used in Off-Axis Tensile Tests . . . . .	92
XV	Strain Gage Characteristics, Off-Axis Study . . . . .	93
XVI	Fracture Orientations, Off-Axis Compression . . . . .	95
XVII	Summary of Compressive Fracture Data (Off-Axis Study) . . . . .	99
XVIII	Summary of Tensile Fracture Data (Off-Axis Study) . . . . .	109

## LIST OF SYMBOLS

### SYMBOLS FREQUENTLY USED

$\sigma_{1,2,3}$	. . .	principal stresses
$\sigma_A$	. . .	axial stress in cylindrical specimen
$\sigma_H$	. . .	hoop stress in cylindrical specimen
$\sigma_{T_a}$	. . .	uniaxial tensile strength, with-grain direction
$\sigma_{T_c}$	. . .	uniaxial tensile strength, across-grain direction
$e_A$	. . .	axial strain
$e_H$	. . .	hoop strain
$\theta$	. . .	angle between load axis and parent billet axis

## Section 1

### INTRODUCTION

A need exists for data on the mechanical behavior of ATJ-S graphite under multiaxial loads. In particular, multiaxial failure data are needed to guide the design of thermostructurally loaded ATJ-S components. At present, no experimentally verified failure criterion exists.

A biaxial test program of limited scope (room temperature, tension-tension only) was recently conducted on ATJ-S (special process) graphite at MDAC-West (Reference 1). Some biaxial data is also reported in Reference 2. However, there is a clear need for more data, particularly with respect to the effects of elevated temperature, off-axis loading, and triaxial stress states.

The current program has the following objectives:

- A. To provide on-axis biaxial test data on ATJ-S graphite at room and elevated temperature in the across-grain tension/with-grain tension and the across-grain compression/with-grain tension quadrants.
- B. To provide test data at room temperature on the strength of ATJ-S under off-axis loading.
- C. To evaluate the feasibility of conducting meaningful triaxial tests and, if the evaluation warrants, recommend a triaxial test program for possible future effort.

This interim report describes the nature of the program and presents, in a preliminary manner, the results of the biaxial and off-axis test efforts.

## Section 2

### BACKGROUND

#### 2.1 Material Anisotropy

ATJ-S graphite is mechanically orthotropic. When fabricated in the form of a cylindrical billet, the axis of the billet coincides with one principal material direction (the across-grain direction). The other two principal material directions lie in the plane perpendicular to the billet axis and the material is isotropic in that plane. Directions within the plane of isotropy are referred to as with-grain directions. Because the material is weaker in the across-grain direction, a billet may be thought of as behaving somewhat like a stack of weakly-bonded circular platelets as suggested in Figure 1a.

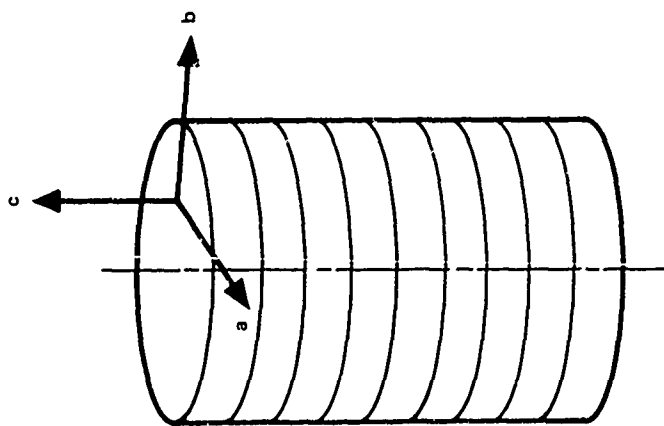
Figure 1a is somewhat simplified because a typical billet will probably not be uniformly anisotropic; that is, the principal material directions, and the difference between with-grain and across-grain properties, may vary somewhat from location to location within a single billet.

When describing the behavior of ATJ-S under stress, it is necessary to specify the magnitudes of the applied principal stresses and their orientation with respect to the principal material directions. Figure 1b shows the terminology used here. The c axis is the across-grain direction while the a and b axes denote any two mutually perpendicular with-grain directions; the 1, 2, and 3 directions refer to principal stress directions;  $\theta$  is the angle between the c axis and the 3 direction;  $\phi$  is the angle between the 2 direction and the intersection of the a-b and 1-2 planes. Thus five independent parameters ( $\sigma_1$ ,  $\sigma_2$ ,  $\sigma_3$ ,  $\theta$  and  $\phi$ ) are to be considered in describing the multiaxial failure envelope for ATJ-S graphite, in addition to the usual variables such as temperature, rate of stressing, volume under stress, environment, etc.

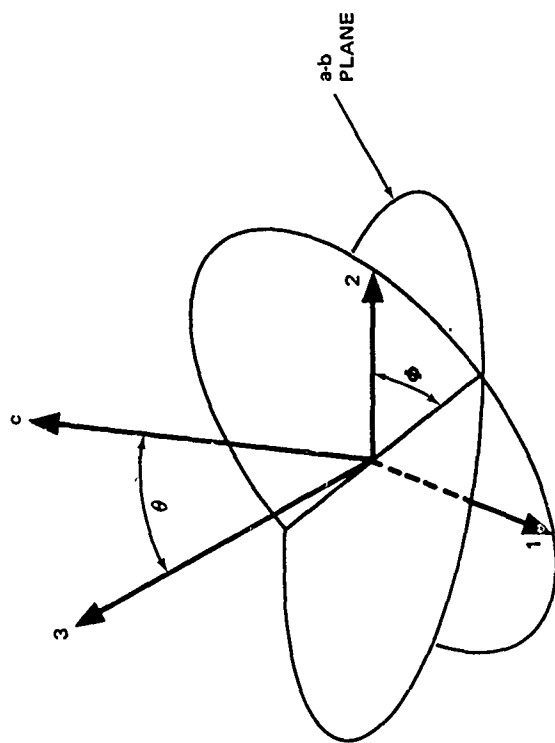
When  $\theta$  is zero, the stress state is referred to as being "on-axis"; when  $\theta$  is non-zero, the stress state is "off-axis".

**Preceding page blank**





a. BILLET AXES



b. COORDINATE NOMENCLATURE

Figure 1. Material and Stress Axes

## 2.2 Conditions of Interest

To narrow the scope of the problem, it is useful to consider the type of stress states to be expected in the applications of immediate interest. The prime applications involve externally heated, thermally stressed bodies of revolution. The heat input, and therefore the stress situation, is approximately axisymmetric; the axis of the body coincides with the across-grain or "c" direction of the material.

From considerations of symmetry, it may be shown that  $\phi$  is zero for such components, and that the off-axis stress states of primary interest may be specified in terms of  $\theta$  alone.

The temperatures of interest range from about room temperature up to above 5,000°F (at the external surface). However, the interior regions, where tensile stress may be expected to approach the failure level, are not expected to exceed 3,500°F.

## 2.3 Available Test Techniques

A variety of biaxial and triaxial stress states can be mechanically induced in hollow cylindrical specimens by suitable combinations of axial load, internal pressure, and external pressure. An alternate approach would be to combine the aforementioned loadings with torsion applied to the ends of the cylinder. However, a facility capable of applying torsion in combination with other loads is not available to this program. An obvious restriction in both approaches is that the radial stress can only be compressive.

For ATJ-S, the only way of excising a cylindrical specimen so that the stress state is homogeneously oriented with respect to the material anisotropy is to align the cylinder axis with the across-grain (or "c") direction. This corresponds to the Type I specimen shown in Figure 2. As suggested in the figure, a varying wall thickness would be necessary to control the failure location

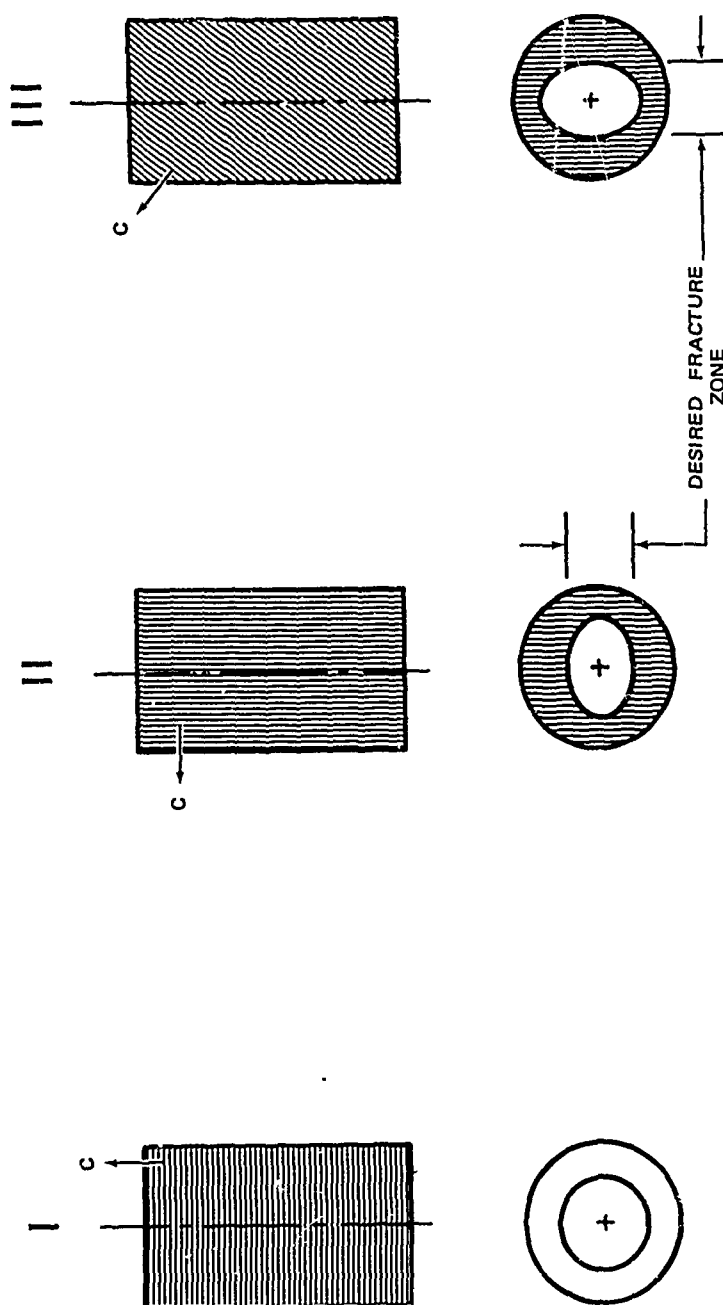


Figure 2. Cylindrical Specimen Orientations

in specimen Types II and III. To avoid the complications implicit in making, testing, and interpreting data from Type II and III specimens, only Type I specimens are considered in the current program. This restriction implies that:

- A. Testing of off-axis orientations of multiaxial stress-states is precluded.\*
- B. Of the two with-grain stresses, one (corresponding to the radial direction) must always be compressive (or zero).

Biaxial tests under internal pressure and axial load can be conducted in the MDAC facility at Santa Monica which has been used (References 1 and 3) to test graphite under biaxial stress states up to 4000°F. Triaxial tests can be conducted, at room temperature only, in a high-pressure facility of the type available at Pennsylvania State University (PSU) as described in Reference 11. The PSU facility is capable of applying axial load, internal pressure, and external pressure simultaneously to generate any desired triaxial stress state (with the obvious exception of triaxial tension) in a hollow cylindrical specimen. Strains at the external wall of the specimen can be measured using strain gages. The pressure capacity of the system exceeds the uniaxial compressive strength of ATJ-S graphite by one order of magnitude.

Off-axis tests can readily be conducted in uniaxial tension and compression. Some problems attend the off-axis testing as a result of unsymmetrical deformations of the specimens (References 4 and 5). These effects can be minimized in tension (as noted in Reference 5) by providing a relatively long gage section. In compression, however, short specimens are necessary to avoid buckling; off-axis tests in compression should therefore be accompanied by an analytical estimate of the true stress state at failure.

---

\*With the exception of equi-biaxial tension, see Section 3.2

### Section 3

#### SCOPE AND STATUS OF CURRENT PROGRAM

##### 3.1 Biaxial Tests

It may be noted that, for ATJ-S, there are seven independent on-axis biaxial quadrants:\*

	<u>a</u>	<u>b</u>	<u>c</u>
Quadrant 1	+	0	+
Quadrant 2	+	0	-
Quadrant 3	-	0	-
Quadrant 4	-	0	+
Quadrant 5	+	+	0
Quadrant 6	+	-	0
Quadrant 7	-	-	0

The quadrants selected for investigation in the current program are the first two (Numbers 1 and 2) listed above, primarily because they are the most readily explored with the existing biaxial facility at MDAC-West.

However, the biaxial failure picture would be incomplete without some definition of behavior in the other quadrants, particularly Numbers 4, 5, and 6 listed above. With the possible exception of quadrant 5, these might eventually be investigated (at room temperature) in a triaxial facility.

In selecting biaxial stress states to be tested, it is helpful to postulate an idealized fracture envelope and consider which stress-states would be most effective in revealing the difference between actual material behavior and the assumed ideal. Somewhat arbitrarily, but with available biaxial data for graphites (References 1,2,3 and 6) in mind, the idealized envelope selected consists of the combination of a maximum principal-stress envelope and a maximum shear-stress envelope.

\*In the tabulation + denotes tensile stress and - denotes compressive stress in the a, b, or c direction.

This combined envelope is shown as a dotted line in Figure 3. Several stress-ratios which might be effective test conditions are also shown. Of particular interest are the following stress states.

<u>Nominal Axial-to-Hoop Stress Ratio</u>	<u>Remarks</u>
1:0	Across-grain uniaxial reference
1:1	Applies to off-axis study (Section 3.2); fills in between 1:0 and "corner".
$\sigma_{T_a} : \sigma_{T_c}$	Approximately 1:1.2 stress state; explores "corner" of tension-tension quadrant.
1:2	Readily tested (requires no axial load); fills in between "corner" and 0:1.
0:1	With-grain uniaxial reference.
-1:1	For ATJ-S this stress state is close to the "corner" in compression-tension quadrant

With the exception of the -1:1 stress state, biaxial data has been obtained on ATJ-S material at room temperature in a previous effort at MDAC (Reference 1). The current program is intended to supplement that data at room temperature and to provide some data at elevated temperature. The elevated temperature selected for test is 2000°F because it appears (Reference 7) that ATJ-S exhibits the lowest tensile strain-to-failure at temperatures in the range 1500 to 2500°F.

The biaxial test matrix is given in Table I. The tests have been completed and the data is presented in Section 4 of this report.

### 3.2 Off-Axis Tests

Under equibiaxial stress, such as the 1:1 stress state, the direction of the principal stresses is not unique; this may be inferred from, for example, the fact that the appropriate Mohr's circle vanishes into a point. Therefore the 1:1 on-axis test is actually an off-axis test. This being so, an economical way of estimating the off-axis effect on

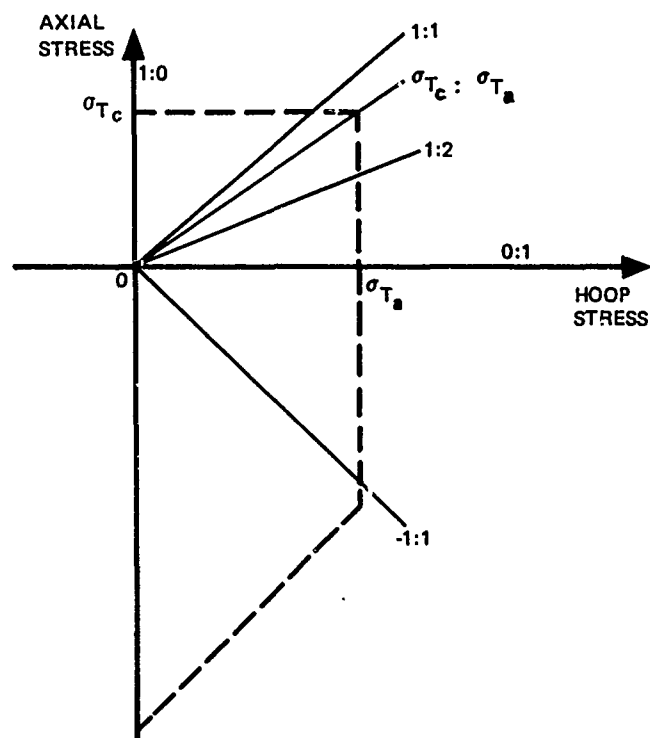


Figure 3. Biaxial Stress States

TABLE I  
BIAXIAL TEST MATRIX

<u>Stress State</u> Ratio, Axial to Hoop Stress <sup>(1)</sup>	Number of Test Points (2) (3)	
	Room Temperature	2000°F
1:0	5 <sup>(4)</sup>	4
1:1	— <sup>(4)</sup>	—
1:X <sup>(5)</sup>	5 <sup>(4)</sup>	7
0:1	5 <sup>(4)</sup>	6
-1:1	4	5
Totals	19	22

NOTES

- (1) All specimens are biaxial cylinders (Figure 9) with axis aligned with across-grain direction.
- (2) Crosshead speed 0.02 to 0.05 in./min; test to failure under simultaneous axial load and internal pressure. Measure failure load and pressure.
- (3) Axial and hoop strains measured with strain gages at room temperature and with optical extensometers at elevated temperature.
- (4) Some data available, Reference 1
- (5) Stress state in biaxial tension; X approximates ratio of average uniaxial with-grain strength to average uniaxial across-grain strength.



is to supplement the 1:1 test with some uniaxial off-axis tests at various off-axis angles  $\theta$  (Figure 4) and from the data estimate the likely form of the failure envelope (dotted line in Figure 4). The test matrix, Table II, includes tensile tests at room temperature at angles  $\theta$  of 0 degrees, 45 degrees, 70 degrees, and 90 degrees. The emphasis on angles greater than 45 degrees is based on off-axis results for filamentary composite materials which suggest that the 45-degree tensile strength might be rather close to the 0-degree strength.

Available evidence (Figure 20 of Reference 8) suggests that compressive failure of ATJ-S takes place by shear at an angle approximately 45 degrees to the loading axis. Biaxial data for AXF graphite (Reference 3) suggest that in a portion of the compression-tension quadrant a critical shear stress theory may apply. For ATJ-S, it would be of interest to determine how the critical shear stress varies with orientation; for example, the layer-structure model suggests that compressive strength would be least when the load is oriented 45 degrees to the c-axis because the maximum shear stress would then act on the weakest plane. It seems that a knowledge of off-axis compressive strengths could aid in estimating the off-axis effect on the compression-tension failure envelope. The test matrix, Table II, includes compressive testing at angles  $\theta$  of 0 degrees, 45 degrees, and 90 degrees; these angles should reveal the extremes of compressive strength variation. One additional orientation, selected at 70 degrees, is intended to fill in the trend.

The planned off-axis tests have been completed. A preliminary description of the results is presented in Section 5 of this report.

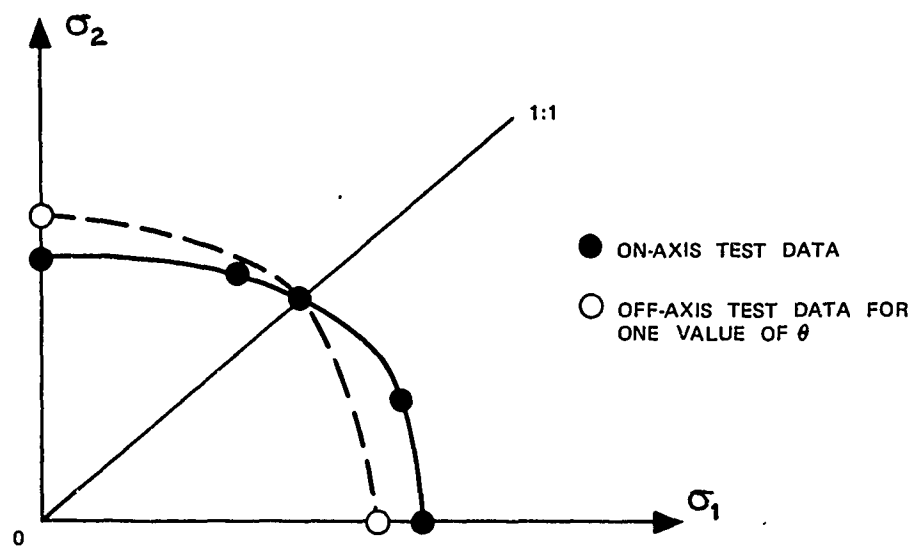


Figure 4. Off-Axis Biaxial Failure Envelope

TABLE II  
OFF-AXIS TEST MATRIX  
(ROOM TEMPERATURE)

	<u>θ, Load Axis Angle from c Direction</u>			
	<u>0°</u>	<u>45°</u>	<u>70°</u>	<u>90°</u>
Tension	3	3	3	3
Compression	3	3	3	3
NOTES				
(1) Uniaxial specimens.				
(2) Crosshead speed 0.05 in./min; two axially oriented strain gages on each specimen				

### 3.3 Triaxial Test Development

The on-axis triaxial envelope for ATJ-S occupies eight octants in principal stress space. Because of the equivalence of the a and b with-grain directions, only six octants require independent investigation:

	<u>a</u>	<u>b</u>	<u>c</u>
Octant 1	+	+	+
Octant 2	+	+	-
Octant 3	+	-	+
Octant 4	+	-	-
Octant 5	-	-	+
Octant 6	-	-	-

Octant No. 1 is beyond the present scope of study because adequate triaxial tension tests have not been developed. A variety of triaxial tension tests have been attempted on other materials (for example, see page 178, Reference 9). The problems associated with sufficiently precise definition of the actual stresses at failure lead to the conclusion that adequate definition of the triaxial tension failure envelope for graphite is beyond present experimental capabilities. However, the problem merits further study in the hope that a useful technique can be developed. Octant No. 6, triaxial compression, is of little interest to current component designs. Octant No. 2 is eliminated from consideration at this time because the requirement that both with-grain stresses be tensile imposes the experimental difficulties noted in Section 2.3.

The loads and pressures required to investigate the remaining three octants (Numbers 3, 4, and 5) can readily be applied. The knowledge of the triaxial failure surface which might be gained by conducting tests in these octants might be of direct help in component design; also, it would probably be useful in assessing the validity of theoretical failure criteria. The feasibility of obtaining useful triaxial fracture data is dependent upon several considerations:

- A. Accurate load and pressure measurement capability.
- B. Ability to seal the specimen material from the pressurizing medium.
- C. Ability to maintain accurate alignment of the specimen relative to the axial load to minimize parasitic bending strains.
- D. Ability to measure specimen strains during loading.
- E. Ability to design specimens which do not fail prematurely in buckling under compressive stresses, and which do not exhibit excessive stress variations in the gage section.

Under the current program, the use of solid and hollow cylindrical specimens, subjected to internal and external pressures and to tensile or compressive axial loads, is being investigated. It is planned to study the experimental aspects of the problem by using the triaxial facility at Pennsylvania State University. At this time preliminary specimen and fixture designs have been completed and are being reviewed for experimental feasibility and for conformance to the desired stress uniformity and buckling resistance.

TABLE III  
BILLET CHARACTERISTICS

ATJ-S Billet Number	Approximate Dimensions, Inch			Bulk (1) Density G/CC	Acoustic Velocities, In/Microsec (2)	
	Length	Outside Diameter	Hole Diameter	Hole Depth	Axial	Radial
1CO-15	10 1/4	7 1/2	2 3/4	6 3/8	1.85	.0864-.0874 .1005-.1040
16K9-27	10 1/4	7 1/2	2 3/4	6 3/8	1.86	.0869-.0884 .1041-.1064
10V9-27	5 3/4	7 3/8	2 3/4	3 1/4	1.84	.0861-.0872 .1003-.1022

(1) Bulk Density from Weight & Volume; Volume measured by immersion in water after applying waterproof coating (approximate thickness = .002 inch).

(2) Acoustic Velocities measured at 1 MHZ.

Axial Velocities measured at 5 inch diameter circle, six measurements.

Radial Velocities measured at 2 inch intervals along length at six angular positions.

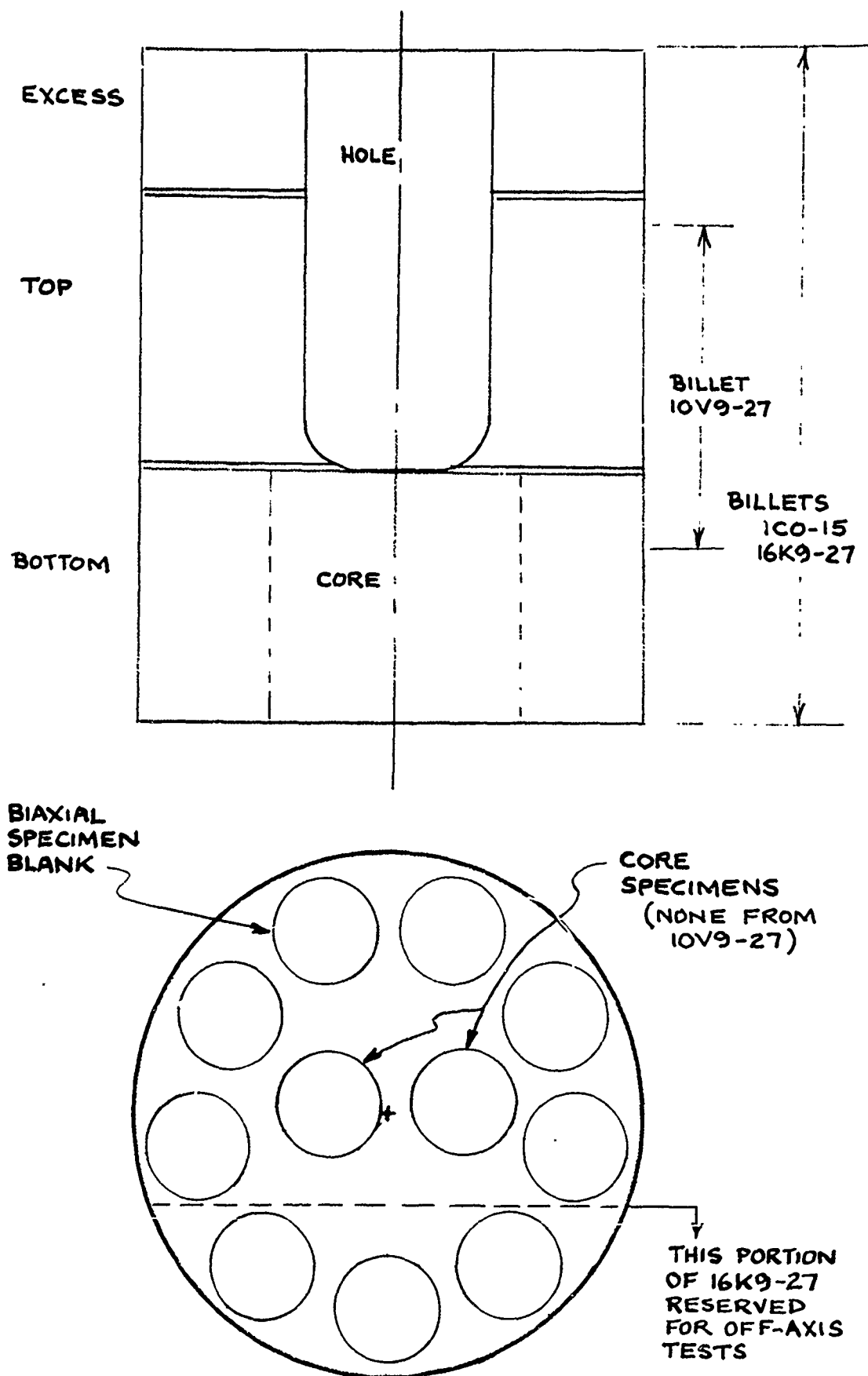


Figure 5. Billet Cutting Plans - Schematic

TABLE IV  
CHARACTERISTICS OF BIAXIAL SPECIMEN CORES

Specimen Number	Bulk Density (grams/cc)	Electrical Resistivity <sub>3</sub> ( $\Omega$ cm X $10^3$ )	Acoustic Velocity (in/ sec)
1	1.840	1.009	0.0861
2	1.847	1.015	0.0859
3	1.843	1.024	0.0854
4	1.848	1.031	0.0857
5	1.842	1.020	0.0861
6	1.849	1.007	0.0868
7	1.842	0.998	0.0868
8	1.848	0.995	0.0871
9	1.842	0.996	0.0870
10	1.846	0.996	0.0868
11	1.843	0.988	0.0869
12	1.847	0.997	0.0864
13	1.836	0.992	0.0868
14	1.844	0.991	0.0865
15	1.837	0.975	0.0874
16	1.847	0.987	0.0864
17	1.841	0.991	0.0870
18	1.846	0.993	0.0863
19*	1.847	1.053	0.0873
20	1.853	1.058	0.0876
21*	1.853	1.070	0.0868
22	1.855	1.073	0.0871
23*	1.855	1.071	0.0871
24	1.856	1.083	0.0866
25*	1.855	1.053	0.0878
26	1.851	1.075	0.0874
27*	1.854	1.060	0.0880
28	1.853	1.052	0.0882
29*	1.852	1.051	0.0878
30	1.852	1.042	0.0884
31	1.835	1.066	0.0851
33	1.834	1.071	0.0847
35	1.836	1.057	0.0854
37	1.831	1.042	0.0857
39	1.828	1.047	0.0856
41	1.828	1.046	0.0857
43	1.827	1.048	0.0856
45	1.827	1.052	0.0856
47	1.830	1.059	0.0854
1S	1.843	1.002	0.0864
2S	1.843	1.002	0.0863
3S	1.847	1.059	0.0874
4S	1.848	1.065	0.0873

\* These specimen cores are six inches long.



TABLE V  
BILLET CHARACTERIZATION (SPECIMEN CORE DATA) (1)

AJ-S Billet Number	Number Of Specimens	Bulk Density (2) G/CC	Electrical (3) Resistivity MilliOhm-Cm	Acoustic (4) Velocity in/Microsec
100-15	20	1.836-1.849	.975-1.031	.0854-.0874
16K9-27	14	1.847-1.856	1.042-1.083	.0866-.0884
10V9-27	9	1.827-1.836	1.042-1.071	.0847-.0857

(1) Specimen cores taken from center of biaxial specimen blanks per sectioning plans.

(2) Density by dry weight and measured volume.

(3) Electrical resistivity in across-grain direction

(4) Acoustic velocity in across-grain direction measured at 1 MHz.

TABLE VI  
AVERAGE CHARACTERISTICS OF BILLET REGIONS (1)

ATJ-S Billet	Region	Bulk Density G/CC	Electrical Resistivity MilliOhm-Cm	Acoustic Velocity In/Micro Sec
1CO-25	Top	1.841	.999	.0866
	Bottom	1.847	1.001	.0864
	Core	1.843	1.002	.0864
16K9-27	Top	1.853	1.060	.0875
	Bottom	1.853	1.065	.0875
	Core	1.848	1.062	.0874
10V9-27	Middle	1.831	1.054	.0854

(1) Measurements on biaxial specimen cores.

TABLE VII

## SPECIMEN ALLOCATIONS

Parent Billet (ATJ-S)	Billet Region	Specimen Number	Test Temperature and Stress State <sup>(1)</sup>							
			70°F				2000°F			
			1:0	1:X	0:1	-1:1	1:0	1:X	0:1	-1:1
1CO-15	Top	1		X						
		3			X		X			
		5						X		
		7							X	
		9								
		11	X							
		13		X				X		
		15								
		17								X
	Bottom	2	X							
		4				X				
		6			X					
		8				X				
		10							X	
		12(2)					X			
		14							X	
		16						X		
		18								
	Core	1-S				X				
		2-S								X
16K9-27	Top	19						X		
		21							X	
		23							X	
		25			X					
		27		X						
		29	X							
	Bottom	20	X							
		22(3)								
		24		X			X			
		26						X		
		28								
		30			X					
	Core	3-S						X		
		4-S								X

(continued next page)

TABLE VII (Cont'd)

Parent billet (ATJ-S)	Billet Region	Specimen Number	Test Temperature and Stress State <sup>(1)</sup>							
			70°F				2000°F			
			1:0	1:X	0:1	-1:1	1:0	1:X	0:1	-1:1
10V9-27	Middle	31	X							
		33		X				X		
		35								
		37								X
		39					X			
		41								X
		43			X					
		45				X				
		47						X		
Total Number Specimens			5	5	5	4	4	7	6	5

(1) Stress state given as ratio of axial to hoop stresses.

(2) Specimen 12 broken accidentally before test

(3) Specimen 22 damaged in machining

References 1 and 3. Biaxial stresses are obtained by combining axial load with internal pressure applied to a hollow cylindrical specimen.

The axial loads are applied in a fixture designed to limit bending strains in the specimen. Alignment checks performed before each series of tests show that the bending strains introduced into the biaxial specimen are less than 3% of the average axial strain both in tensile and compressive loading.

All tests were conducted using approximately radial loading. That is, the pressure was manually controlled to increase in proportion to the axial load so that the ratio of axial stress to hoop stress was approximately constant.

4.2.1 Room Temperature Tests - As indicated in Figure 6 a thin rubber balloon was used to prevent penetration of the pressurizing fluid (water containing soluble oil) into the graphite specimen. Two strain gages were used to monitor strains. One gage was oriented axially, the other circumferentially. Both gages were Micromeasurements Type EA-06-125AD-120; this gage type has a gage factor of 2.10 and a transverse sensitivity factor of +0.8%. The gages were applied with Eastman 910 cement to the external surface at midlength.

4.2.2 2000°F Tests - As indicated in Figure 7, a metal foil bladder was used to seal the pressurizing medium (argon). The bladder was a seamless electrodeposited nickel tube 0.002 to 0.003 inches thick. At 2000°F the flow strength of the nickel bladder is low and at failure of the graphite specimen accounts for less than two percent of the load and pressure carrying capacity of bladder/specimen combination. Strains were measured optically using a Physitech Model 440 extensometer aimed at graphite "flags" mechanically attached to the specimen for axial strains, and an Optron Model 800 extensometer aimed at the diametral extremes of the specimen gage section for hoop strains. Figure 8 shows the flags and the relation of optical sighting points to the specimen. Axial sightings were at opposite sides of the specimen to minimize the effects of bending. The

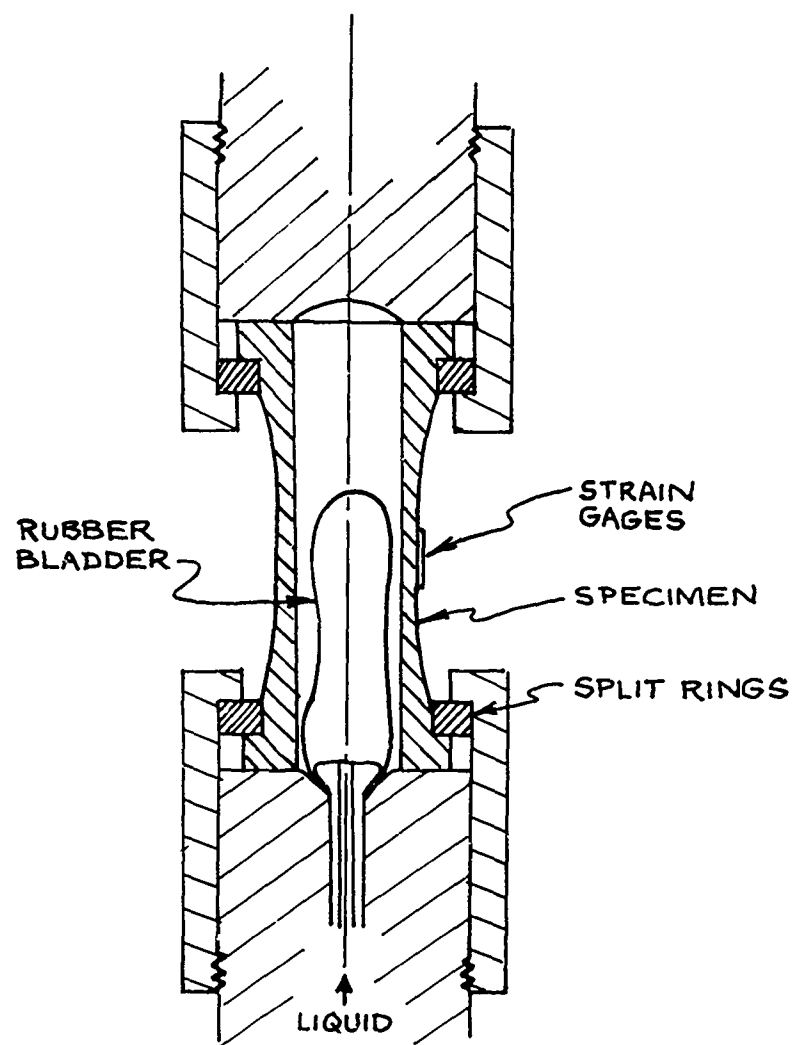


Figure 6. Room Temperature biaxial Test Set-Up

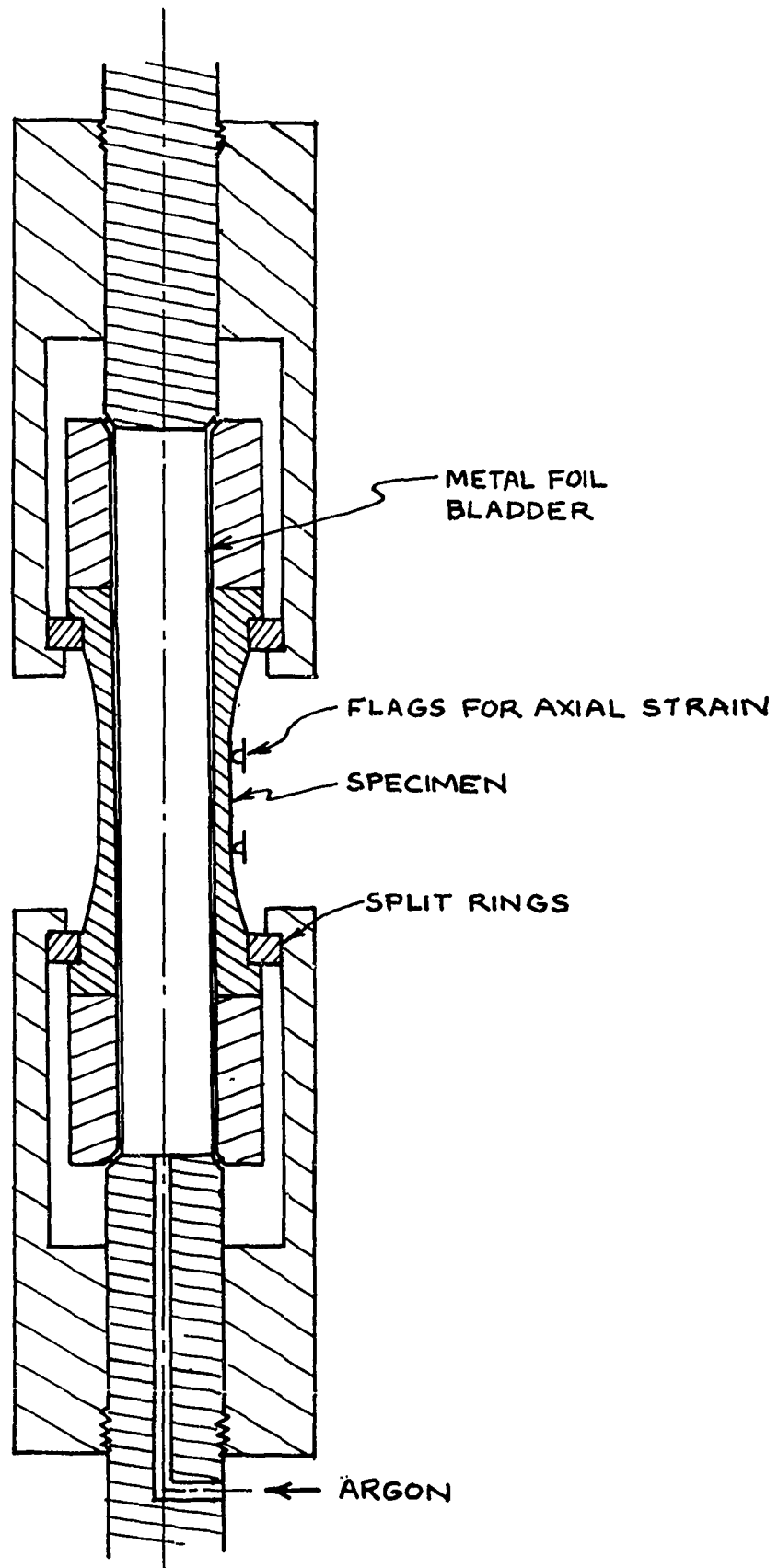


Figure 7. Elevated Temperature Biaxial Test Set-Up

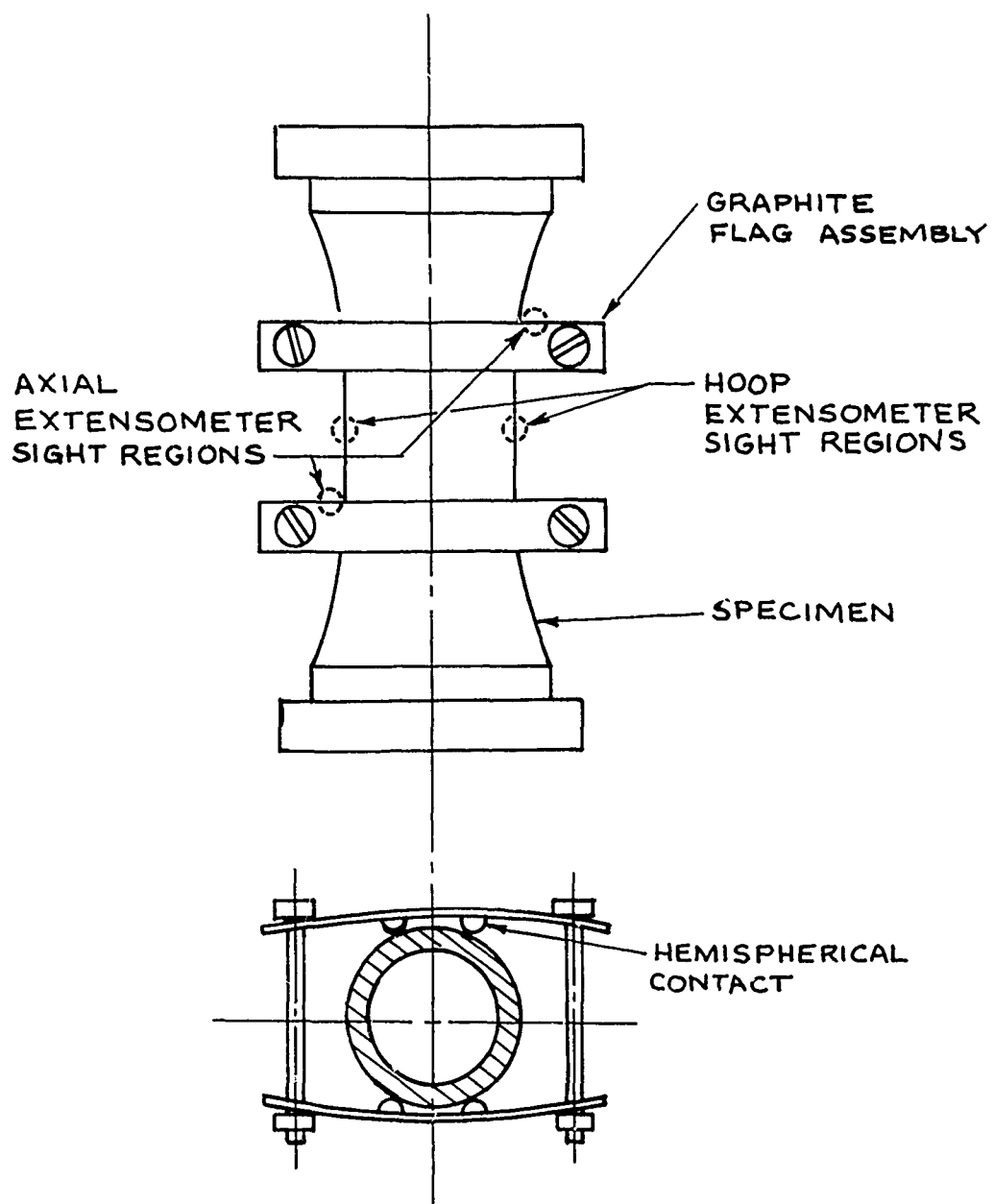


Figure 8. Biaxial Specimen and Flag Assembly for Strain Measurement at Elevated Temperature



flags were designed to be flexible so they exert little diametral constraint on the specimen while maintaining contact in spite of diametral strains. Calibration tests on the optical extensometers show that the strain data is repeatable and accurate within approximately  $\pm .0002$  inches per inch.

4.2.3 Data Reduction - Stresses were calculated from the loading data using the following equations:

$$\sigma_A = \frac{L + \pi r_{ib}^2 P}{\pi(r_o^2 - r_i^2)}$$

$$\sigma_H = \frac{P r_{ib}}{r_o - r_i}$$

where

$\sigma_A$  = axial stress, psi

$\sigma_H$  = hoop stress, psi

$L$  = measured load, lb\*

$P$  = internal pressure, psi

$r_o$  = outer radius of gage section, in.

$r_i$  = inner radius of gage section, in.

$r_{ib}$  = effective inner radius, in.

For tests at room temperature  $r_{ib}$  was taken as equal to  $r_i$  on the assumption that the rubber bladder acts like a fluid under pressure. For tests at 2000°F,  $r_{ib}$  was taken as the nominal internal radius of the nickel bladder,  $r_{ib} = r_i - 0.003$ .

It may be noted that the equation for hoop stress is the thin-wall approximation and thus provides only an approximate value of stress. The reader is referred to the stress analysis described in Reference 1,

\*The measured load may be about one percent less than the true load sustained by the specimen because of friction between the load train and the guide bushings used to provide alignment (Reference 1; see also Figure 47).

and in Section 4.3 of this report, for an estimate of the stress gradients in the gage section of the specimen.

Strains were obtained from the strain gage and extensometer readings in the usual manner. In the case of strain gages the readings were corrected for the transverse sensitivity of the gage using the transverse sensitivity factor supplied by the gage manufacturer.

#### 4.3 Biaxial Specimens

The specimen used at both room and elevated temperature is shown in Figure 9. The specimen is longer than that used in the study reported in Reference 1; the longer specimen was selected because it reduces the nonuniformities in stress, as described in Section 4.3.2. The wall thickness used is 0.050 inch as in previous work (References 1 and 3). Some doubts were expressed in Reference 1 as to the ability of so thin a wall to represent the bulk behavior of the material; to help resolve these doubts, the experimental study briefly described in Section 4.3.1 was conducted under a concurrent MDAC program.

4.3.1 Wall Thickness Study - Hoop tension tests were conducted on ATJ-S graphite ring specimens of two different wall thicknesses. The specimens were hollow cylindrical rings of uniform wall thickness and were tested under internal pressure and zero axial load at MDAC in a fixture patterned after that in Reference 10.

The specimen dimensions and test results are summarized in Table VIII. The specimen dimensions were selected to give equal volumes and equal ratios of radius to thickness for both wall thicknesses so as to minimize the potential effects of volume and thick-wall stress gradients on the comparison of results.

It is seen that increasing the wall thickness does not increase the average strength of the specimens, and that the .050-inch wall specimens give strength values closer to those expected in the with-grain direction for this material. This result suggests that there would be no advantage to increasing the wall thickness of the biaxial specimen.

NOTES

1. UNSPECIFIED TOLERANCES  $\pm 0.010$
2. UNSPECIFIED SURFACE FINISH

16

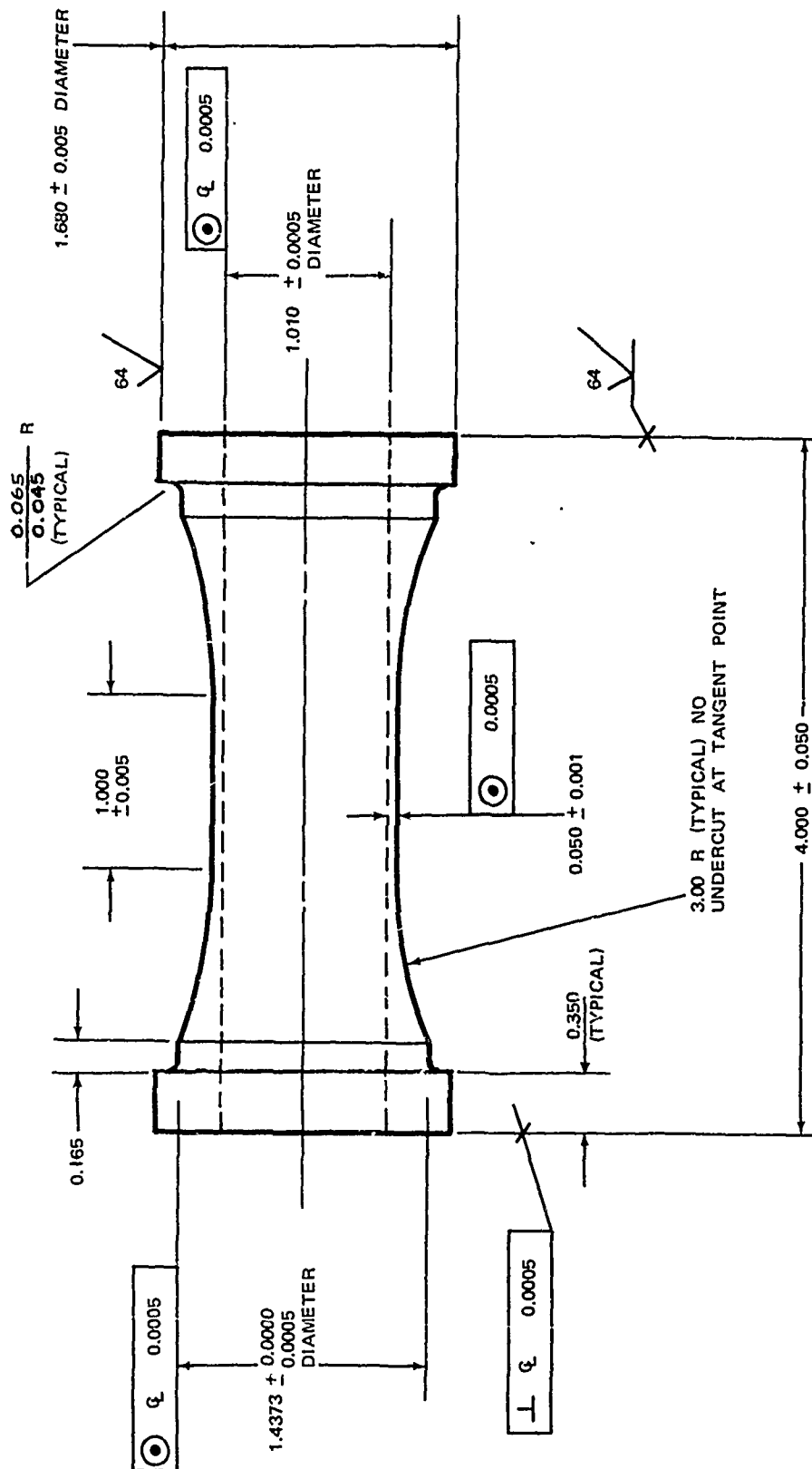


Figure 9. Biaxial Specimen (Current Program)

TABLE VIII  
NOT REPRODUCIBLE

RESULTS OF WALL-THICKNESS STUDY

Nominal Specimen Dimensions, Inch			Internal (2) Pressure at Burst, psi	Loop Stress (3) at Burst, psi
Wall Thickness	Inner Diameter	Height		
0.050	1.000	2.000	Specimen (1) Number	
			1A	4120
			1B	4655
			1E	5600
			1F	5580
			1h	5415
0.062	1.640	0.750	Average	
			2-1A	4530
			2-2A	3925
			2-4A	4925
			2-5A	5020
			2-F	4580
Average			458	4594

(1) All specimens excised from single slab of ATJ-S graphite, so that the cylindrical axis corresponds to the across-grain direction.

(2) Tests conducted at a pressurization rate of 1200 psi/min.

(3) Thin wall approximation.

4.3.2 Biaxial Specimen Analysis\* - Stress analysis of two biaxial specimen configurations was conducted to select the best design for this program. The configurations are shown in Figures 9 and 10. The 4.0 inch long specimen (Figure 9) is the standard configuration used at MDAC-West for biaxial strength tests. The 3.15 inch long specimen (Figure 10) was used in a recent study (Reference 1) and was designed to that length for the purpose of conserving material. While material conservation was not a major consideration in specimen selection for the current program, it was initially considered desirable to use the same specimen as in Reference 1 for the purpose of data comparison.

The short (3.15 inch) specimen was previously analyzed (Reference 1) to determine the stress distributions under various loading conditions. It was determined from these analyses that the combination of internal pressure and axial tension resulted in the most severe stress nonuniformities in the specimen. The stress distribution for this case is shown in Figure 11. The increase in the axial and hoop stresses near the end of the gage section is a result of discontinuities in specimen stiffness between the thin wall section and the heavy ends, and the eccentricity of the axial load application relative to the thin section. Both effects cause cylindrical bending stresses in the specimen which, in biaxial tension, add to produce the stress nonuniformities shown.

Using the same analytical technique and assumptions (Reference 1), the long (4.0 inch) specimen was analyzed in this study for the combination of internal pressure and axial tensile loading, for comparison to the analytical results for the short specimen.

The stress analysis results for the 4.0 inch long specimen are shown in Figure 12. Comparison of the stress distributions to those previously predicted for the short (3.15 inch long) specimen indicates that the 4.0 inch specimen is more favorable. The differences between peak and nominal stresses are about 1/2 of those in the shorter specimen. This reduction is presumed to be a result of a more gradual transition in

---

\*by B. R. Lyons and J. C. Schutzler

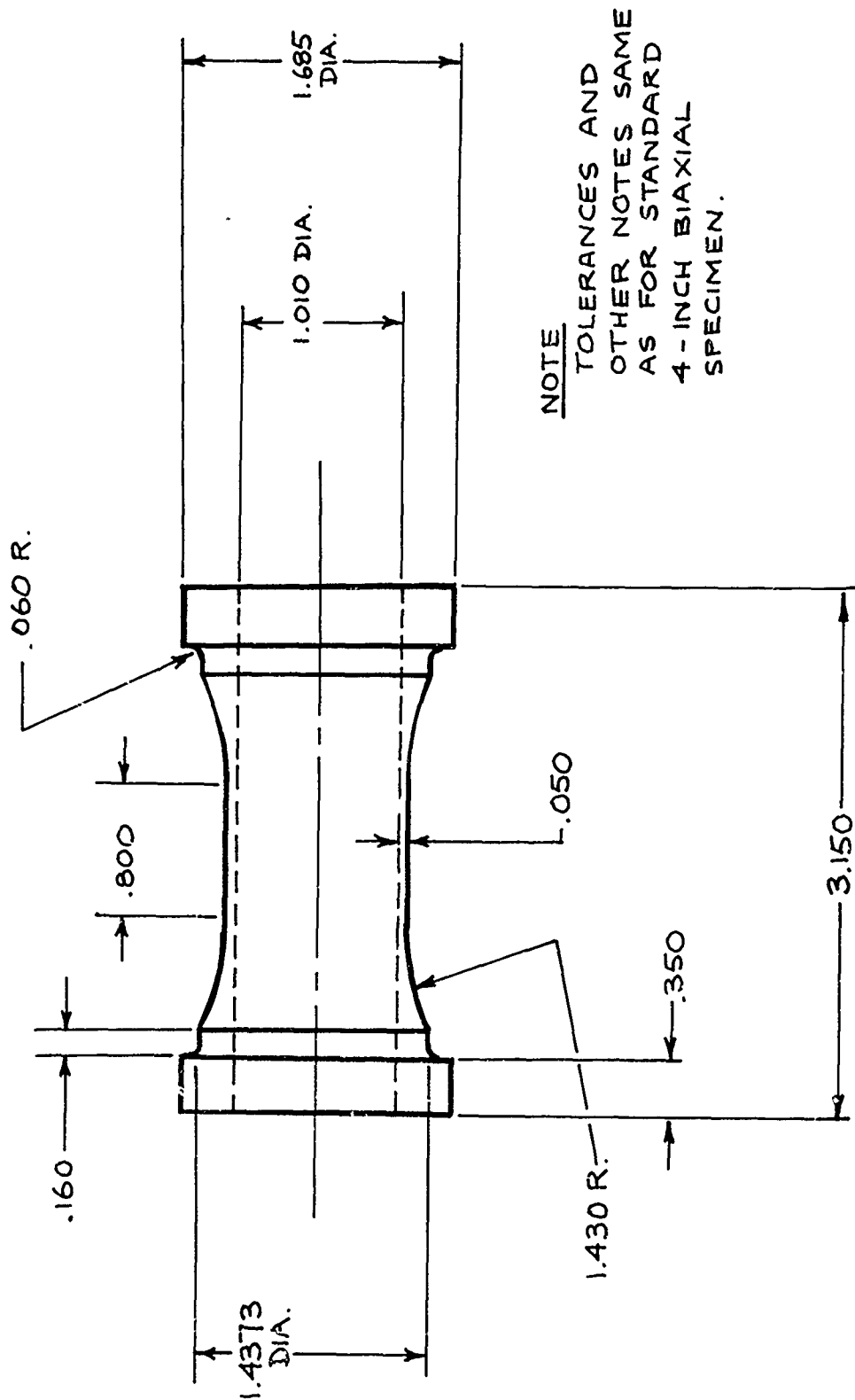


Figure 10. Short Biaxial Specimen (Reference 1)

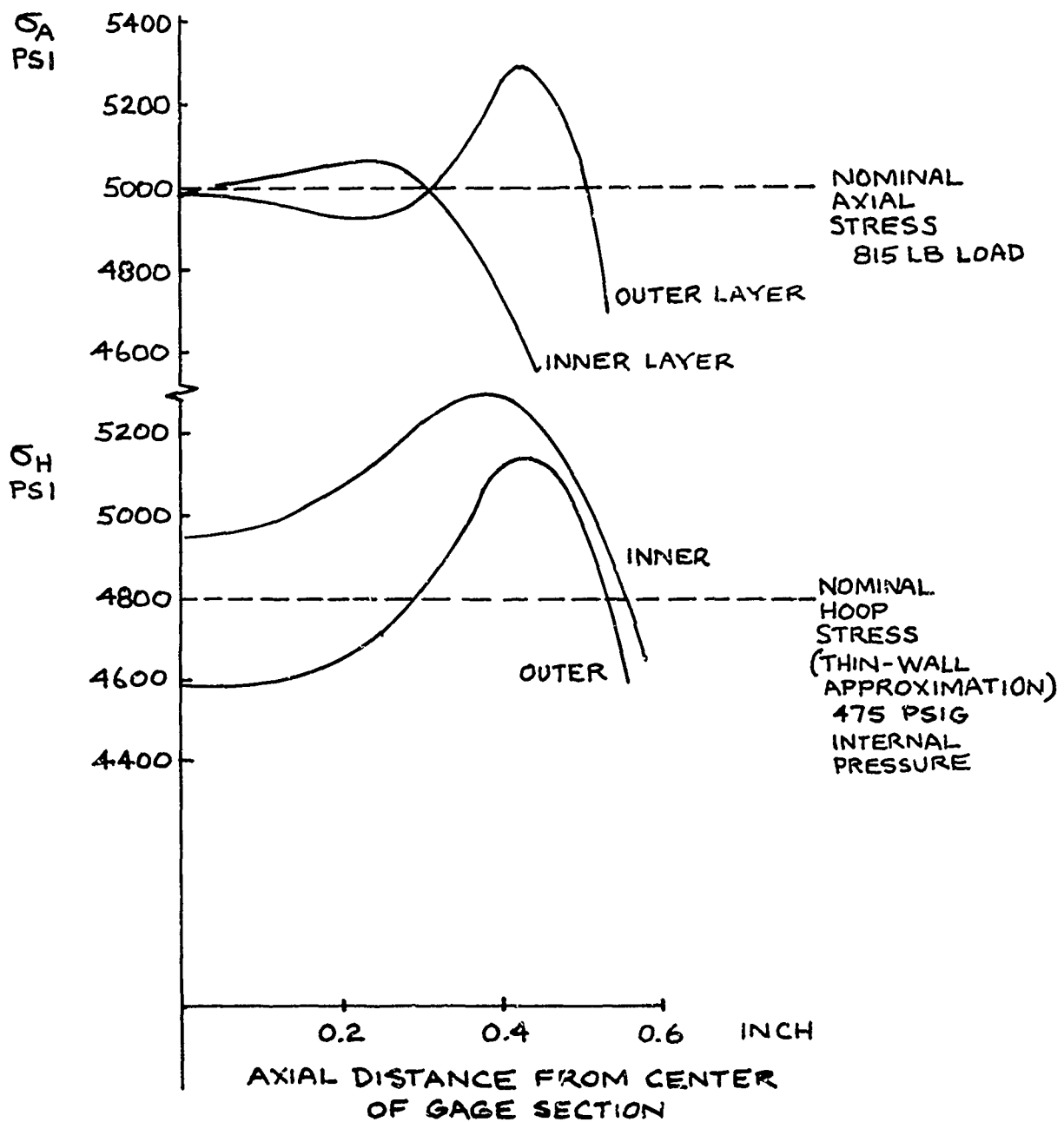


Figure 11. Stress Distribution in Short Biaxial Specimen

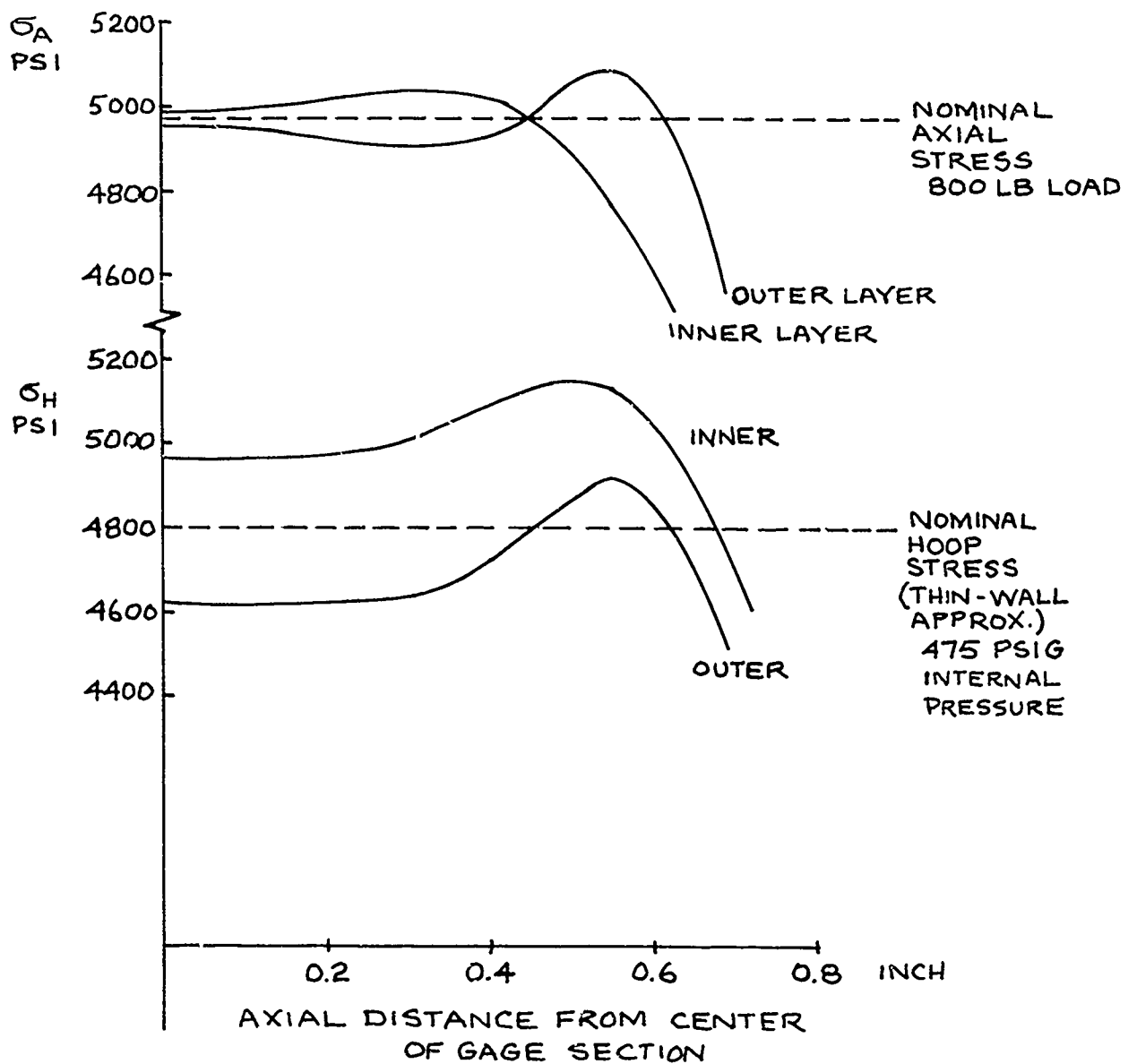


Figure 12. Stress Distribution in 4-Inch Biaxial Specimen



stiffness between the gage section and the heavy ends. On the basis of these comparisons, the standard 4.0 inch long specimen was selected for use in this program.

4.3.3 Inspection of Specimens - All specimens were inspected for conformity to the dimensional tolerances shown in Figure 9. No significant deviations were discovered during the dimensional inspection, which was conducted using standard machine-stop inspection practices. The wall thickness was measured directly using a dial gage set-up rather than by taking the difference between outer and inner diameters because it was found that the action of a three-point inner-diameter micrometer could deform the specimen wall enough to cause error in the wall thickness measurement. The actual wall thicknesses varied between .0490 to .0505 inches from specimen to specimen.

All specimens were sent to the Air Force Materials Laboratory for X-ray inspection of the gage section. No defects were discernible on the radiographs; however, some radiographs have been returned to AFML for image-enhancing treatment to determine whether some of the lower strengths measured in biaxial testing might be attributable to defects discernible under enhanced conditions.

The exterior surface of the gage section was inspected visually after being wiped with alcohol. A fair number of small pits on some specimens was discovered in this manner. However, there appears to be no correlation between the location of fracture and the location of these pits. The lack of correlation may be due to the existence of more severe pits at the inner-diameter surface (which was not inspected because of its relative inaccessibility) or may imply that such surface pits are not as effective as other types of defects in reducing strength.

#### 4.4 Fracture Patterns

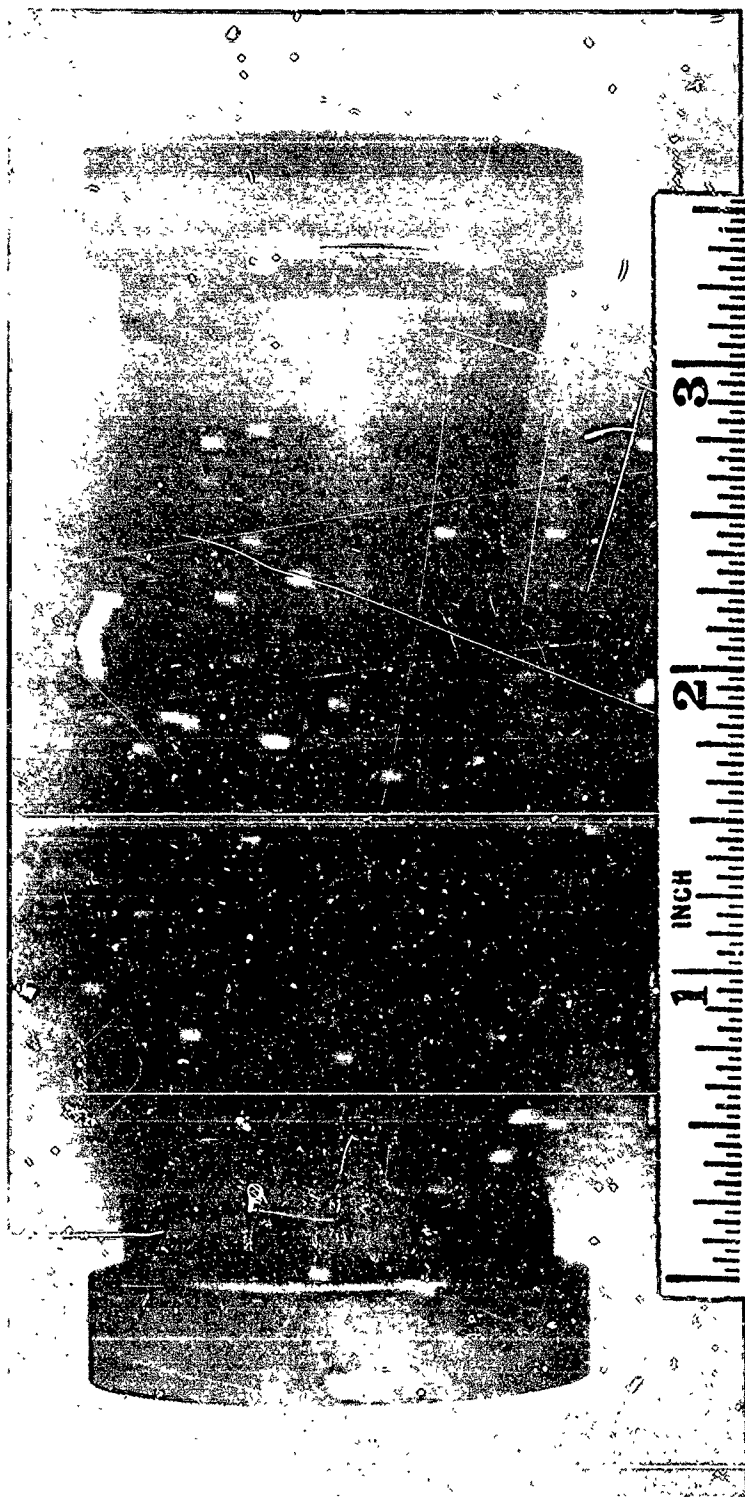
Photographs showing the typical appearance of fracture crack patterns

observed in the biaxial tests at 70°F are shown in Figures 13 through 18. The specimens were reconstructed after failure with the aid of adhesive tape. The original crack segment at which fracture initiated is usually determinable by following the crack bifurcation patterns back to their apparent origin. Figure 16 shows a particularly clear example; the original crack is identified with an arrow. The orientation of the original crack with respect to the specimen axis may be summarized as follows:-

- 1) In uniaxial tension (under axial load applied along the specimen axis) the crack is perpendicular to the axis (Figure 13).
- 2) In uniaxial hoop tension (under internal pressure) and also under axial compression combined with hoop tension, the original crack is parallel to the specimen axis (Figures 14 and 15).
- 3) In biaxial tension where the axial stress and the hoop stress are nearly equal, the crack orientation is random (Figures 16, 17, and 18).

These observations, which are no different than those noted in References 1 and 3, imply that the failure plane is normal to the maximum principal tensile stress in all the stress states tested with the exception of near-equibiaxial tension. In near-equibiaxial tension the angular variation of normal tensile stress is small and the fracture plane tends to be randomly oriented.

At 2000°F, the specimens shattered upon failure into too many pieces to conveniently reconstruct the crack pattern (Figure 19 shows only part of the remains of a typical specimen). However, limited evidence tends to show that the initial crack orientations follow the same trends



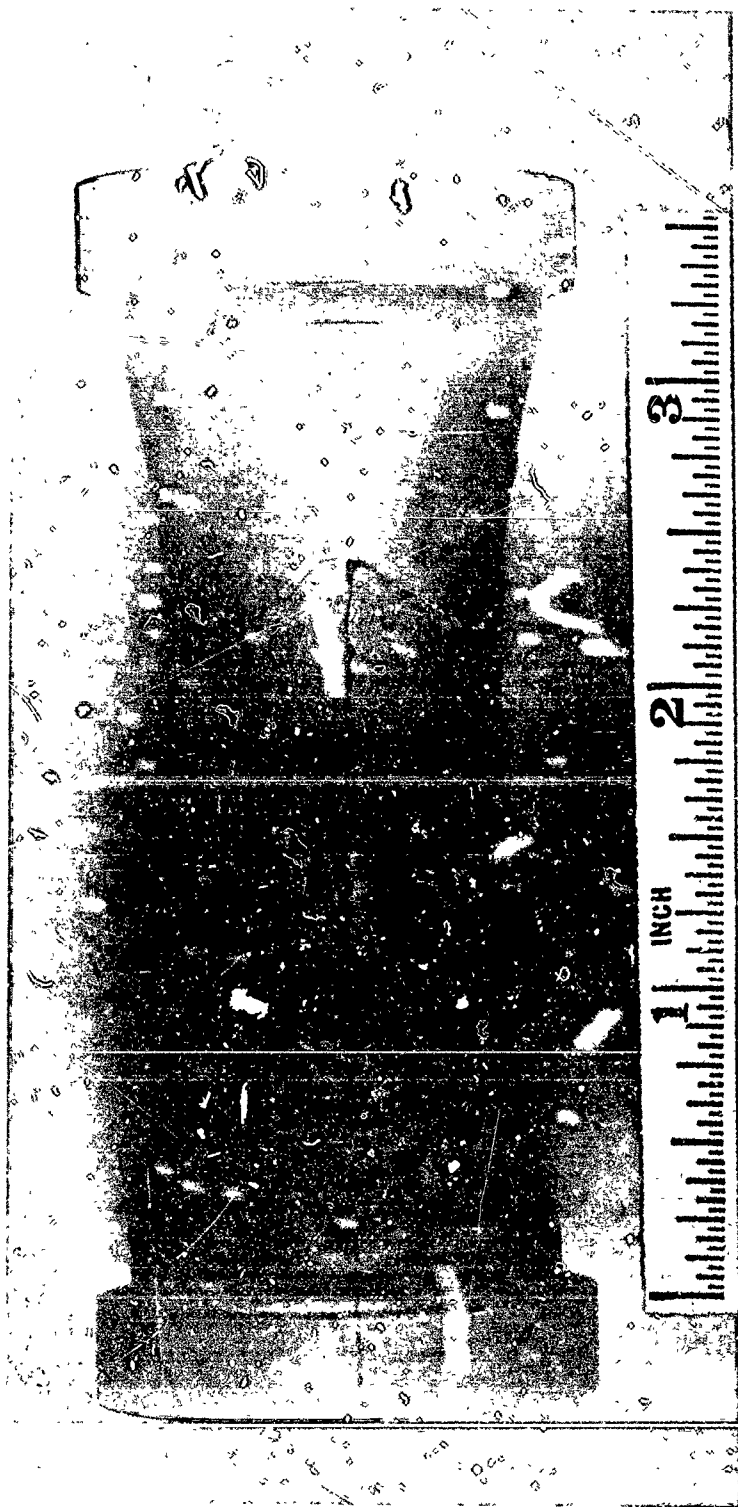
SPECIMEN NO. 11  
AXIAL-TO-HOOP STRESS RATIO 1:0  
TEST TEMPERATURE 70°F  
(ATJ-S GRAPHITE, BIAxIAL TEST)

Figure 13. Specimen After Uniaxial Tension Test at 70°F



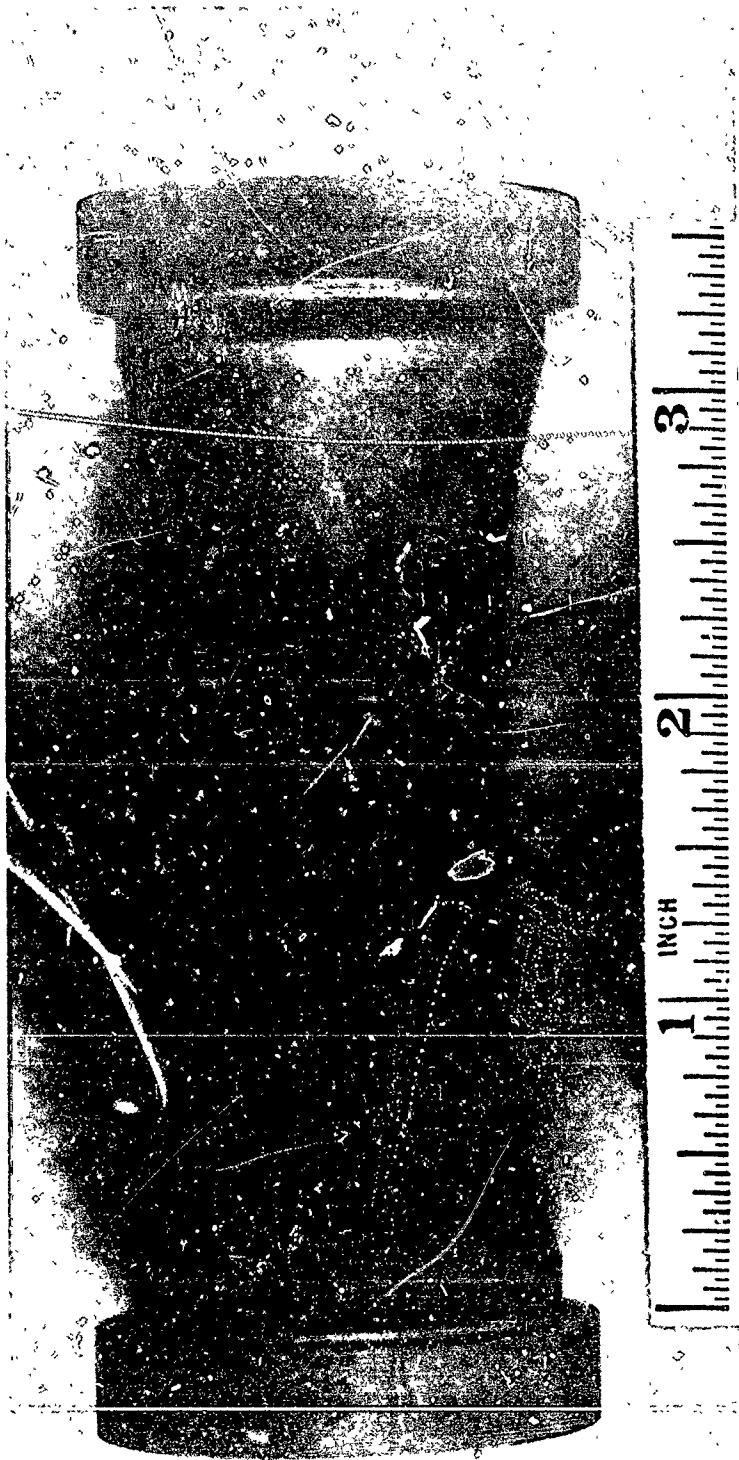
SPECIMEN NO. 30  
AXIAL-TO-HOOP STRESS RATIO 0:1  
TEST TEMPERATURE 70°F  
(ATJ-S GRAPHITE, BIAxIAL TEST)

Figure 14. Specimen After Hoop Tension Test at 70°F



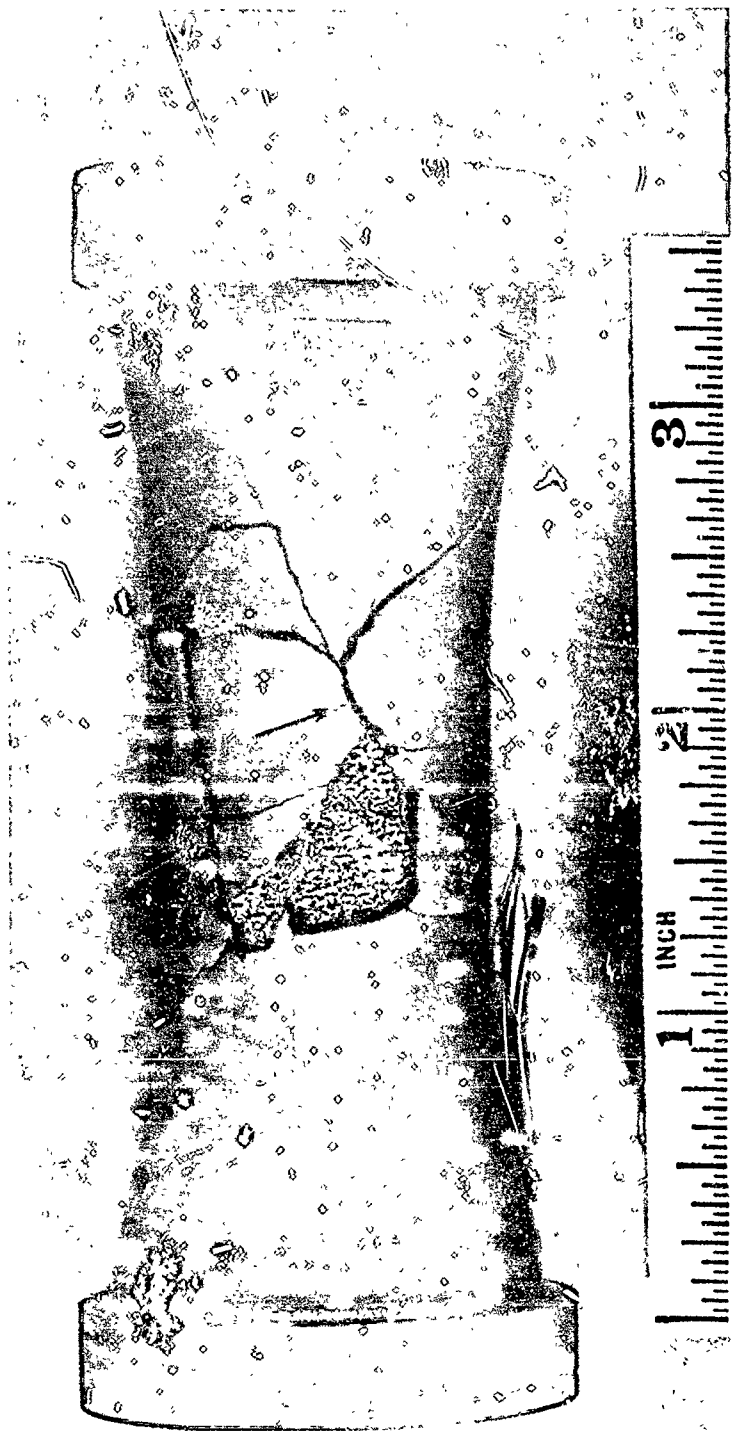
SPECIMEN NO. 4  
AXIAL-TO-HOOP STRESS RATIO - 1:1  
TEST TEMPERATURE 70°F  
(ATJ-S GRAPHITE, BIAxIAL TEST)

Figure 15. Specimen After Compression-Tension Test at 70°F



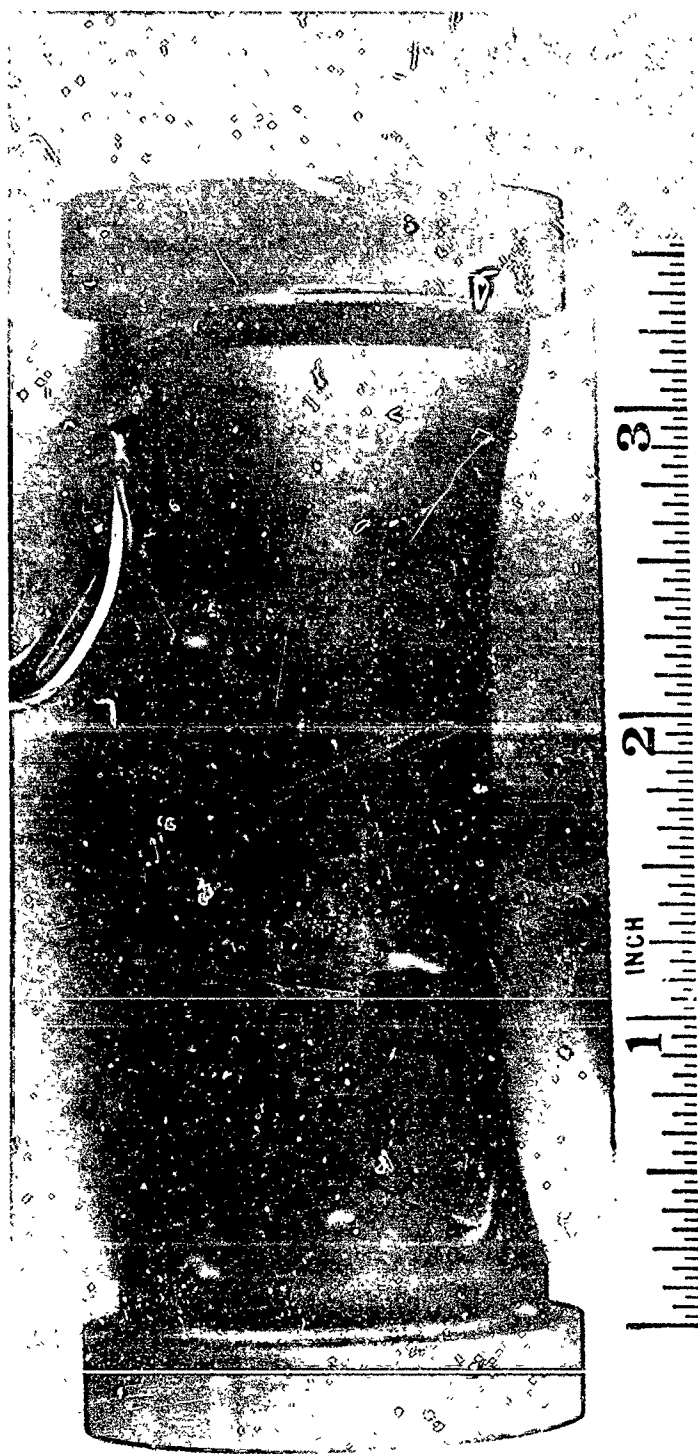
SPECIMEN NO. 24  
AXIAL-TO-HOOP STRESS RATIO 1:1.26  
TEST TEMPERATURE 70°F  
(ATJ-S GRAPHITE, BIAxIAL TEST)

Figure 16. Specimen 24 After Biaxial Tension Test at 70°F



SPECIMEN NO. 1  
AXIAL-TO-HOOP STRESS RATIO 1:1.26  
TEST TEMPERATURE 70°F  
(ATJ-S GRAPHITE, BIAxIAL TEST)

Figure 17. Specimen 1 After Biaxial Tension Test at 70°F



SPECIMEN NO. 13

AXIAL-TO-HOOP STRESS RATIO 1:1.26

TEST TEMPERATURE 70°F

(ATJ-S GRAPHITE, BIAxIAL TEST)

Figure 18. Specimen 13 After Biaxial Tension Test at 70°F





Figure 19. Typical Remains of Biaxial Specimen Tested at 2000°F

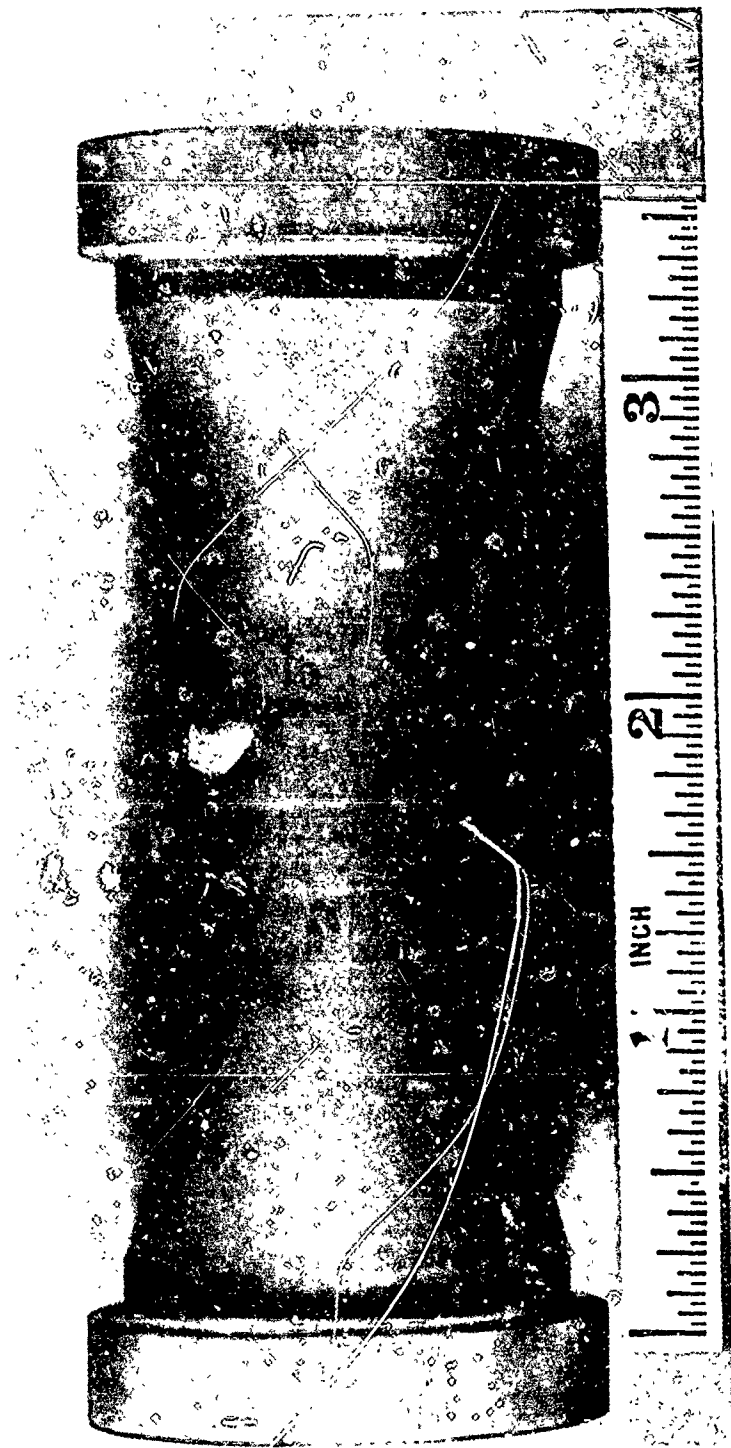
observed at 70°F. Figure 20 shows a typical uniaxial failure at 2000°F in which, as expected, the fracture plane is normal to the applied tensile stress. Figures 21 and 22, incomplete with respect to the reconstruction of the graphite specimen, show the tear in the nickel bladder which presumably followed the original crack in the graphite. Figure 21 shows that the original crack in compression-tension was axially oriented, and Figure 22 shows that the original crack in near-equibiaxial tension was at an "odd" angle.

#### 4.5 Fracture Data

The failure data are summarized in Table IX for room temperature tests, and in Table X for 2000°F. The table for room temperature results includes a listing of the parameters  $\theta$ ,  $X$  and  $\alpha$ , defined in Figure 23, which characterize the location of the midpoint of the initial crack and its orientation. It may be seen, in Table IX, that the midpoints of all initial cracks tend to occur within the uniform-wall-thickness gage section of the specimen; however, as Figure 12 shows, the uniform-stress section of the specimen is only about one half the length of the one-inch gage section; thus the actual stresses at failure might vary from the nominal tabulated stresses (obtained from the equations of Section 4.2.3) by a few percent, in addition to the usual "thick-wall" effect, depending on the location of the fracture.

The stresses and strains measured at failure are plotted in Figures 24 through 27. To aid in interpreting the data different symbols are used to identify the parent billet of each specimen. The dotted lines in Figures 24 and 26 indicate the approximate lower-bound of the room temperature data previously reported in Reference 1.

At the start of the program it was hoped that the three billets of ATJ-S used in the biaxial tests would be sufficiently alike in properties that the mechanical data might be pooled to give biaxial failure envelopes of some significance for similar billets of ATJ-S. Unfortunately, as the strength data in Figures 24 and 25 show, the three billets are dis-



SPECIMEN NO. 26  
AXIAL-TO-HOOP STRESS RATIO 1:0  
TEST TEMPERATURE 2000°F  
(ATJ-S GRAPHITE, BIAxIAL TEST)

Figure 20. Specimen After Uniaxial Tension Test at 2000°F



SPECIMEN NO. 17

AXIAL-TO-HOOP STRESS RATIO - 1:1

TEST TEMPERATURE 2000°F

(ATJ-S GRAPHITE, BIAxIAL TEST)

Figure 21. Specimen and Nickel Bladder After Compression-Tension Test at 2000°F



SPECIMEN NO. 15  
AXIAL-TO-HOOP STRESS RATIO 1:1.10  
TEST TEMPERATURE 2000°F  
(ATJ-S GRAPHITE, BIAxIAL TEST)

Figure 22. Specimen and Nickel Bladder After Biaxial Tension Test at 2000°F

TABLE IX

## SUMMARY OF BIAxIAL FAILURE RESULTS AT 70°F

(ATJ-S GRAPHITE)

Nominal Stress State	Specimen Number	FAILURE CONDITIONS				FRACTURE CRACK CHARACTERISTICS			
		Axial Stress (psi)	Hoop Stress (psi)	Axial Strain	Loop Strain	Orientation, $\theta_c$	Axial Location, X (in.)	Circumferential Location, $\alpha$	Remarks
1:0	2	4010	---	.0056	-.0004	90°	1.2	255°	$\alpha \pm 20^\circ$
	11	4060	---	.0058	-.0004	85°	1.7	170°	
	20	3980	---	.0054	-.0004	90°	1.6	275°	
	29	3900	---	.0049	-.0004	90°	2.0	0°	
	31	3750	---	.0052	-.0003	90°	2.0	88°	
1:1.26	1	3480	4420	.0051	.0041	30°	2.0	5°	machining marks (not near fracture)
	13	3030	3810	.0040	.0032	0°	1.2	355°	
	24	3870	4900	.0056	.0038	60°	2.0	250°	
	27	3550	4490	.0047	.0035	45°	1.1	190°	
	35	2860	3610	.0037	.0028	30°	1.7	230°	
0.15:1	43	637	4000	-.0002	.0031	0°	1.7	300°	
0:1	3	---	4640	-.0003	.0040	0°	1.8	0°	crack 1/16" from strain gage pieces missing
	6	---	5010	-.0004	.0042	0°	?	200°	
	30	---	4710	-.0003	.0035	0°	1.6	250°	
-0.1:1	25	-400	4890	-.0008	.0034	0°	2.0	160°	fracture through strain gage
-0.6:1	8	-2440	3860	-.0031	.0034	0°	1.7	20°	
-1:1	1-S	-4180	4260	-.0062	.0044	0°	1.5	250°	
	4	-4620	4680	-.0076	.0051	0°	1.3	285°	
	45	-3560	3720	-.0051	.0034	0°	?	120°	

- Notes.
- 1) Hoop stress from thin-wall approximation.
  - 2) Strains measured with strain gages at mid-length of exterior surface.
  - 3)  $\theta_c$ , X, and  $\alpha$  are defined in Figure 23.
  - 4) Gage length lies between  $X = 1.15$  and  $X = 2.15$ .

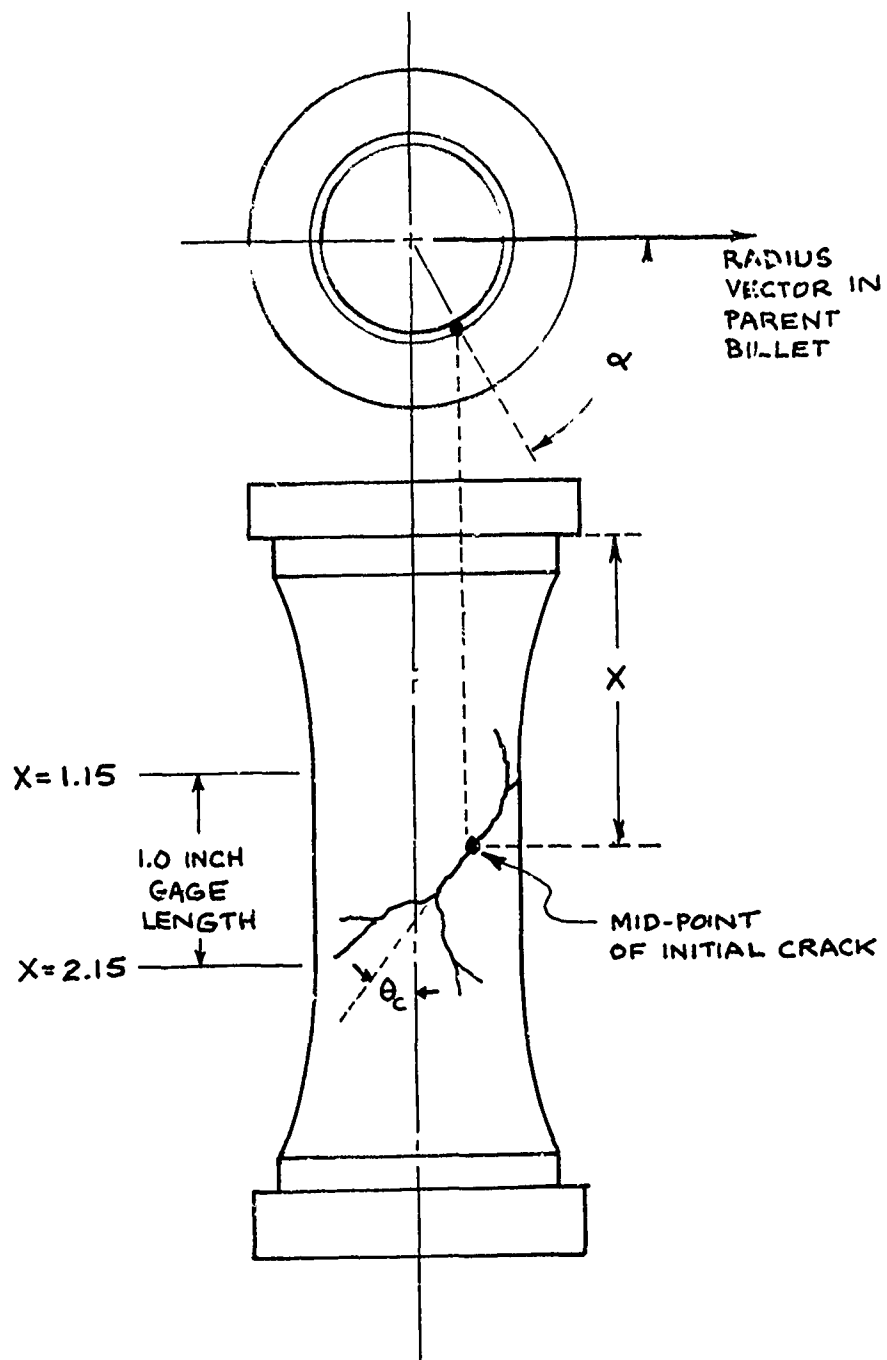


Figure 23. Nomenclature for Crack Location and Orientation

TABLE X  
SUMMARY OF BIAXIAL FAILURE RESULTS AT 2000°F  
(ATJ-S GRAPHITE)

Nominal Stress State	Specimen Number	FAILURE CONDITIONS			
		Axial Stress (psi)	Hoop Stress (psi)	Axial Strain	Hoop Strain
1:0	5	4910	---	.0058	-.0005
	14	4680	---	.0051	-.0004
	26	5180	---	.0053	-.0006
	39	4340	---	.0049	-.0006
1:1.10	7	4110	4570	.0038	.0032
	15	3390	3730	.0032	.0026
	3-S	4600	5070	.0043	.0032
1:1.20	33	4090	4930	n.d.	n.d.
1:1.35	18	3520	4700	.0033	.0030
	19	4430	5860	.0040	.0043
	28	3930	5380	.0026	.0035
0:1	9	0	5120	-.0007	.0033
	16	12	5120	-.0006	.0031
	21	18	6750	n.d.	.0041
	47	-24	5300	n.d.	.0035
-0.1:1	10	-600	5930	n.d.	.0036
	23	-740	7030	n.d.	.0041
-1:1	17	-4820	4920	-.0062	.0041
	2-S	-4700	4840	-.0057	.0038
	4-S	-4130	4140	-.0034?	.0035
	37	-3960	4040	-.0044?	.0035
	41	-4620	4750	-.0064	.0038



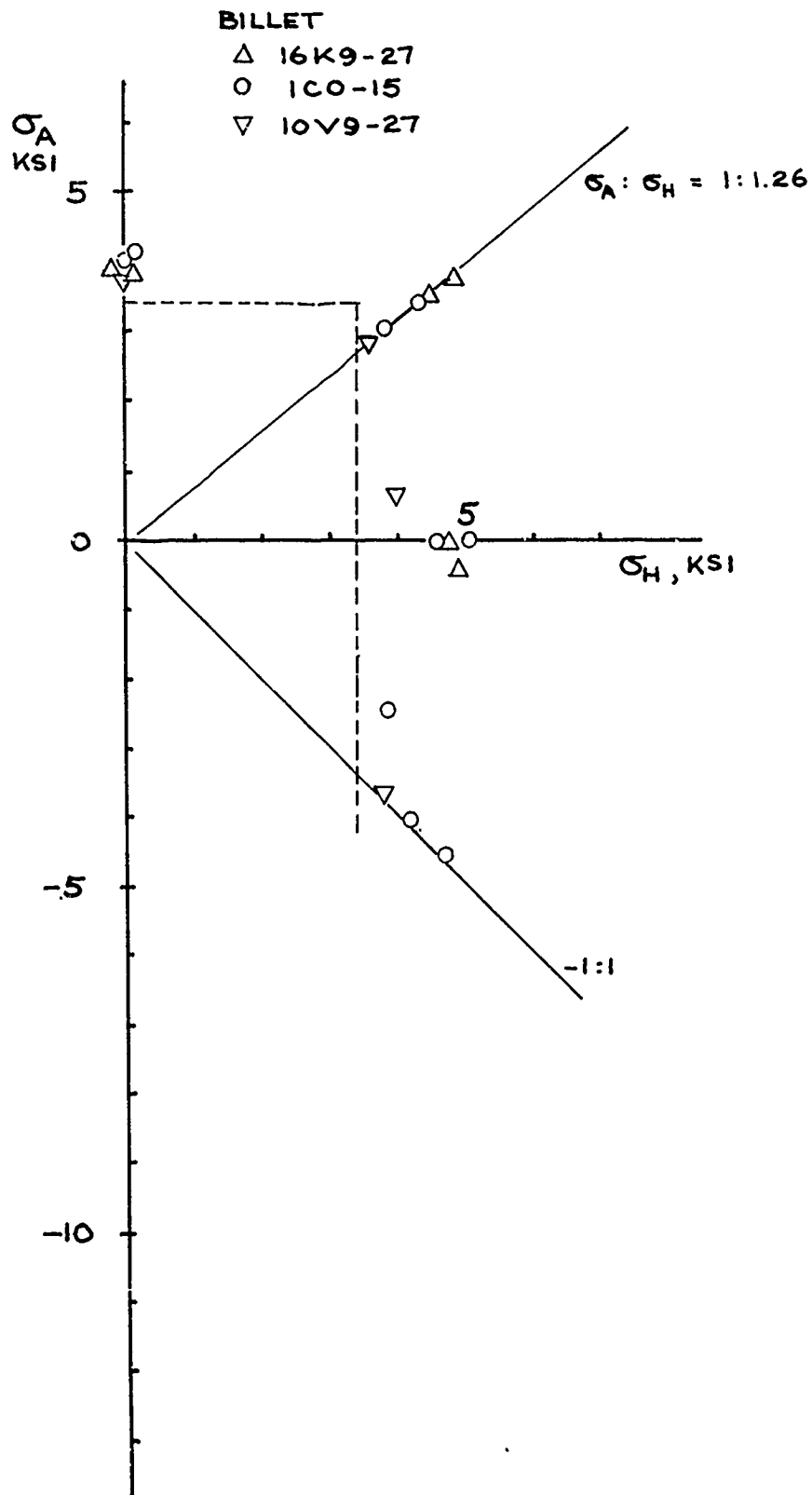


Figure 24. Biaxial Failure Stresses at 70°F (ATJ-S)

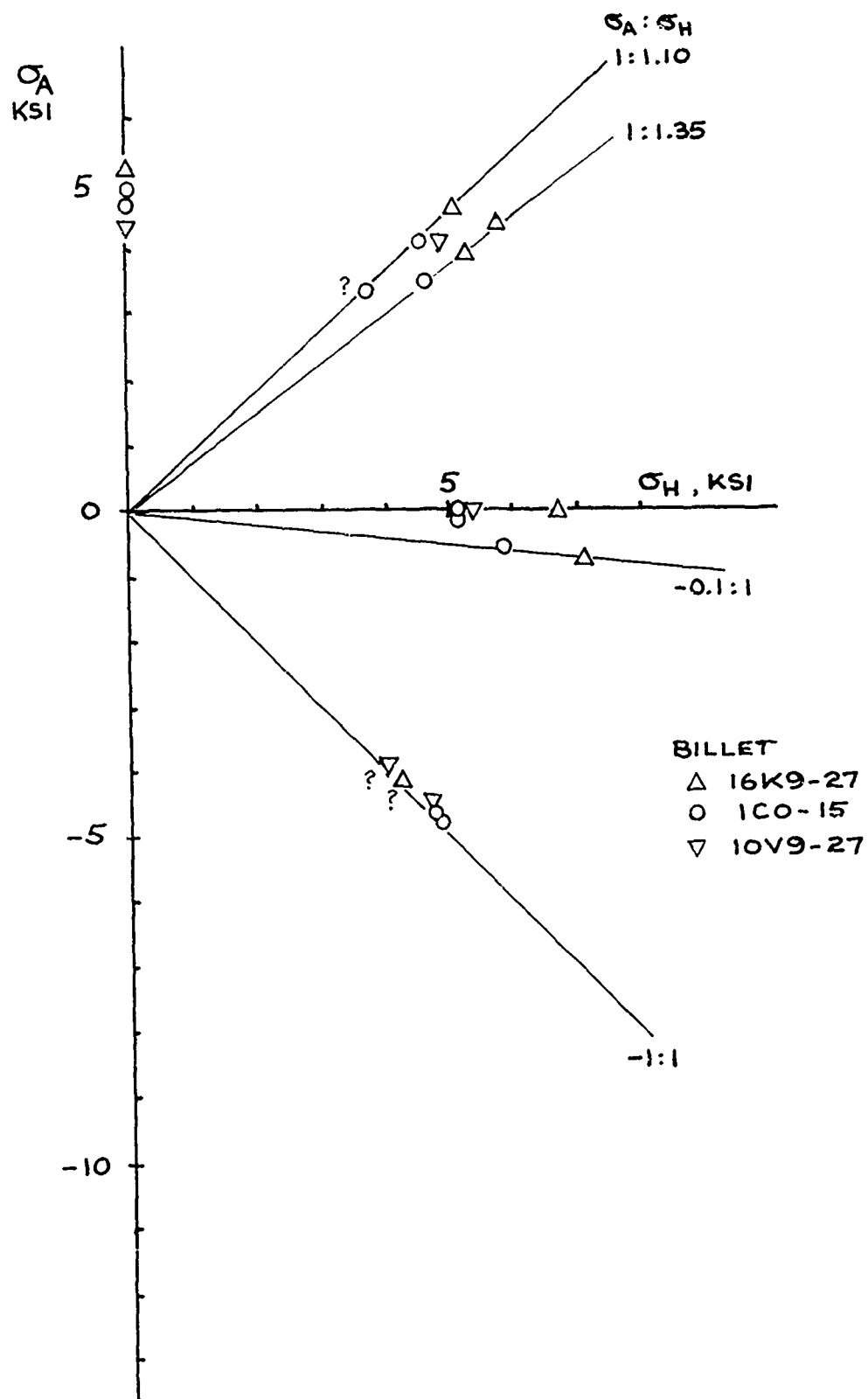
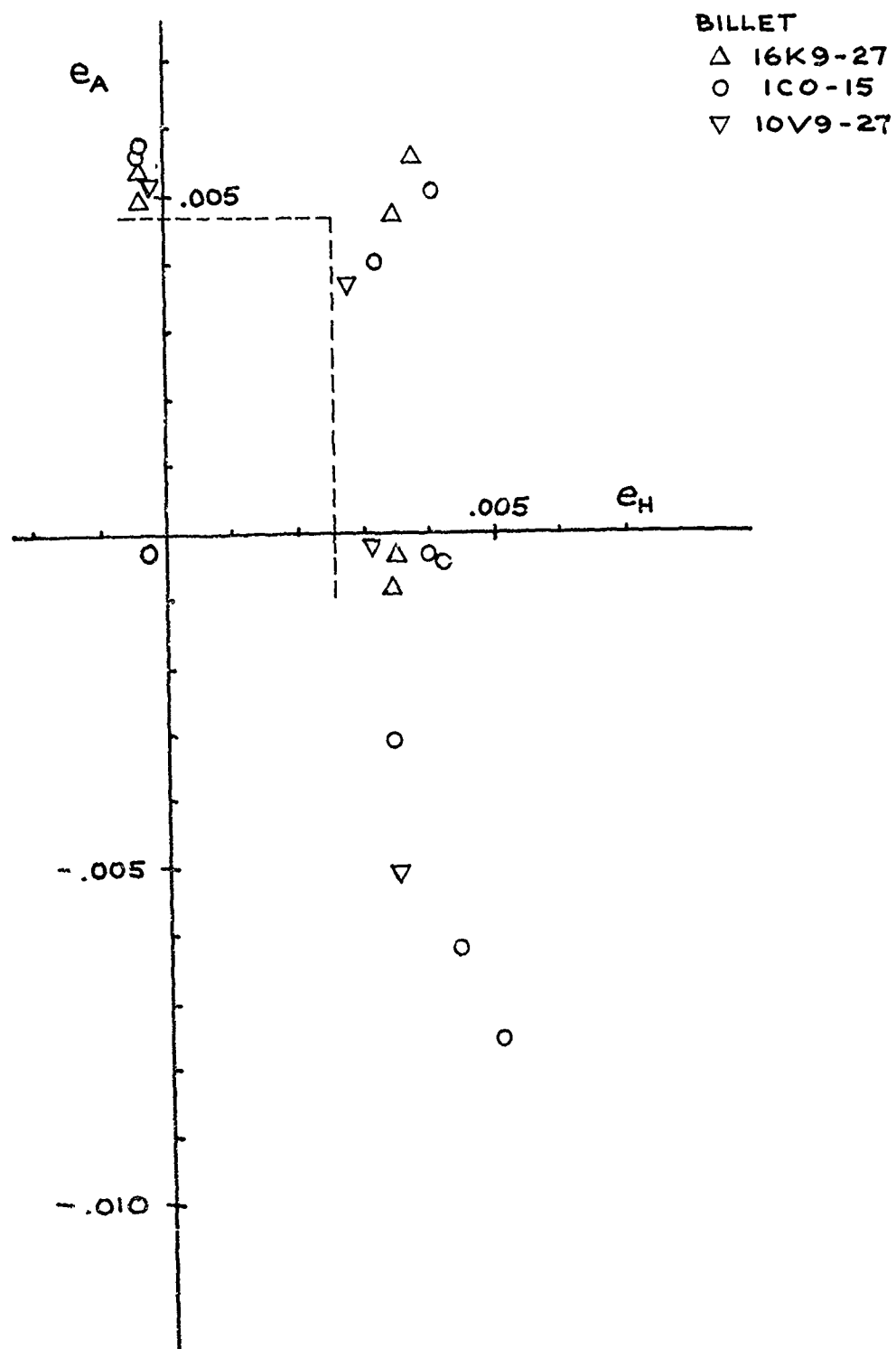
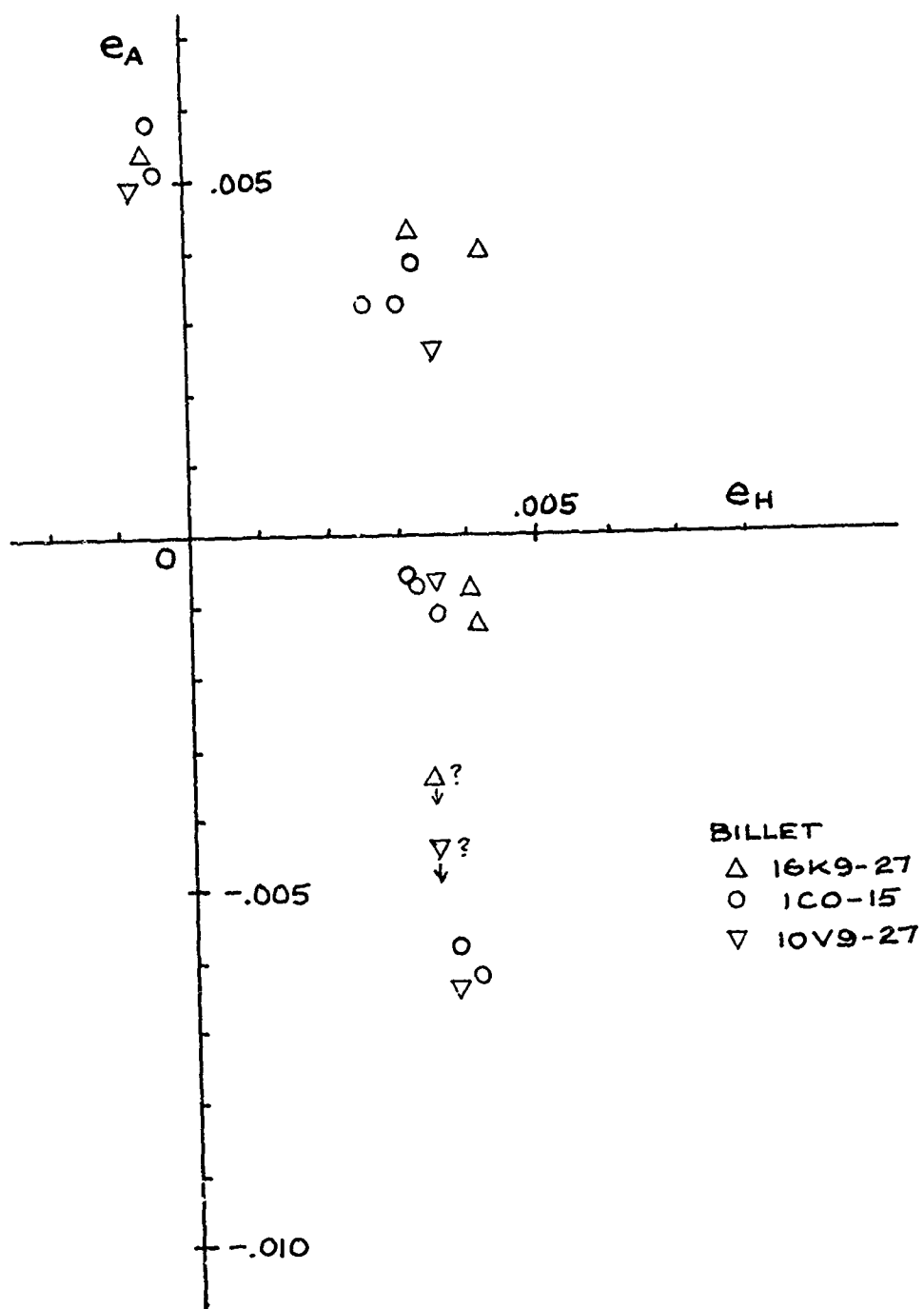


Figure 25. Biaxial Failure Stresses at 2000°F (ATJ-S)





cernibly different in biaxial behavior. Billet 10V9-27 is generally distinctly weaker than the other two at room temperature, but seems to be similar to 1C0-15 at 2000°F; billet 16K9-27 appears to be the strongest at 2000°F and in the 1:1.26 stress state at room temperature, although in compression-tension at 2000°F an anomalously low strength was obtained. At room temperature billet 1C0-15 appears closer in strength to 16K9-27 than to 10V9-27. Because of these differences among billets it is doubtful that simply averaging the strengths obtained in each stress-state, from specimens representing each of only three disparate billets, would have much significance.

The data for each billet show that the average tensile strength in the with-grain (hoop) direction tends to be reduced somewhat by the application of either a tensile or compressive stress in the across-grain direction, both at 70°F and 2000°F. The magnitude of this strength reduction appears to vary from billet to billet. However, more data points would be necessary to substantiate and quantify these tentative conclusions.

For the design analysis of components, the lower-bound envelope of strength is probably of greater interest than the average or median envelope. It seems noteworthy that, at room temperature, none of the data points violate the lower bound of the biaxial strength data reported in Reference 1. This lower bound, shown as the dotted line in Figure 24, appears nearly isotropic and conforms well to a maximum principal stress envelope.

It should be noted that, whereas the stress states are biaxial (except for a small radial compressive stress resulting from the internal pressure), the strain states are distinctly triaxial because the radial strains are not necessarily negligible. In the absence of direct measurement, the radial strains might be analytically estimated if an adequate constitutive

law were available for the material (see Section 4.6). Furthermore, the strains were measured at the external surface of each specimen. It may be shown that the hoop strain gradient across the wall thickness is greater than the corresponding stress gradient; therefore, the maximum hoop strains experienced by the specimen might be significantly (by ten percent or more) different from the measured values presented in Figures 26 and 27.

#### 4.6 Stress-Strain Behavior

The results of Reference 1 showed that the tensile strains measured in biaxial tension were larger than would be estimated from uniaxial tensile stress-strain curves and the constitutive relations that are commonly used (for example Reference 12) in stress analysis of graphite components. This finding is corroborated by the results obtained here. Figure 28 shows the strains measured on biaxial specimens in various stress states at a stress level such that the maximum principal stress is 3500 psi. The data points in biaxial tension lie on the same trend line that was reported in Reference 1. The data show that, instead of the stiffening of strain response which might be expected from Poisson's ratio effects, there exists a biaxial "softening" effect which produces slightly higher strains in biaxial tension than in uniaxial tension. The strains measured at 2000°F (Figure 29) follow a similar trend.

As pointed out in Reference 1, these findings suggest that revision of, presently used constitutive relations is necessary before accurate stress analysis of ATJ-S components can be conducted.

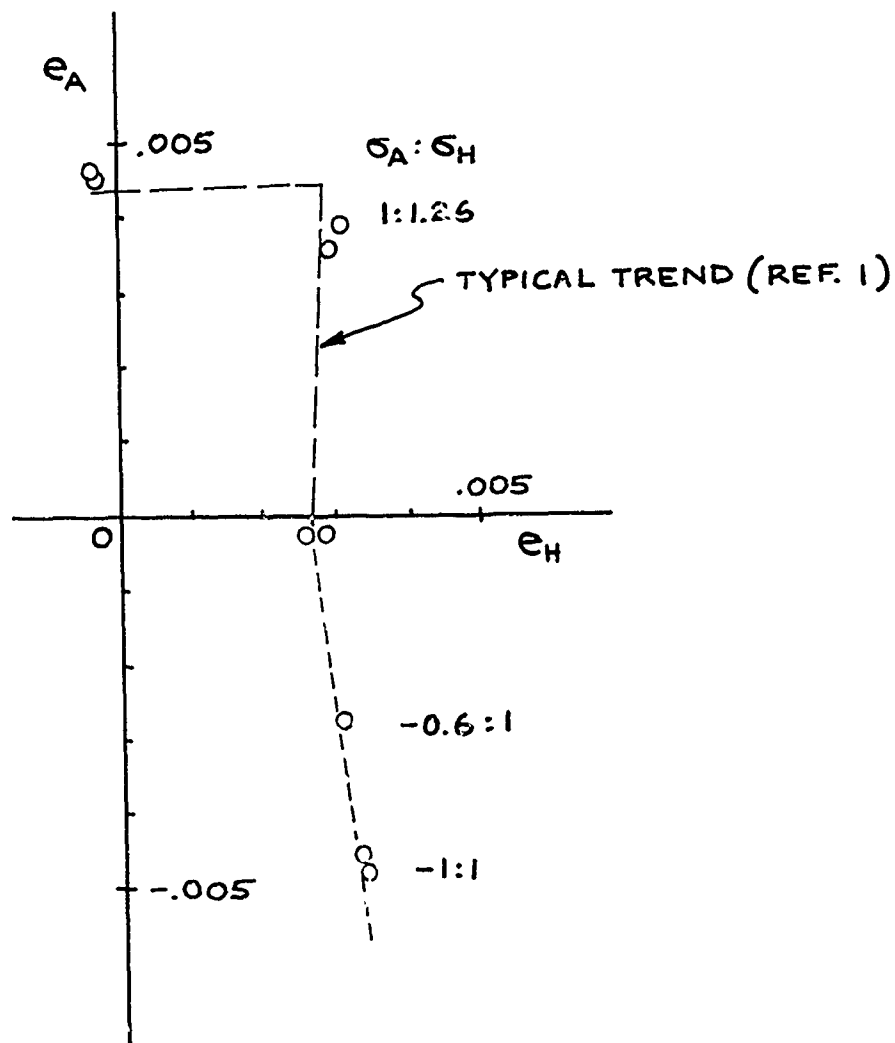


Figure 28. Biaxial Strain Response at 70°F. Measured at Outer Surface of Specimens from ATJ-S Billet 1C0-15 at 3500 psi Maximum Principal Stress

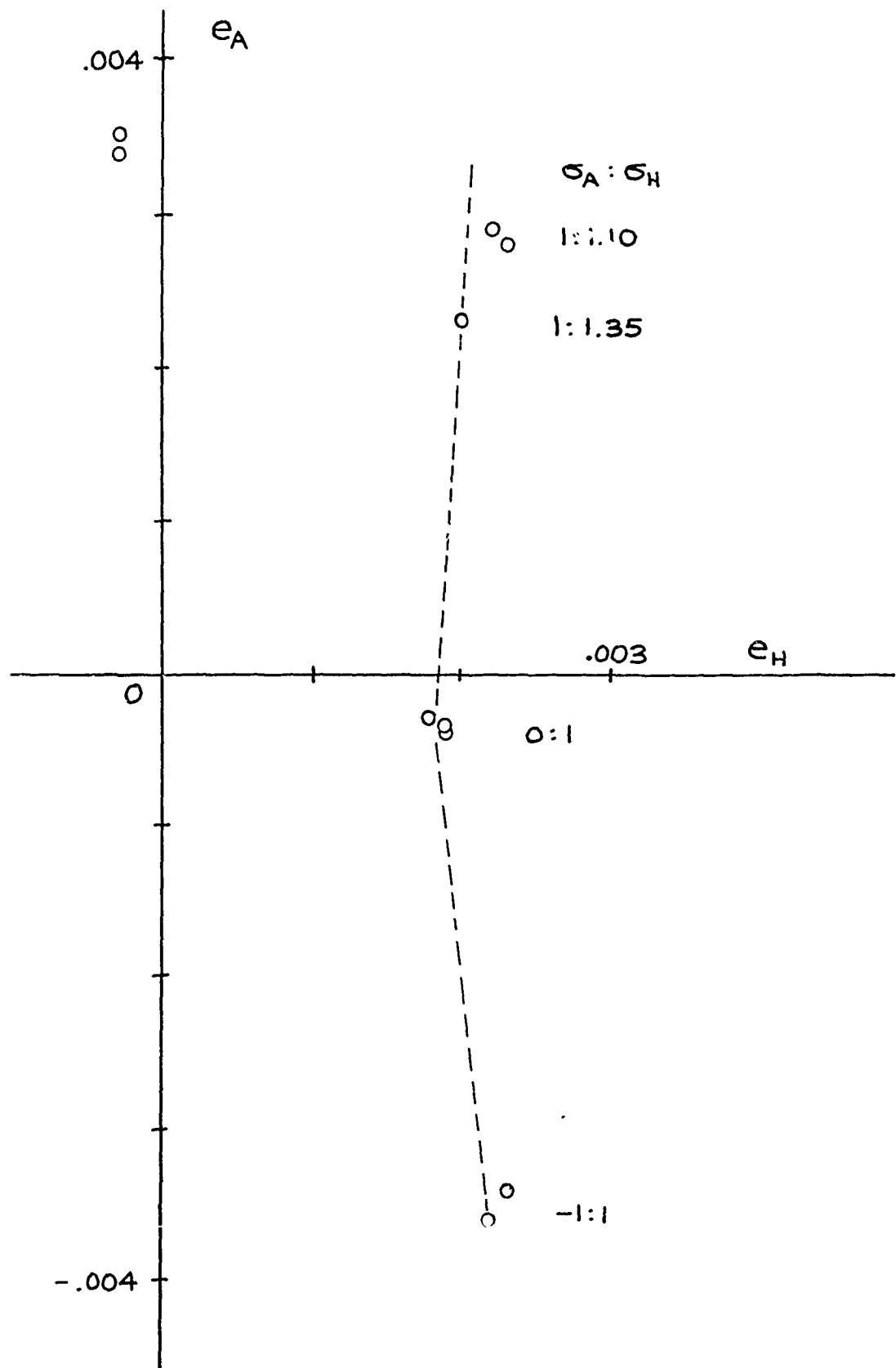


Figure 29. Biaxial Strain Response at 2000°F, Measured at Outer Surface of Specimens from ATJ-S Billet 1C0-15 at 3500 psi Maximum Principal Stress



## Section 5

### OFF-AXIS TESTS

#### 5.1 Material and Anisotropy

The off-axis tests were conducted on material cut from ATJ-S billet 16K9-27. The characteristics of this billet, which was also used for some biaxial specimens, have been summarized in Section 4.1. Figure 30 shows how billet 16K9-27 was cut; the sections used for the off-axis study were:

- P-I used for off-axis tensile specimens (Figure 31)
- P-II, used for on-axis tensile specimens (Figure 32)
- P-III, used for measurements of acoustic velocity as function of direction (Figure 33).
- P-IV, used for on-axis and off-axis compression specimens (Figure 34)

Acoustic velocities were measured along the axis of each tensile specimen blank (6 inch long by 5/8 inch wide by 1/4 inch thick) and each compression specimen blank (5/8 inch diameter by 2 inch long). These measurements and also the bulk density of each blank are presented in Table XI.

Acoustic velocities were also measured across the diameter of each of the three disks excised from P-III (Figure 33); these measurements were taken at 15 degree intervals around the circumference, and are summarized in Figures 35, 36, and 37. It seems that acoustic velocity is a fairly sensitive indicator of orientation. In each disk the maximum and minimum velocities are obtained in directions that are 90 degrees apart. In the 2-3 disk (Figure 35) the difference between velocity extremes is large and the maximum and minima coincide with the 2 and 3 axes; this suggests that the 2 and 3 axes coincide with the b (with-grain) and c (across-grain) directions of the material. In the 1-3 disk, (Figure 36) the difference between maximum and minimum velocities is approximately the same as in the 2-3 disk, but the directions of maximum and minimum velocities are approximately

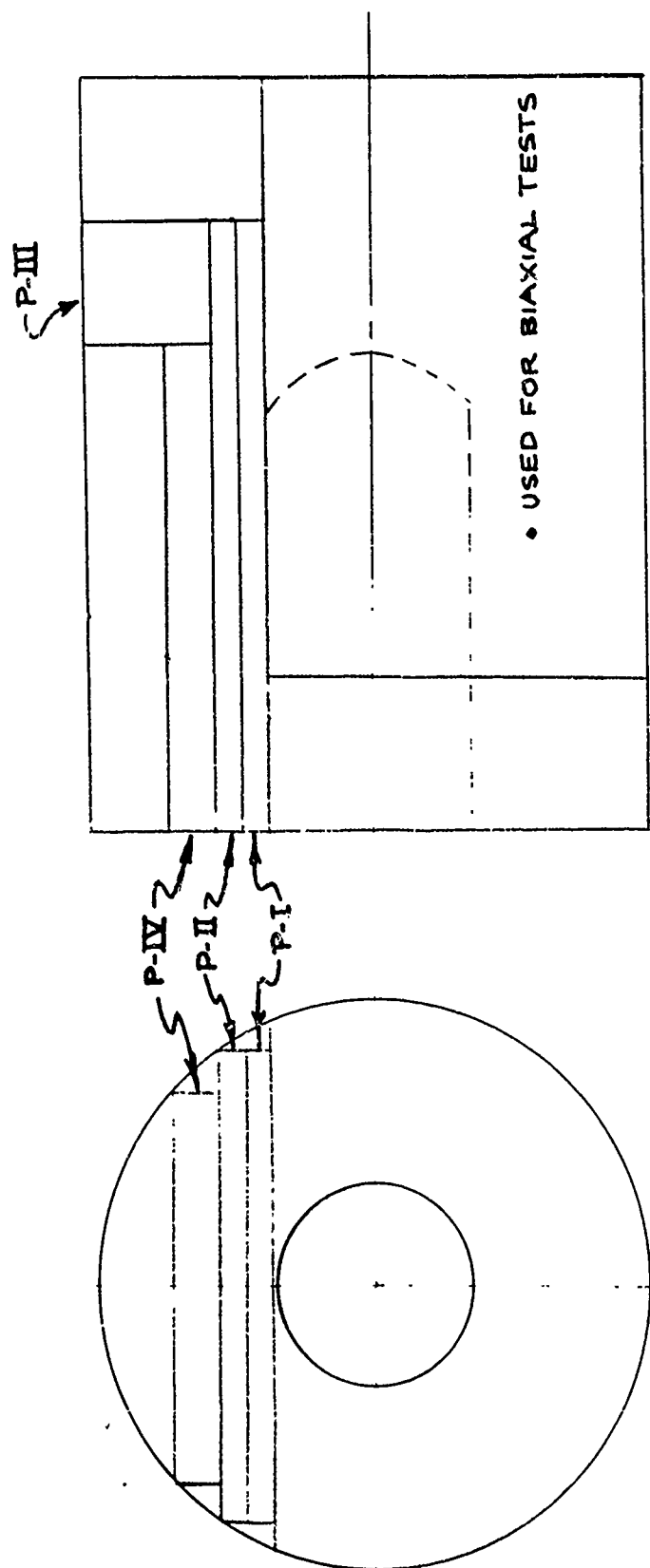


Figure 30. Sectioning Plan, Billet 16K9-27

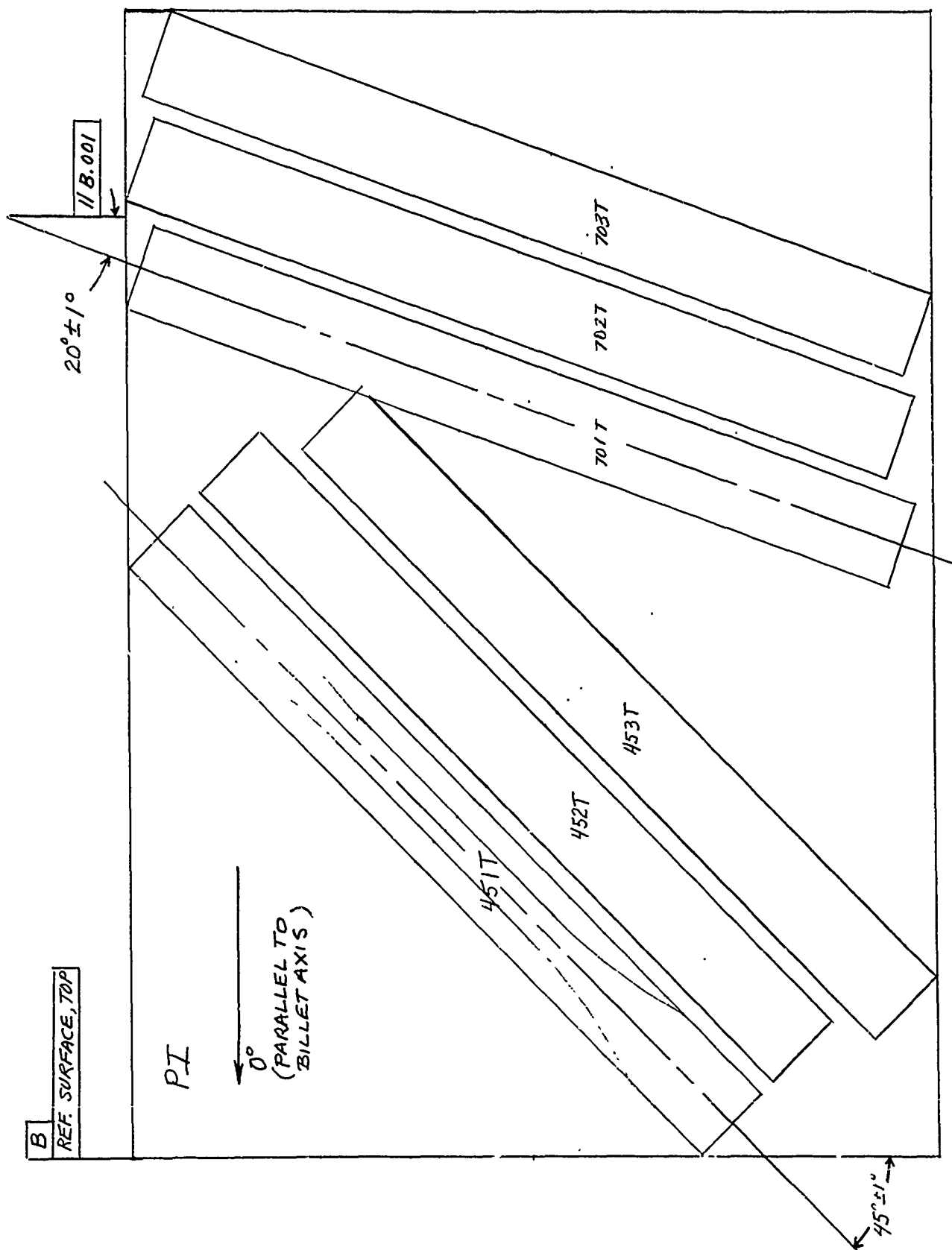


Figure 31. Cutting Plan for 45° and 70° Tensile Specimens

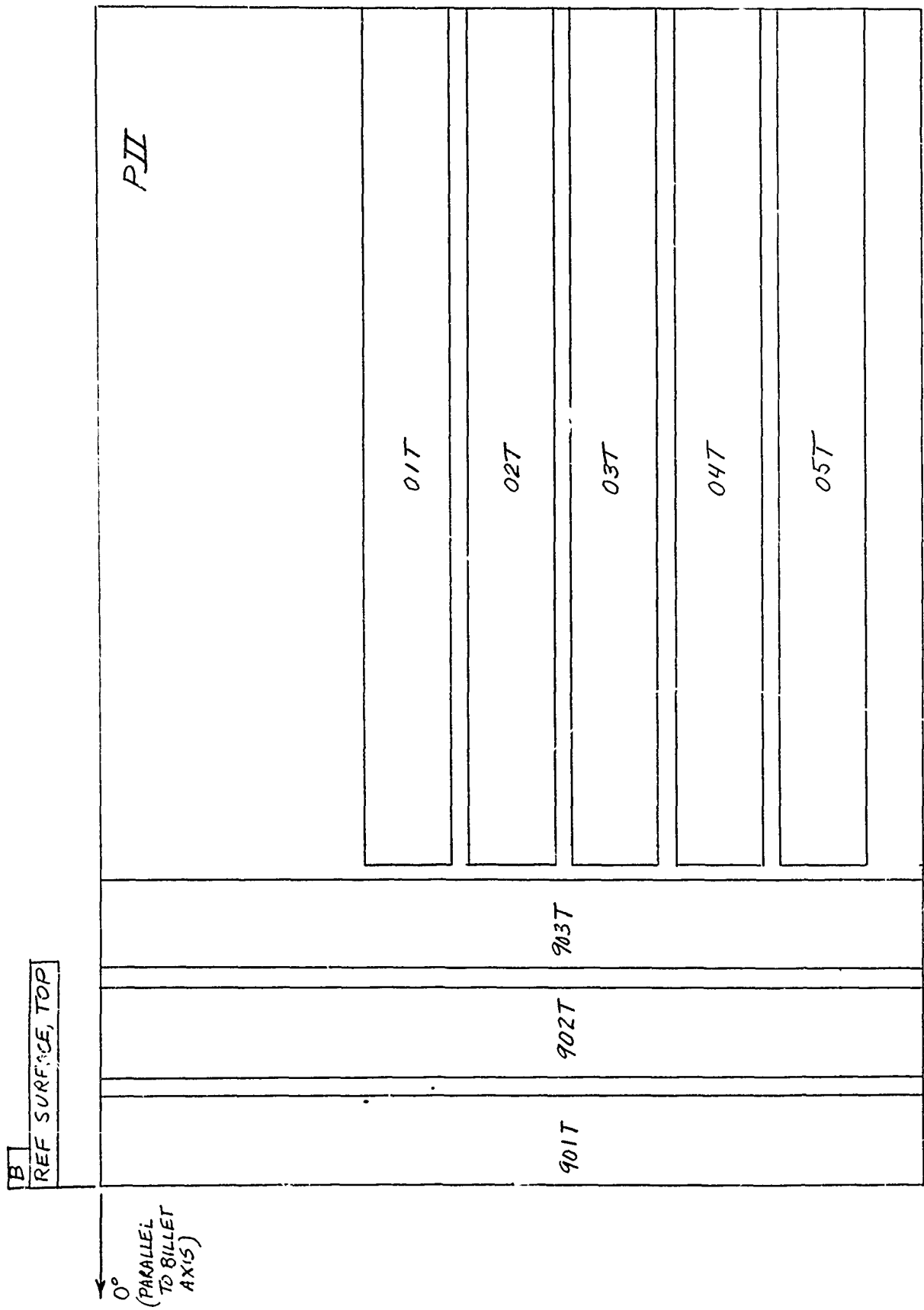
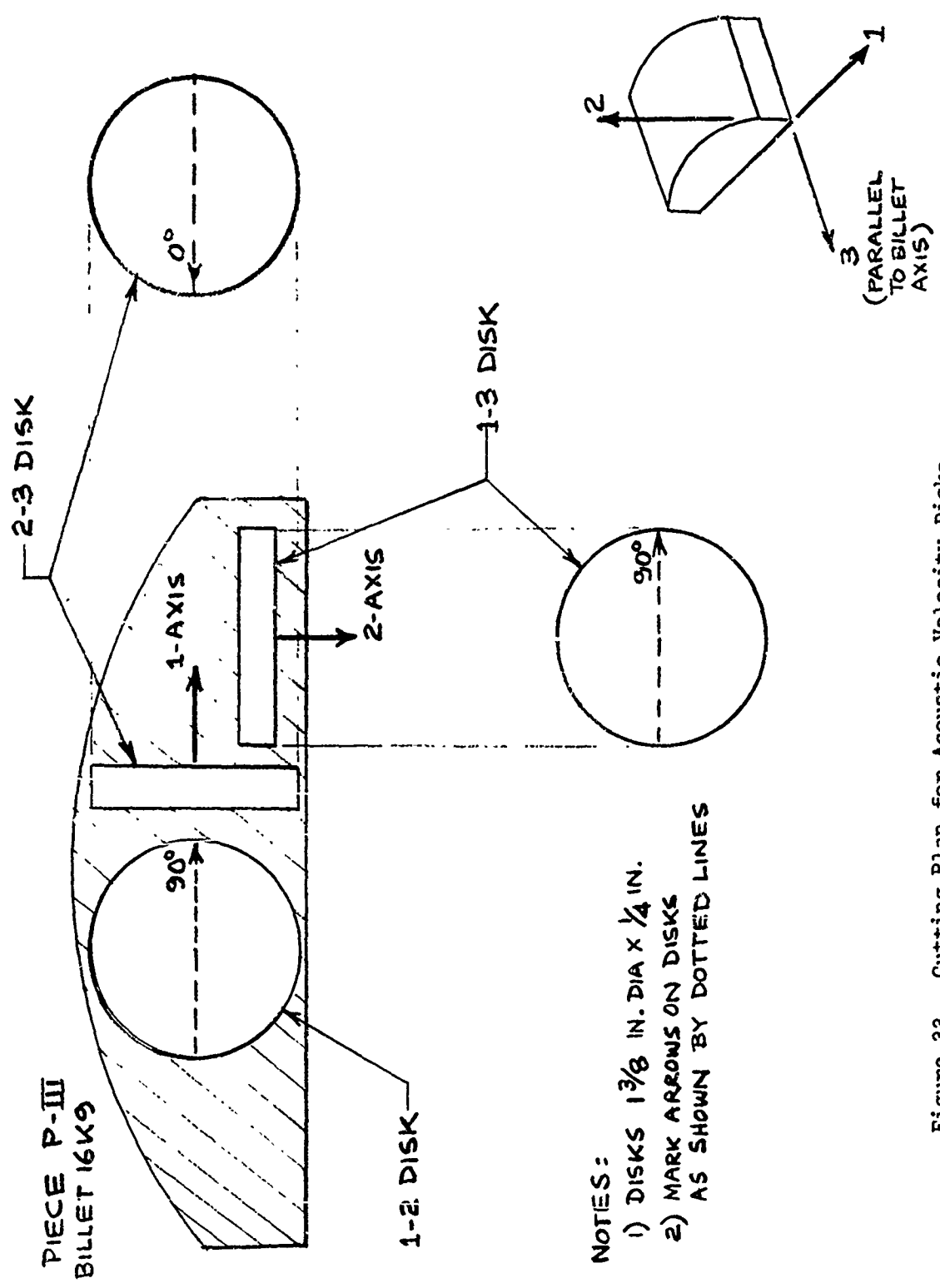


Figure 32. Cutting Plan for 0° and 90° Tensile Specimens



- NOTES:
- 1) DISKS  $1\frac{3}{8}$  IN. DIA X  $\frac{1}{4}$  IN.
  - 2) MARK ARROWS ON DISKS AS SHOWN BY DOTTED LINES

Figure 33. Cutting Plan for Acoustic-Velocity Disks

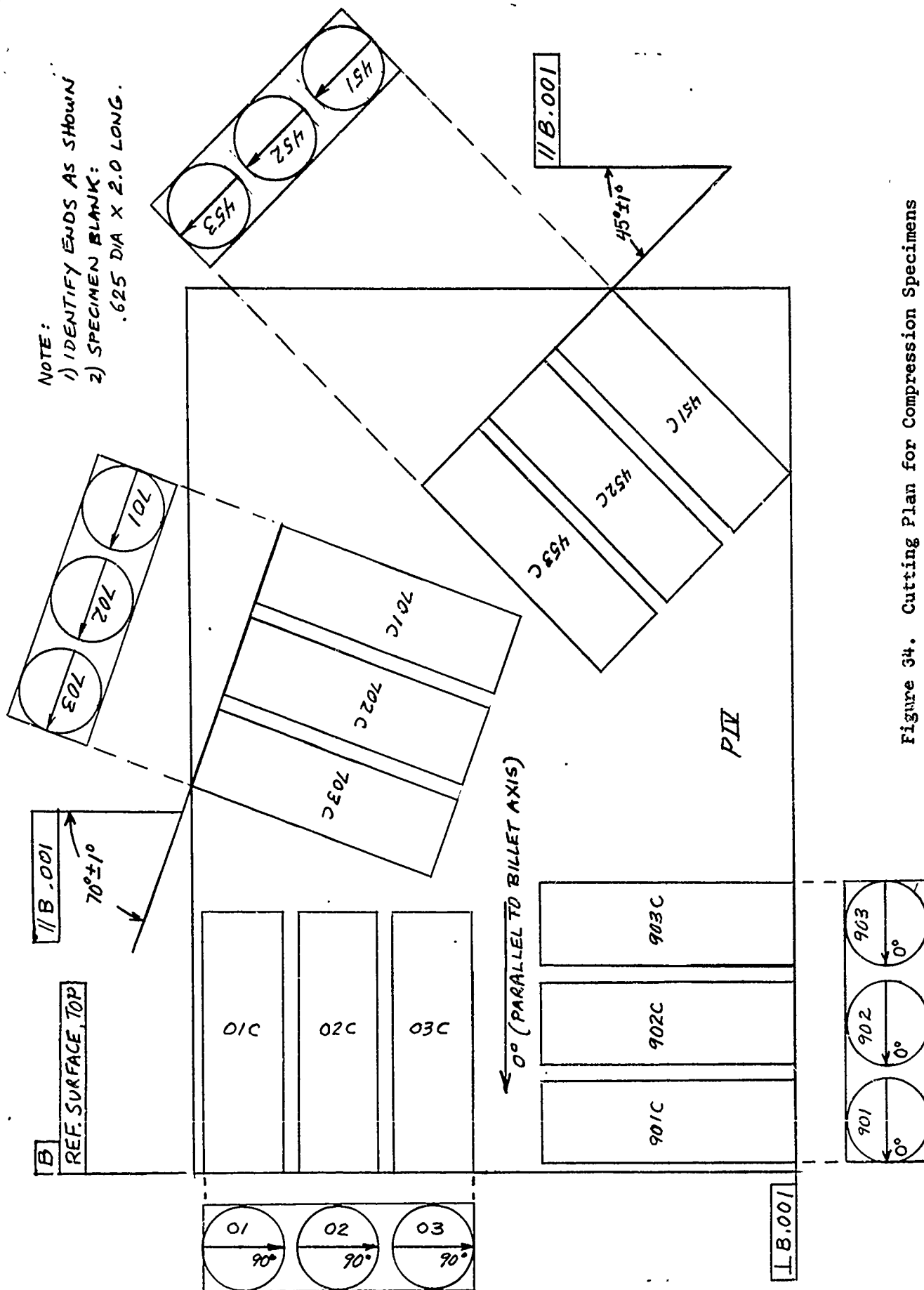


Figure 34. Cutting Plan for Compression Specimens

TABLE XI  
CHARACTERIZATION OF SPECIMEN BLANKS (OFF-AXIS STUDY)

Orientation Angle (1)	Specimen Number (2) (5)	Bulk Density gm/cc (3)	Axial Acoustic Velocity in/microsec (4)
0°	01T	1.850	.0859
	02T	1.849	.0859
	03T	1.848	.0861
	04T	1.851	.0861
	05T	1.857	.0866
	01C	1.854	.0870
	02C	1.854	.0875
	03C	1.855	.0865
45°	451T	1.853	.0925
	452T	1.852	.0943
	453T	1.849	.0936
	451C	1.854	.0942
	452C	1.851	.0958
	453C	1.850	.0957
70°	701T	1.849	.1008
	702T	1.850	.1006
	703T	1.851	.1007
	701C	1.847	.1035
	702C	1.848	.1034
	703C	1.854	.1025
90°	901T	1.856	.1040
	902T	1.854	.1031
	903T	1.855	.1025
	901C	1.854	.1048
	902C	1.854	.1040
	903C	1.853	.1036

- (1) Angle between specimen axis and parent billet axis  
(2) T = tensile specimen; C = compression specimen  
(3) By weight and external dimensions  
(4) Measured at 1.0 MHz.  
(5) All specimens from ATJ-S billet 16K9-27.

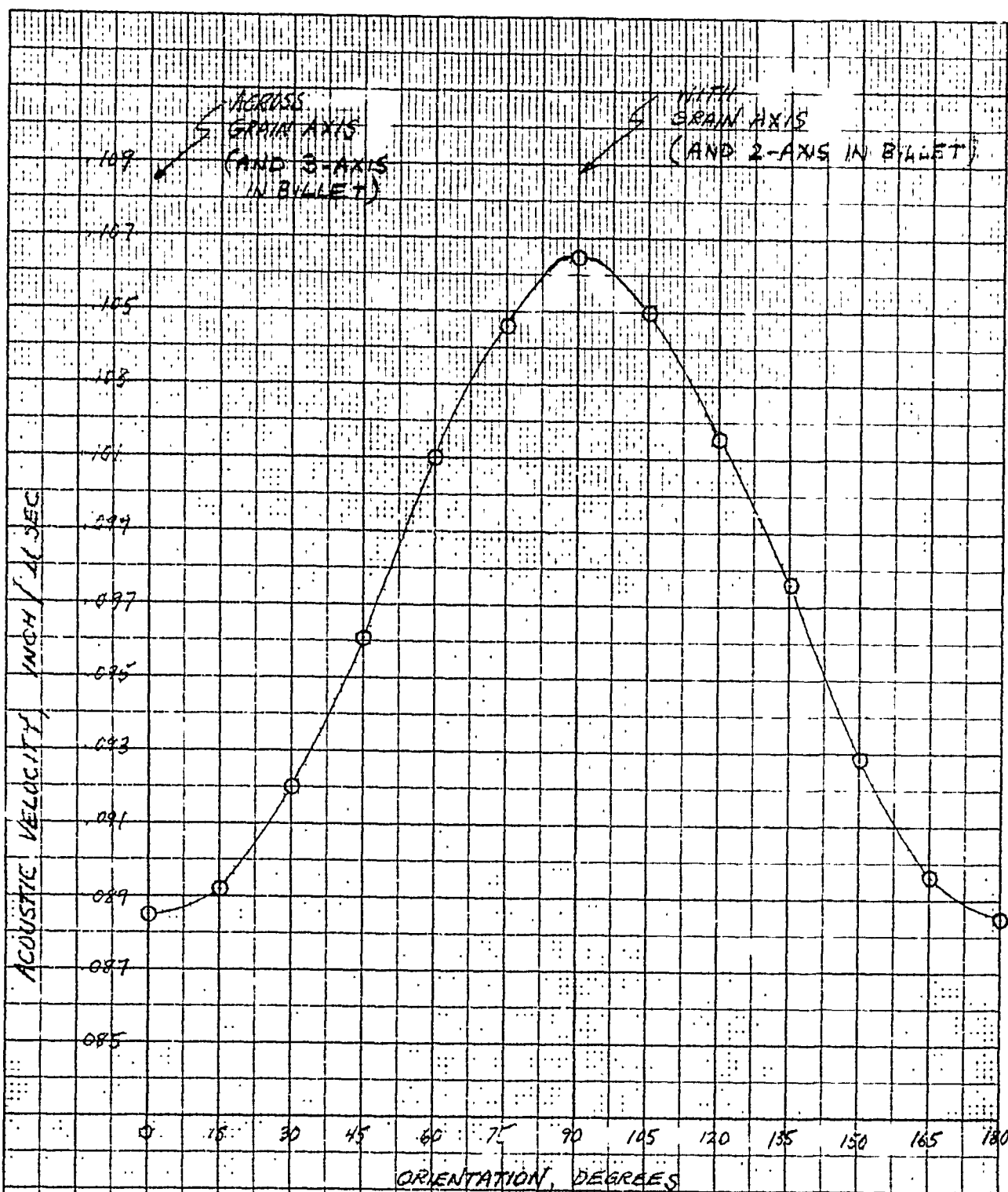


Figure 35. Angular Variation of Acoustic Velocity, Disk 2-5



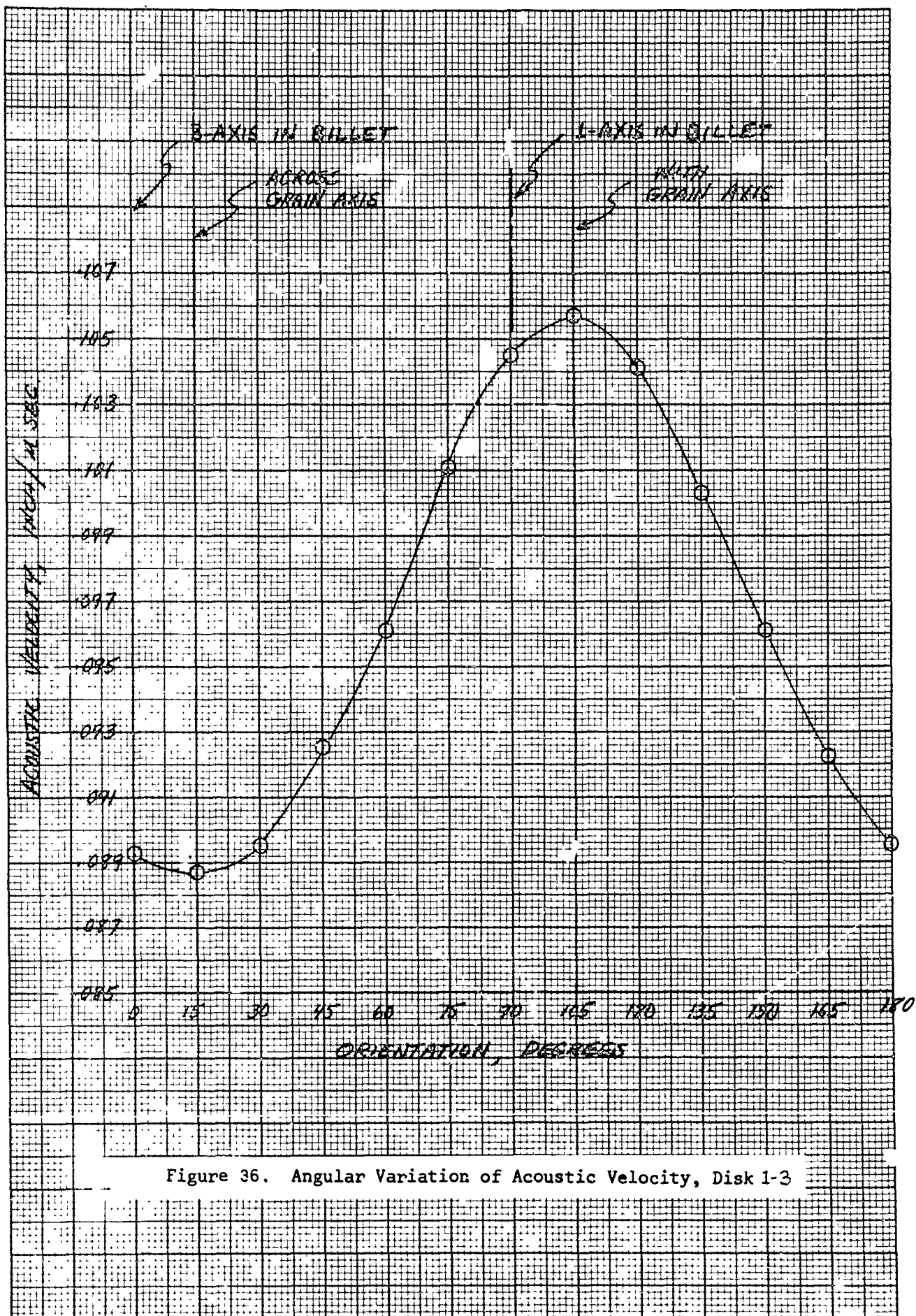


Figure 36. Angular Variation of Acoustic Velocity, Disk 1-3

K-E 10 X 10 TO 1 1/2 INCH  
46 1327  
MADE IN U.S.A.  
KEUFFEL & ESSER CO

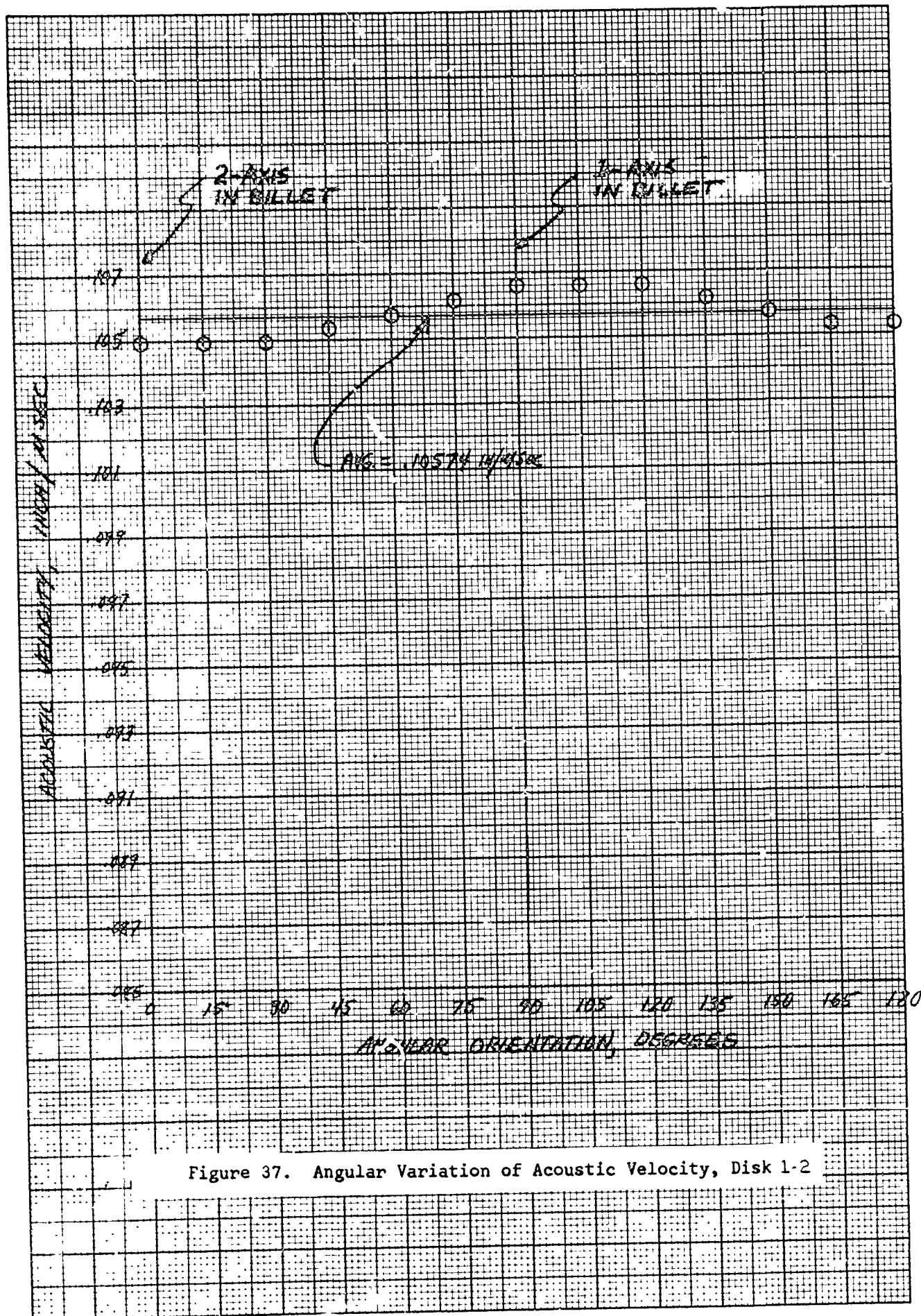


Figure 37. Angular Variation of Acoustic Velocity, Disk 1-2

15° displaced from the 1 and 3 axes; this implies that the true with-grain (a) and across-grain (c) directions in the material do not coincide, in that region of the billet, with the respective nominal directions (perpendicular and parallel to the geometric axis of symmetry of the billet). Similar discrepancies between the nominal geometric axes of a billet and the true principal axes of anisotropy have been measured in ATJ graphite by X-ray techniques (Reference 13). Thus the discrepancy noted in disk 3-1 is not necessarily due to an error in marking the disk orientation. In the 1-2 disk (Figure 37) the difference between maximum and minimum velocities is small leading to the conclusion that the 1-2 plane approximates (within about 15°) the a-b plane of the material.

It seems apparent that excising a mechanical test specimen at a known angle with respect to the geometric axis of the billet does not ensure that the specimen axis has the same angle with respect to the true local across-grain direction in the material. To explore this point, the acoustic velocities measured on the test specimens have been plotted in Figure 38 as a function of nominal geometric angle; also shown in Figure 38 is the expected trend of velocity vs angle of anisotropy (based on the data from disks 2-3 and 1-3). It is seen that the trend of velocities measured on the tensile specimens is approximately parallel to the expected trend except that the velocities in the tensile specimens are generally lower; this apparent low velocity in the tensile specimens may be due to a systematic error in the velocity measurements resulting from the difference in geometry between the tensile specimen and the disks used to generate the expected trend. Because of the agreement between data points and the parallel trend line, it is believed that the geometric angles of the tensile specimens are close to the anisotropy angles, except for the nominal 45° specimens which may actually be closer to 40°. The velocities measured on the compressive specimens also seem to be systematically lower than those measured on the disks; the specimens cut nominally at 70° appear to

LONGITUDINAL  
WAVE VELOCITY  
IN./ $\mu$ -SEC

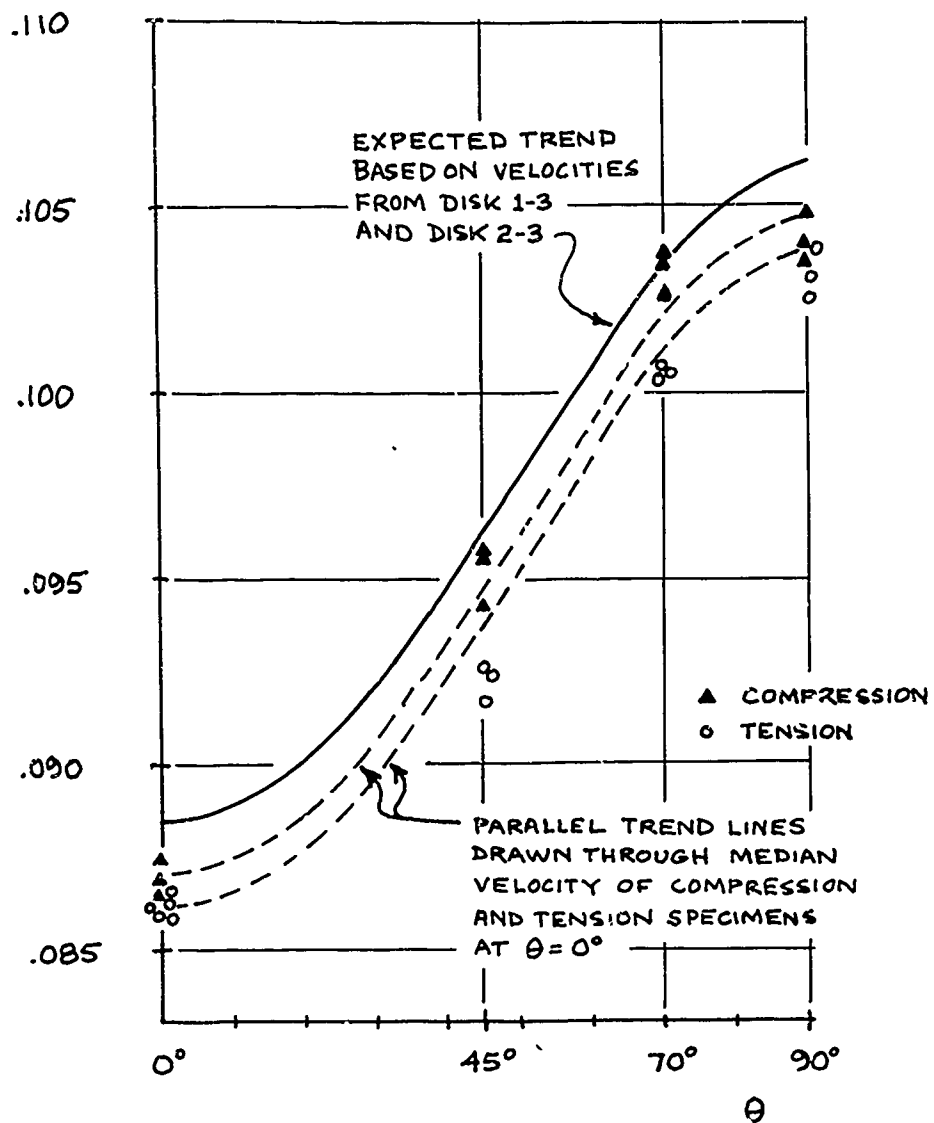


Figure 38. Angular Variation of Acoustic Velocity, Tensile and Compressive specimens.

have, based on the trend line drawn parallel to the expected trend, velocities corresponding to an anisotropic angle close to  $80^\circ$ . These remarks relating the nominal geometrical angles of the specimens to the anisotropy angles are necessarily speculative; they are intended to point out some of the uncertainties in determining the true angle between load axis and true across-grain direction.

## 5.2 Analysis of Shear Coupling Effects\*

When a specimen of ATJ-S with uniform cross-section is loaded uniaxially along the c-axis or along any direction in the a-b plane, the specimen deforms in the manner schematically indicated in Figure 39(a); there are uniform lateral and longitudinal deformations, and the shear strain  $e_{xy}$ , is zero. However, under off-axis loading at some angle  $\theta$  to the c-axis, an unrestrained specimen would tend to deform as shown in Figure 39(b); in addition to the uniform lateral and longitudinal deformations there is a shear strain component  $e_{xy}$ . The shear strain results from the existence of terms in the off-axis matrix of elastic constants which couple shear strains to normal stresses. This phenomenon is referred to as shear coupling. In a real specimen it is virtually impossible to design the load introduction system (grips in tension, loading platens in compression) so that it exerts no restraint against the shear deformation. Under full restraint (rigid grips or platens which allow no rotation or lateral deformation) specimen deformations would be as shown in Figures 39(c) and 39(d). In the case of on-axis loading, a complex state of stress exists near the restrained ends, but at some distance from the ends a state of simple tension exists. In the case of off-axis loading, the moments and shear forces applied by the grips produce complex stress states throughout the specimen.

Full restraint at the specimen ends is probably never achieved in any real test, and the actual degree of restraint may be difficult to analyze. To estimate the potential effects of shear coupling on off-axis strength

---

\*The analyses described in this section were performed by B. R. Lyons

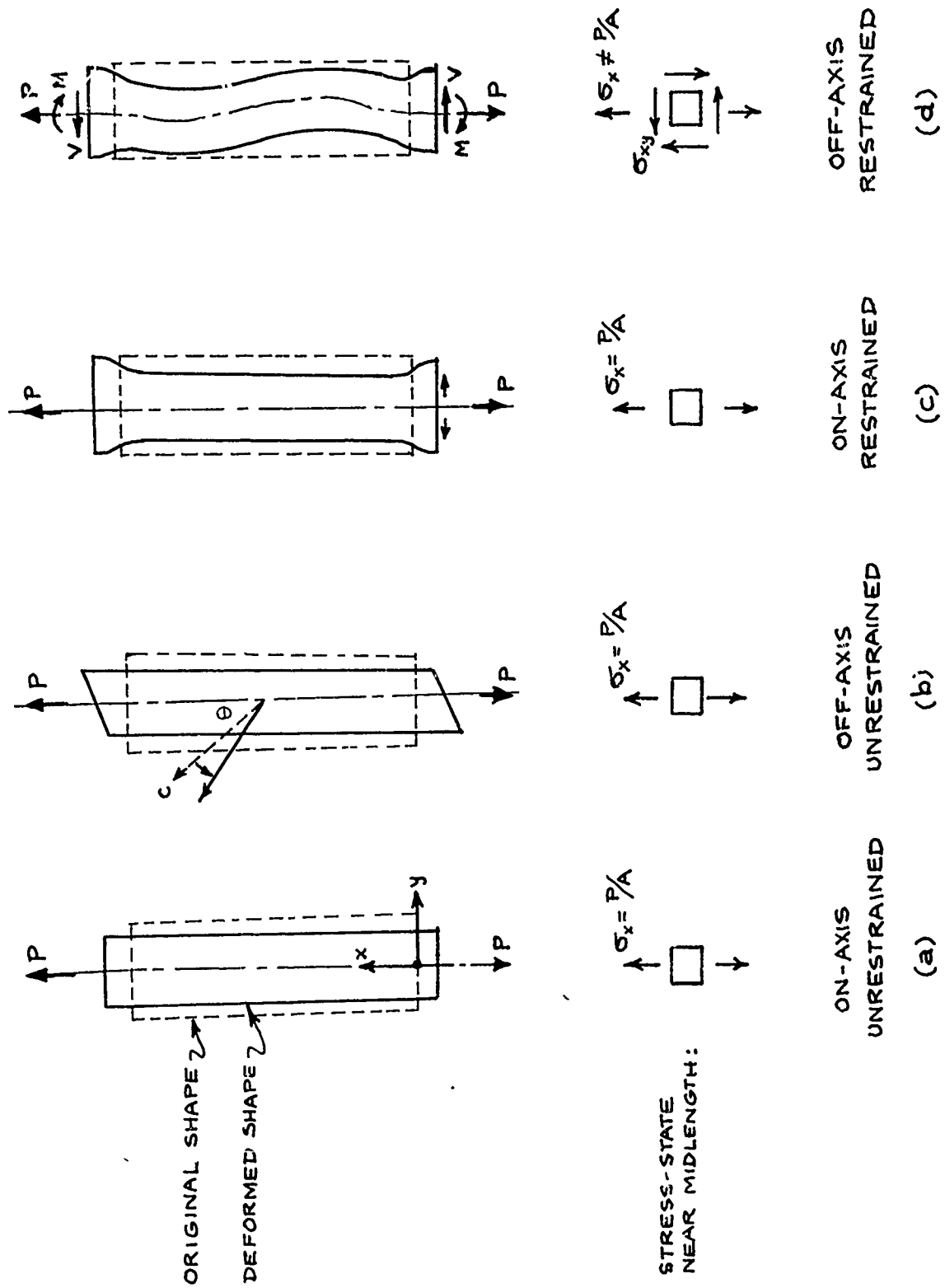


Figure 39. Deformation of Anisotropic Tensile Specimens

data, some simplified analyses of stress distributions in off-axis specimens were performed, as described below.

5.2.1 Simplified Analysis - A closed-form analysis of off-axis shear coupling effects is available in Reference 15. The analysis assumes a flat rectangular-section specimen in a state of plane stress ( $\sigma_{zz} = \sigma_{xz} = \sigma_{yz} = 0$ ), with a partial restraint at the specimen ends:

$$\frac{\partial u}{\partial y} = v = 0; \text{ at } y = 0, x = 0, l$$

where  $u$  = displacement in x-direction  
 $v$  = displacement in y direction

This restraint may be thought of as a "clamping" of the specimen centerline at each end.

The analytical solution of Reference 15 was applied to the case of ATJ-S graphite using the approximate secant elastic constants listed in Table XII. Figure 40 shows some results for specimens with length-to-width aspect ratios of 2 and 6 at an orientation angle of 45°.

For an aspect ratio of 2 the axial stress at specimen mid-length shows a maximum variation of 2% compared to the mean stress. For an aspect ratio of 6 the effect of and restraint on the stresses at the mid-length of the specimen is about 0.4%. The effect of the end restraint is to increase the axial stresses at the ends of the specimen by approximately 12% and 22% for aspect ratios of 6 and 2, respectively. These results indicate that the effect of partial end restraint on the axial stresses at the mid-length of a uniform-section specimen is small. However, the resulting stress concentrations at the ends of the specimen suggest the use of a tapered specimen to prevent failure at the ends.

5.2.2 Tapered Specimen Analysis - A tapered specimen design does not lend itself to an analysis using a closed form solution. Therefore, the

TABLE XII  
ELASTIC MODULI ASSUMED IN SHEAR-COUPLING ANALYSIS

Young's Moduli:

$$E_a = E_b = 1.35 \times 10^6 \text{ psi}$$

$$E_c = 0.70 \times 10^6 \text{ psi}$$

Poisson's Ratio:

$$\nu_{ac} = 0.10$$

Shear Modulus:

$$G_{ac} = 0.475 \times 10^6 \text{ psi}$$

Note: Values above are estimated secant moduli at tensile fracture stress.



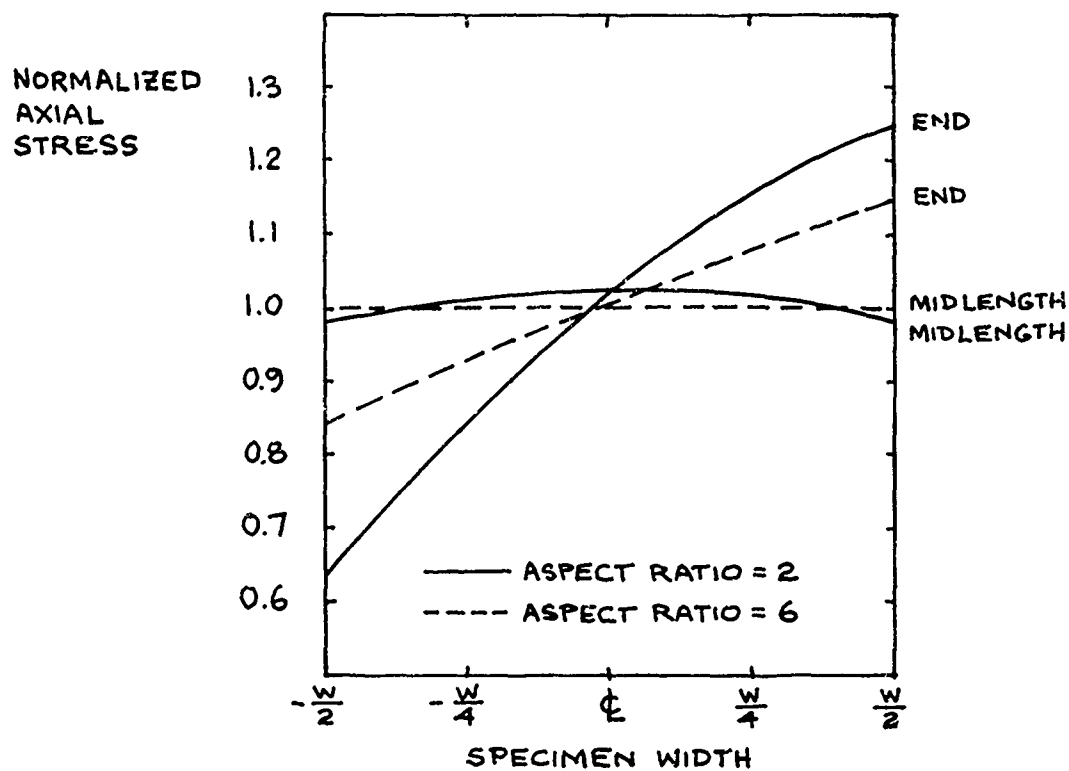


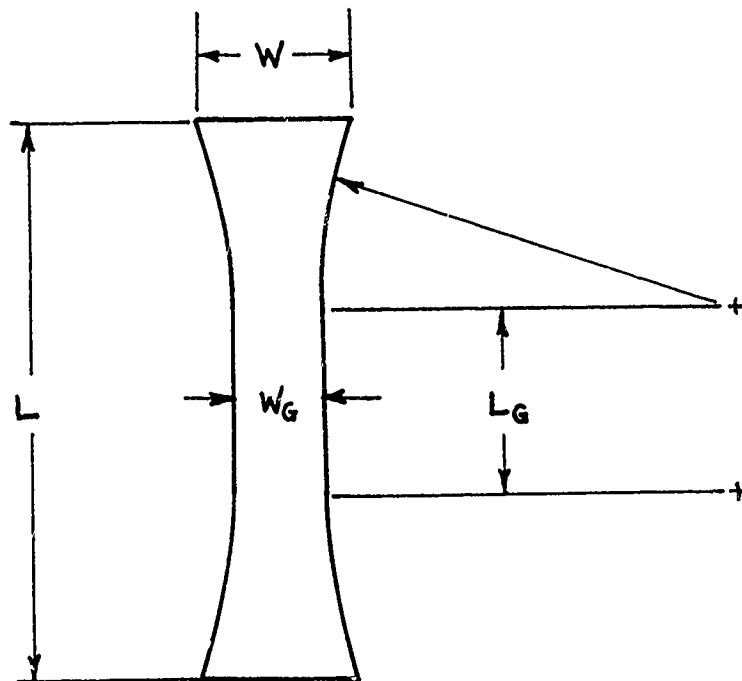
Figure 40. Axial Stresses at Mid-Length and Ends of Partially-Restrained Uniform-Section Off-Axis Specimens

finite element program described in Reference 16 was employed. The finite element model, like the closed form solution, assumes a flat, plane stress, specimen; however, the end conditions are rigid non-rotating grips. The specimens analyzed are shown in Figure 41. Figures 42 and 43 show the stress distribution across the specimens at the mid-length, end, and plane of peak stresses, for a 45° orientation angle. Figures 44 and 45 show the stress distributions along the length of the specimens at the center and near the edge of the tensile and compression specimens respectively.

For the longer specimen, the effect of orientation angle on peak stress concentration is summarized below:

$\theta$ degrees	Ratio of maximum stress to nominal stress
15°	1.02
45°	1.04
70°	1.025
75°	1.02

Although tapering the specimens does not eliminate the higher stresses due to shear coupling, the stress concentrations are significantly reduced. In the case of the short specimen, which corresponds roughly to a typical compression specimen design, the peak stress is about 9% higher than the nominal stress. In the case of the long specimen the peak stress is about 4% higher than the nominal stress. The distribution of axial stress at the midlength of both types of specimens is almost uniform. These calculations were based on full restraint at the specimen ends. Actual restraint is likely to be less severe and, presumably, the actual stress concentrations would be smaller. It should be noted that the analysis was linear, based on estimated secant moduli, and that it applies strictly only to thin flat specimens.



	$\frac{L_G}{W_G}$	$\frac{L}{W_G}$	$\frac{W}{W_G}$
TENSION	8	16	1.5
COMPRESSION	1	4	1.5

Figure 41. Specimen Configurations for Finite-Element Shear-Coupling Analysis

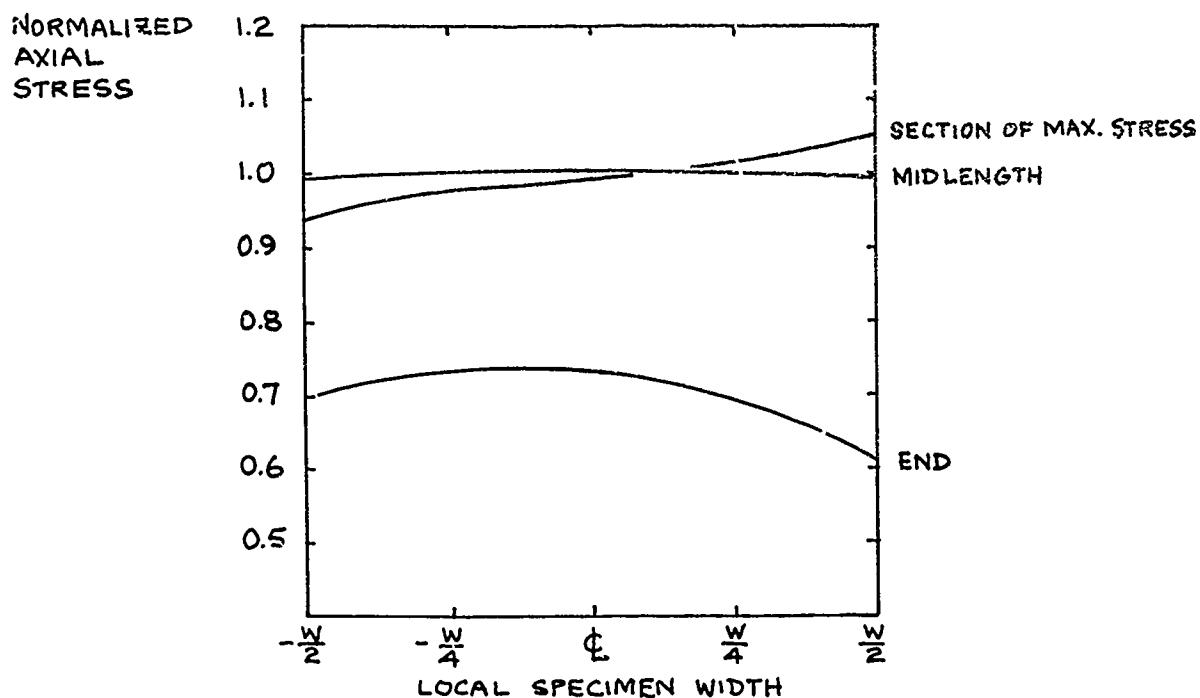


Figure 42. Variation of Axial Stress Across Width of 45° Tensile Specimen

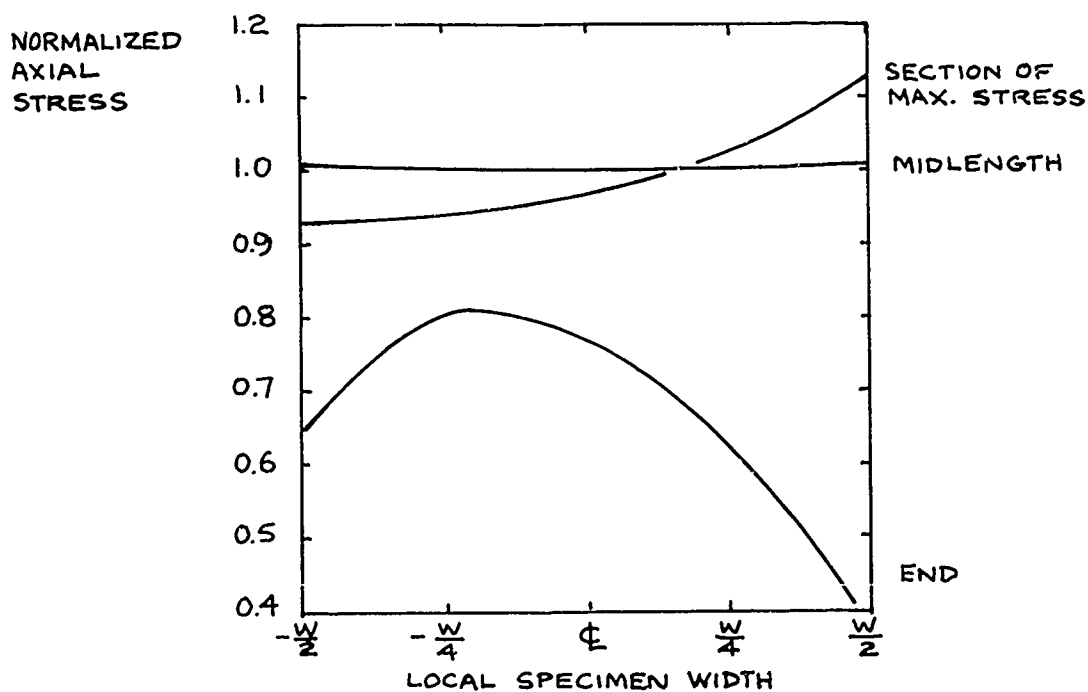


Figure 43. Variation of Axial Stress Across Width of 45° Compression Specimen

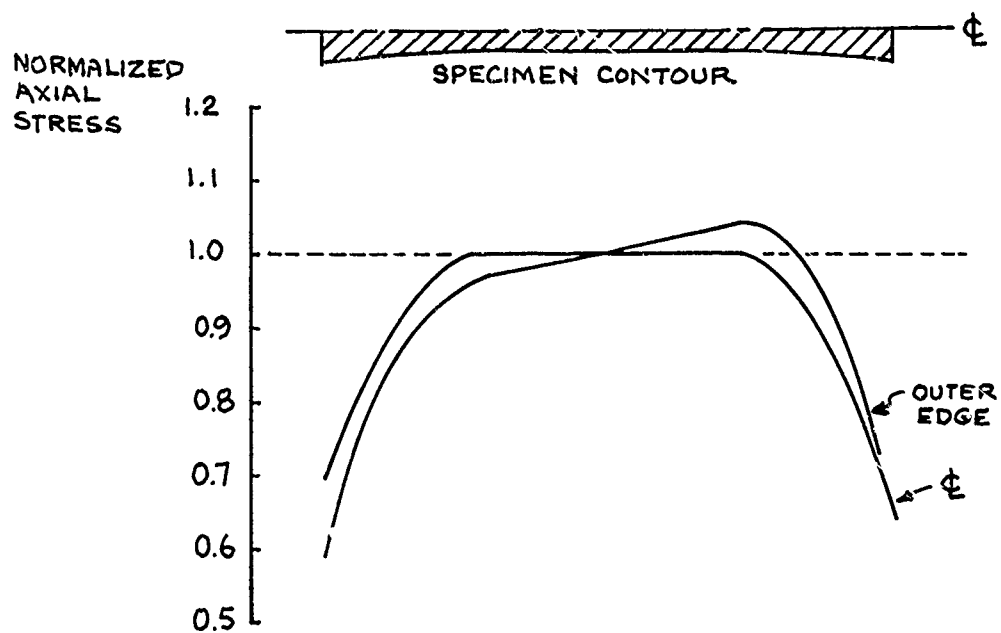


Figure 44. Variation of Axial Stress Along Length of 45° Tensile Specimen

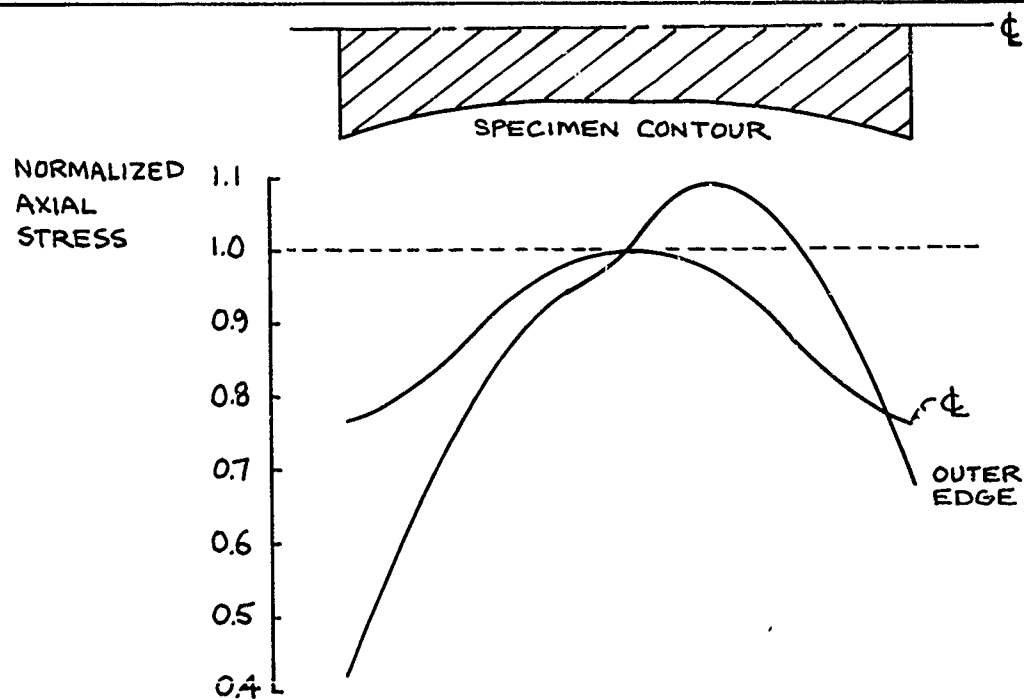


Figure 45. Variation of Axial Stress Along Length of 45° Compression Specimen

### 5.3 Compressive Test Method

The specimen configuration used for compression testing, a circular-section dogbone design, is shown in Figure 46. The ratio of length to diameter is necessarily small to avoid buckling. The specimens were marked during machining to retain knowledge of their orientation within the billet.

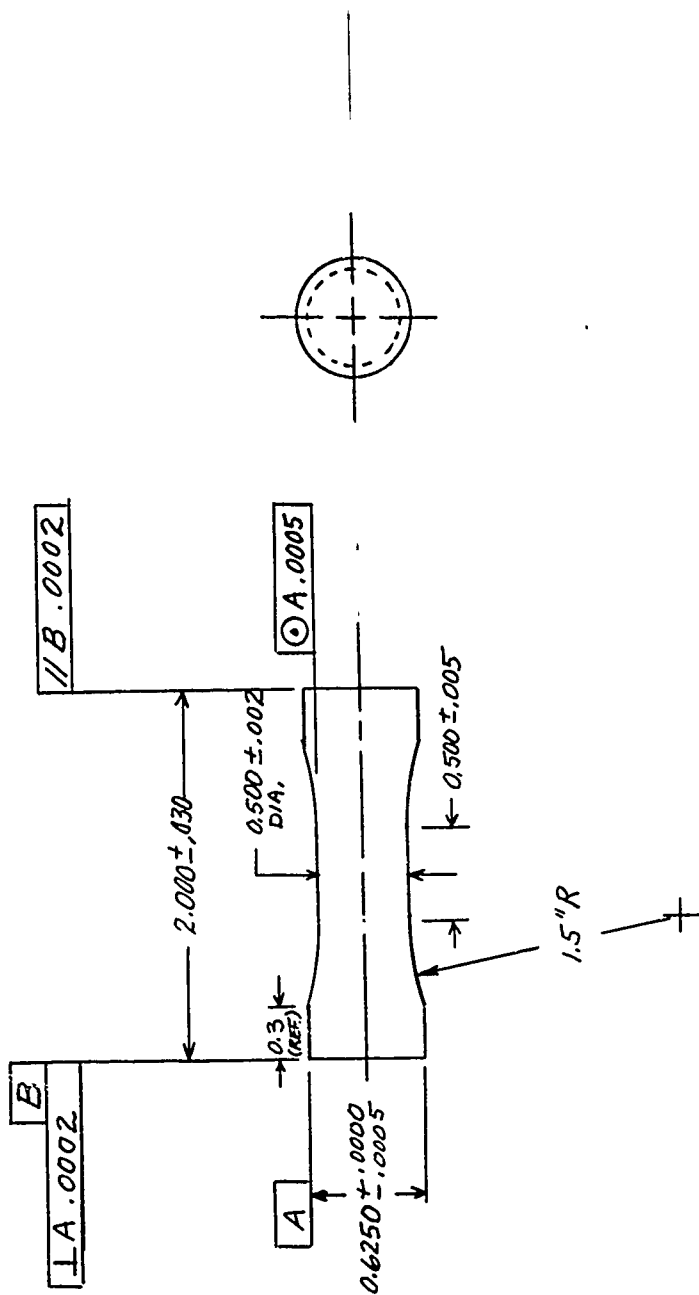
The specimens were tested in the fixture shown in Figure 47. The rigid yoke, guide bushings, and load rods, are the same as used in biaxial testing at room temperature. Loads were applied with an Instron test machine at a cross-head speed of 0.05 inches per minute.

Strains were measured using bonded strain gages mounted at the mid-section of the specimen as indicated in Table XIII. Two axially oriented gages were used in all cases to allow estimates of average axial strain relatively free of the influence of bending. Additional gages were provided in some instances to give transverse strain information.

### 5.4 Tensile Test Method

The tensile specimen used for the off-axis program has a 1/4-inch square cross-section and is tapered in the a-c plane of the material (Figure 48). The length of the gage section (2 inches) is 8 times the width and the total length of the graphite piece is 6 inches. The design was intended to provide sufficient length to minimize the shear-coupling effects discussed in Section 5.2. To further reduce the shear-coupling effects, the load was introduced through pin-loaded aluminum doublers bonded to the graphite using a relatively "soft" adhesive, 3M Company EC2216. The bonding and curing (4 hours at 180°F) of the adhesive was done in a specially-built jig (Figure 49) which ensures that the pin-centers are aligned with the centerline of the gage section.

Rectangular-section specimens, rather than the standard circular-section specimens, were selected because of greater ease in applying strain gages



NOTES:

1. ALL SURFACES MACHINED TO  $\sqrt{32}$  ROUGHNESS OR BETTER.
2. NO UNDERCUTTING PERMITTED WHERE 1.5" R BLENDS INTO REDUCED SECTION.
3. NO CENTERS PERMITTED ON FINISHED PART.

Figure 46. Compression Specimen for Off-Axis Study

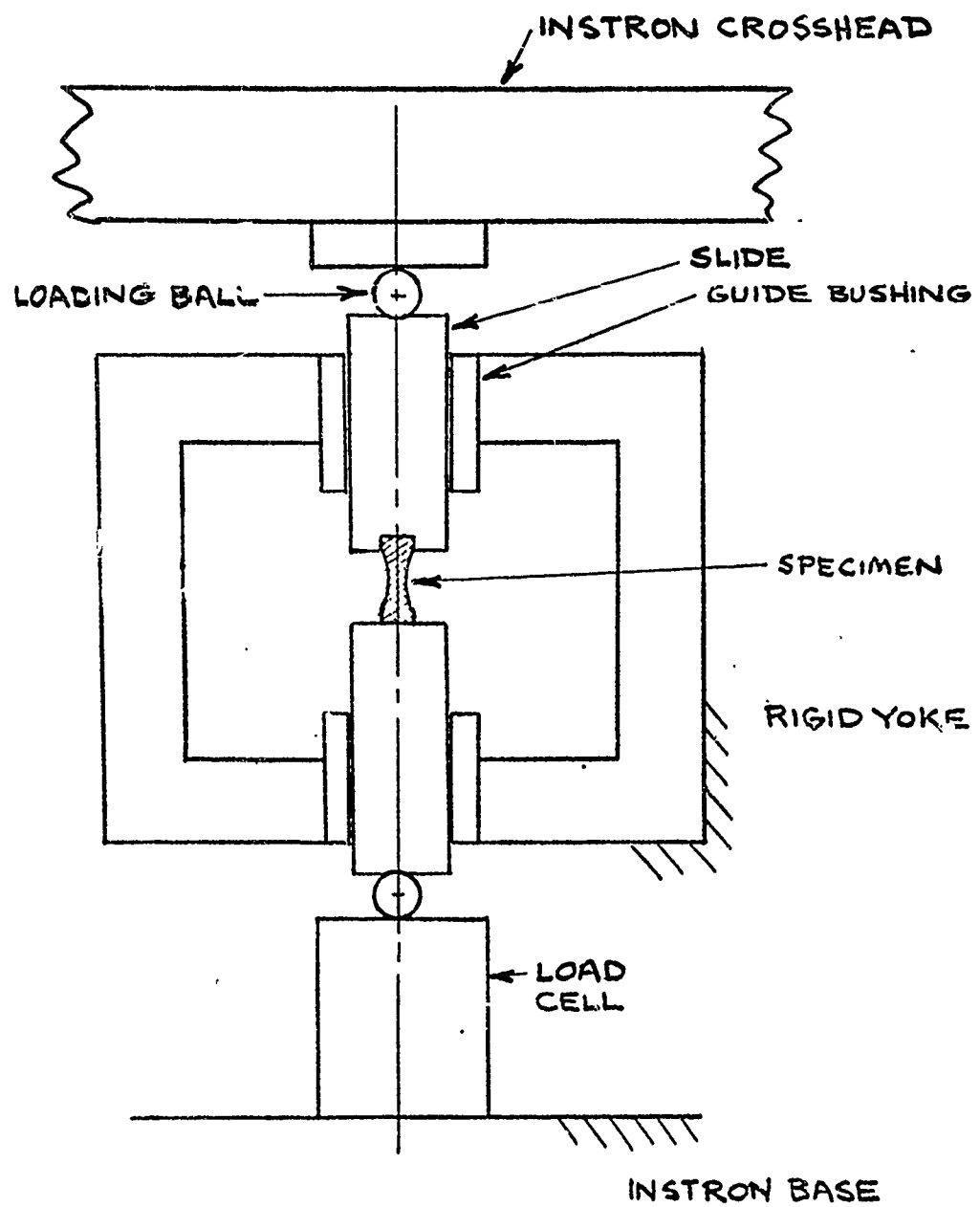


Figure 47. Compression Test Set-Up

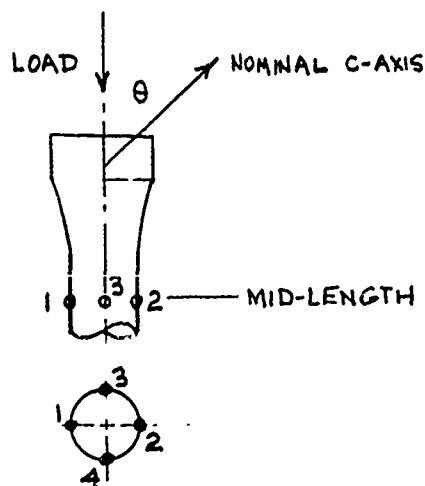


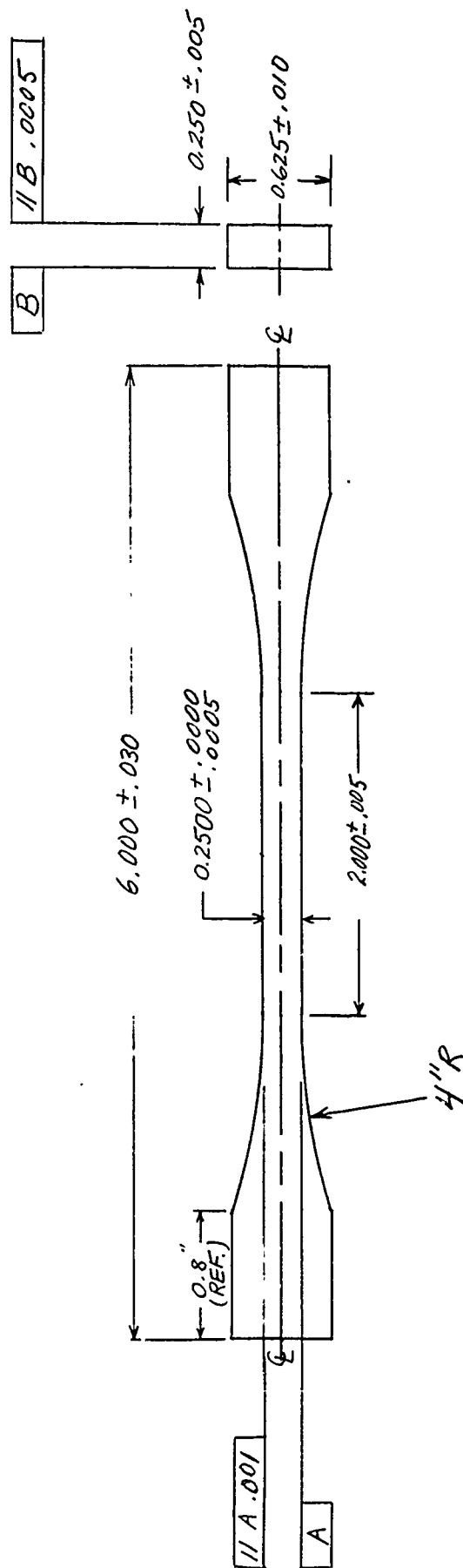
TABLE XIII

## STRAIN GAGES USED IN OFF-AXIS COMPRESSION TESTS

Specimen Number (1)	Strain Gage Position, <sup>(2)</sup> Orientation <sup>(3)</sup> and Type (4)			
	Left #1		Right #2	Front #3
	A	T	A	T
01C, 451C, 701C, 901C	V	-	V	-
02C, 452C, 702C 03C, 453C, 703C	V	IV	V	-
902C, 903C	V	IV	V	IV

- (1) Specimen number code: for example, 01C denotes  $\theta = 0^\circ$ , Specimen #1, compression;  
 (2) Position numbers shown in sketch below. 453C denotes  $\theta = 45^\circ$ , Specimen #3, compression.  
 (3) Orientation: A = axial, T = transverse  
 (4) Strain gage type IV = Micromasurements Inc. Type EA-13-062AK-120  
 (see also Table XV) V = Micromasurements Inc. Type EA-06-125AD-120





NOTES :

1. ALL SURFACES MACHINED TO  $\sqrt{32}$  ROUGHNESS OR BETTER.
2. NO UNDERCUTTING PERMITTED WHERE 4" R BLENDS INTO REDUCED SECTION EDGE.

Figure 48. Tensile Specimen for Off-Axis Study

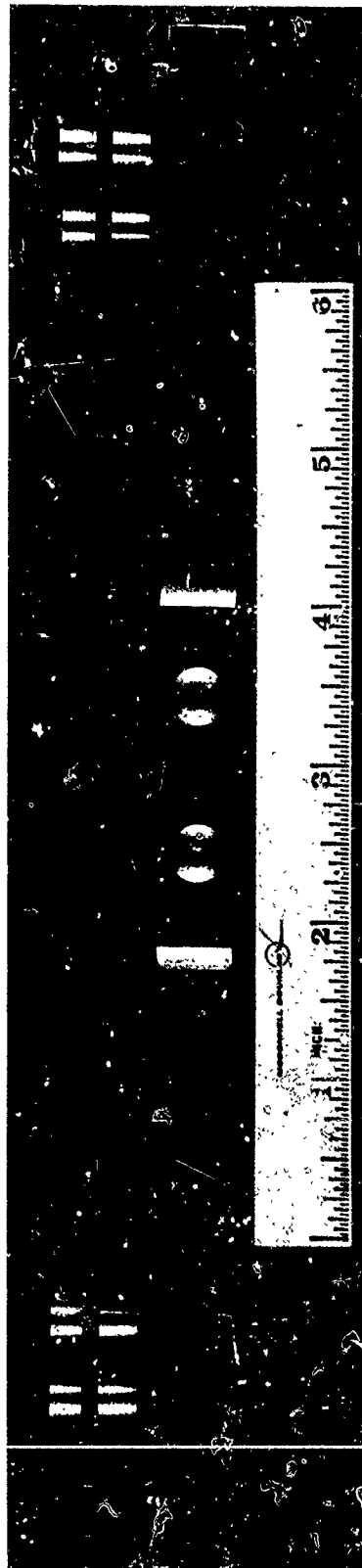


Figure 49. Tensile Specimen and Jig for Doubler Bonding

so that their axis is oriented accurately with respect to the load axis, and so that the plane of strain measurement is well defined with respect to the billet axis.

The specimens were pulled in an Instron test machine at a cross-head speed of 0.05 inches per minute. The load train is shown in Figure 50.

Strain information was obtained using bonded strain gages. A variety of gage positions and orientations was used, as indicated in Table XIV. In addition to measurement of axial strains at the midpoint of the gage section, the strain gages listed in Table XIV permit the measurement of some transverse strains at the mid-length, and axial strains at the tangent point where the gage section blends into the fillet section. The strain measurements at the tangent point are intended to provide a measure of the maximum stress concentration resulting from shear coupling effects since the analysis of Section 5.2 predicts that maximum stresses will occur near the tangent point. Table XV summarizes the manufacturer's information on the characteristics of the strain gages used on both the tensile and compressive specimens.

## 5.5 Results in Compression

5.5.1 Fracture Surfaces - Upon fracture, each compression specimen shattered into several fragments; however, it was possible to reconstruct the specimens. In each specimen, with the exception of specimens 702C and 902C, a well-defined plane of characteristic surface texture was identified as being the primary path of fracture. Typical examples are shown in Figure 51. To the naked eye, these primary planes have a grossly-textured smeared appearance which contrasts with the appearance of typical tensile failures which have a fine-grained "crystalline" appearance. In most cases, the surfaces of what are believed to be secondary fractures in the compressive specimens had the appearance of typical tensile failures.

In some cases the primary fracture surface consisted of two intersecting planes as shown schematically in the sketch in Table XVI. The angles

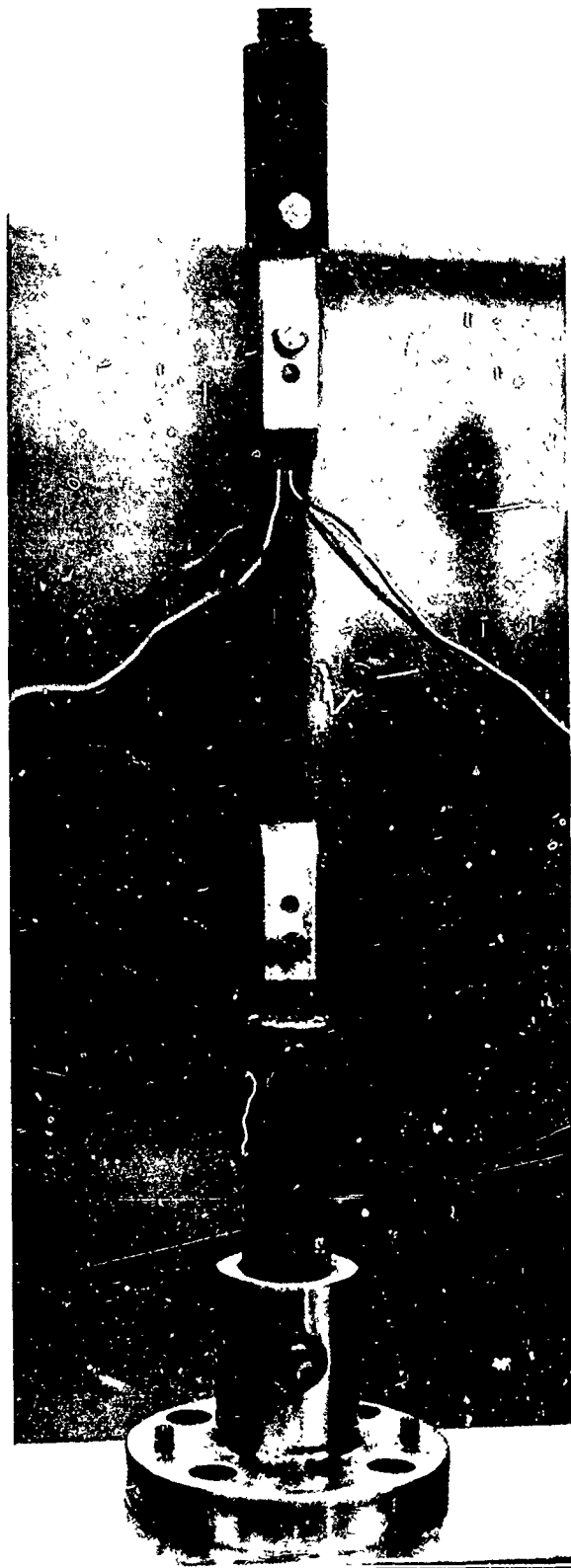


Figure 50. Tensile Load Train for Off-Axis Tests.

TABLE XIV

## STRAIN GAGES USED IN OFF-AXIS TENSILE TESTS

Tensile Specimen Number (1)	Strain Gage Position, <sup>(2)</sup> Orientation, <sup>(3)</sup> and Type <sup>(4)</sup>									
	Mid-Length								Tangent Point	
	Left #1		Right #2		Front #3		Back #4		Left #5	Right #6
	A <sup>(3)</sup>	T	A	T	A	T	A	T	A	A
01T, 451T, 703T, 801T	I	-	I	-	-	-	-	-	I	I
05T	I	-	I	-	I	-	I	-	-	-
04T	-	-	-	-	-	-	-	-	-	-
02T 452T 701T 03T 453T 702T	-	-	-	-	II	III	II	III	-	-
902T, 903T	II	III	II	III	II	III	II	III	-	-

(1) Specimen number code: for example, 01T denotes 0° specimen, number 1, tension;  
453T denotes 45° specimen, number 3, tension.

(2) Strain gage position numbers shown in sketch below.

(3) Orientation: A = axial

T = transverse

(4) Strain gage type: - = No strain gage

I = Micromeasurements Inc. Type EA-06-125BB-210

II = Micromeasurements Inc. Type EA-13-062TT-120, Section 1

(see also Table XV)

III = Micromeasurements Inc. Type EA-13-062TT-120, Section 2

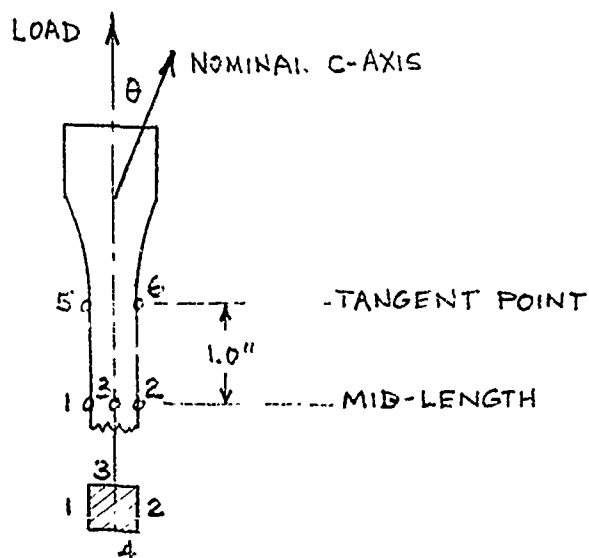


TABLE XV  
STRAIN GAGE CHARACTERISTICS, OFF-AXIS STUDY

Number	Manufacturer's* Designation	Gage Factor	Transverse Sensitivity Percent	Grid Length, Inch	Grid Width, Inch
I	EA-06-125BB-120	2.085	+0.8	0.125	0.088
II	EA-13-062TT-120, Section 1	2.015	+1.7	0.062	0.075
III	EA-13-062TT-120, Section 2	2.035	+1.1	0.062	0.075
IV	EA-13-062AK-120	2.05	+0.9	0.062	0.062
V	EA-06-125AD-120	2.10	+1.3	0.125	0.125

Note: All gages installed using Eastman 910 cement.

\*Micro-Measurements, Romulus, Michigan

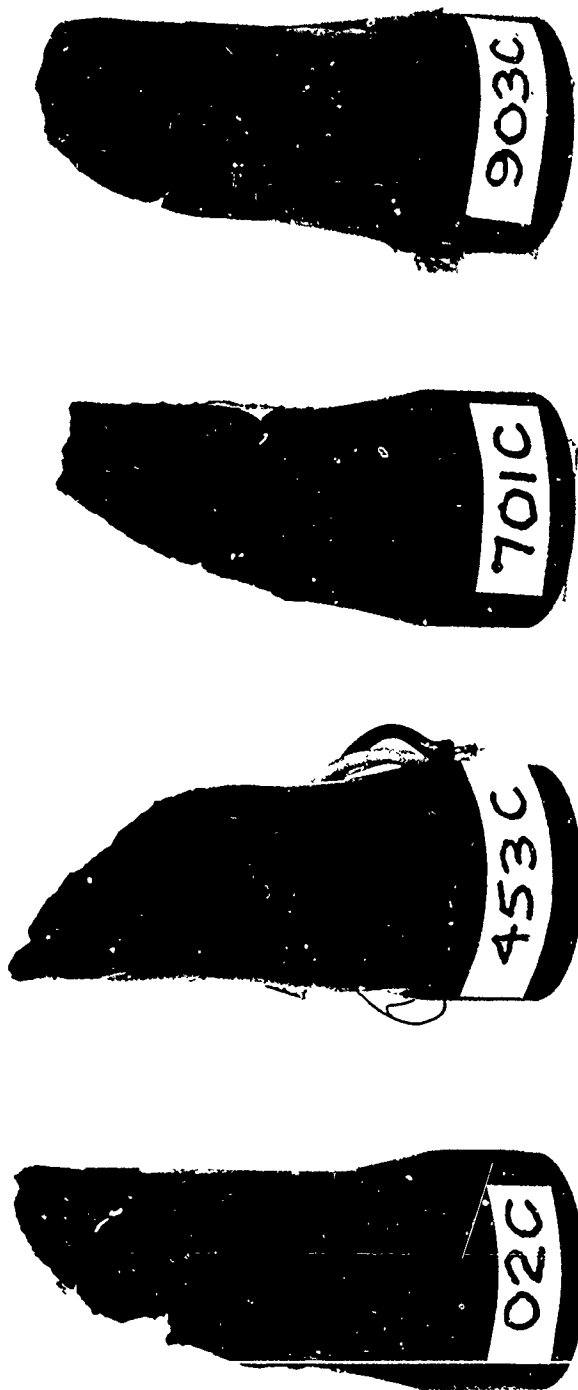


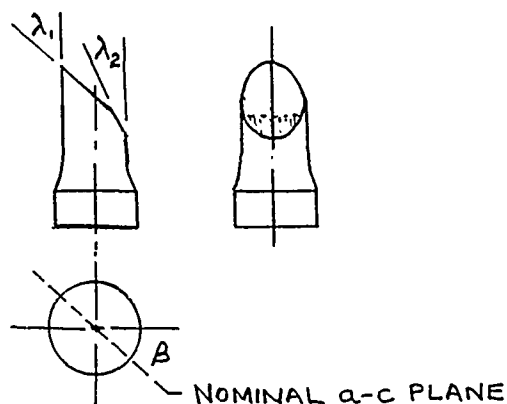
Figure 51. Typical Primary Fracture Planes in Off-Axis Compression Tests



TABLE XVI  
FRACTURE ORIENTATIONS  
OFF-AXIS COMPRESSION (ATJ-S GRAPHITE)

$\theta$	Specimen Number	$\beta$	$\lambda_1$	$\lambda_2$	Remarks
0	01C	0	41°	-	
	02C	50°	41°	-	
	03C	80°	35°	-	
45°	451C	28°	33°	-	
	452C	0°	28°	41°	
	453C	11°	22°	44°	
70°	701C	5°	26°	42°	complex fracture
	702C	(0°)	?	?	
	703C	26°	36°	-	
90°	901C	11°	37°	-	complex fracture
	902C	(5°)	(30°)	?	
	903C	0°	33°	45°	

Note:  $\beta$ ,  $\lambda_1$ , and  $\lambda_2$  are defined in sketch (below) of broken specimen.



between the load axis and the primary fracture planes ranged between  $22^\circ$  and  $45^\circ$  as indicated in Table XVI. When the fracture plane orientations are related to the geometry of the parent billet, as in Figure 52, it is found that:

- a) In the off-axis tests at  $\theta = 45^\circ$  and  $70^\circ$ , the fracture planes seem to lie preferentially so that they make as large an angle as possible with the nominal c-axis of the material; in other words, the fracture tends to occur nearly on the a-b plane.
- b) In the on-axis tests in the across-grain direction ( $\theta = 0^\circ$ ) the fracture plane orientations are approximately  $40^\circ$  to the c-axis. As might be expected from the "layer" model (Figure 1) these planes seem randomly oriented with respect to the plane of the parent slab.
- c) In the on-axis tests in the with-grain direction ( $\theta = 90^\circ$ ) the fracture planes tend to occur so that their normal vector lies in the plane of the parent slab.

These observations seem to support the view that compressive failures occur as a result of shear stresses, and that the plane of lowest shear strength is close to the a-b plane of the material. These conclusions must be tempered by the fact that the mechanisms of compressive failure are poorly understood in general, and by the possibility that in so short a specimen the shear coupling effects may be of overriding significance. Another related factor is that the projected axial length of the primary fracture plane typically is greater than the 1/2-inch gage length of the specimen; thus there are significant stress variations

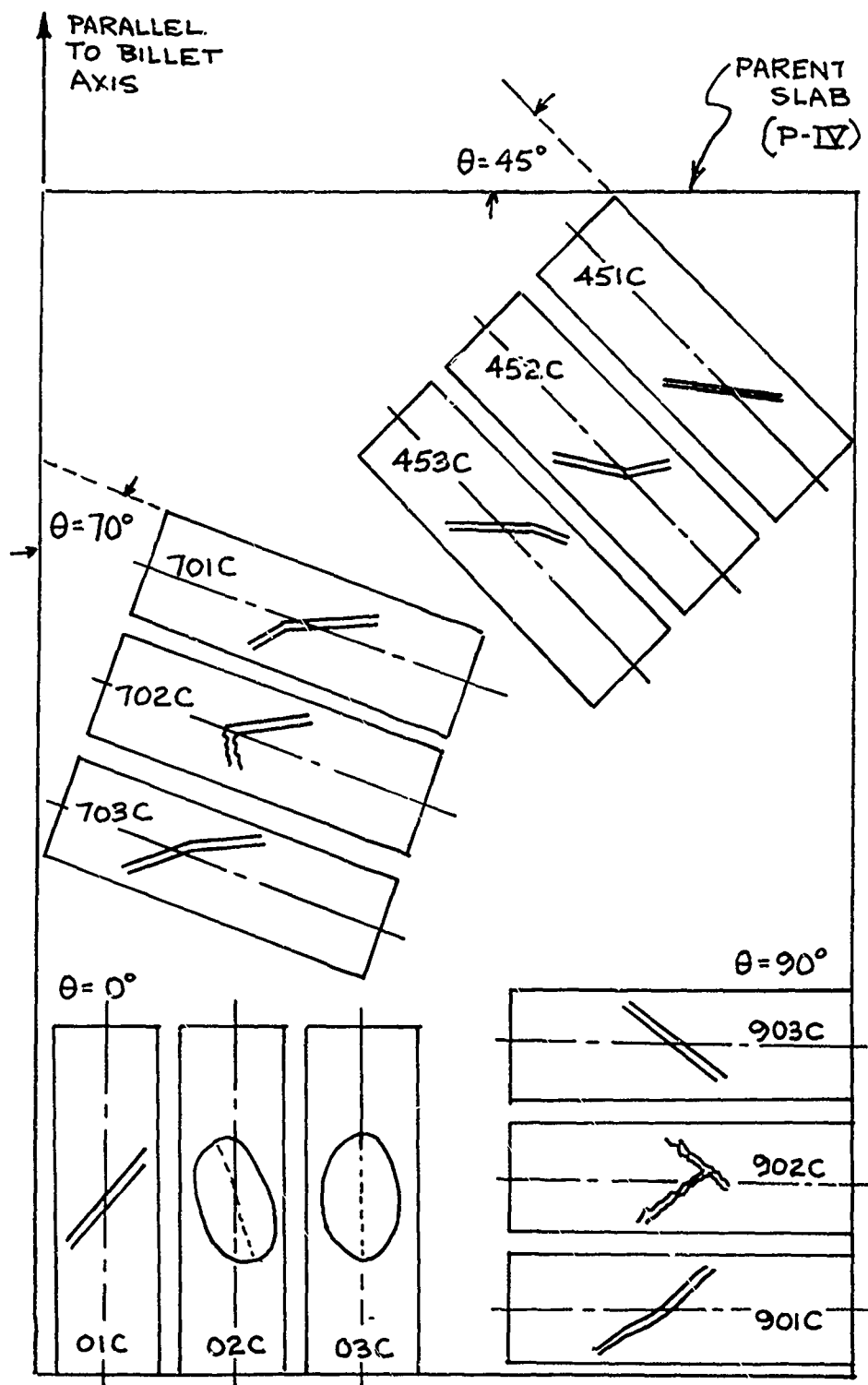


Figure 52. Compressive Fracture Planes in Parent Slab

along the fracture plane (see Figure 45 for general insight, although the analysis was for flat rather than round specimens).

5.5.2 Compressive Data - The strength results are summarized in Table XVII. Figure 53 provides a plot of strength versus  $\theta$ , the angle between load axis and the billet axis of symmetry. Also plotted is the Young's modulus which was taken as the quotient of the nominal stress and average axial strain, measured at a stress level of 500 psi. Figure 54 shows typical axial strain response curves for each orientation and Figure 55 provides a cross plot of strain data at two selected stress levels. Analysis of the transverse strain data was not completed in time for inclusion in this report.

The strength data (Figure 53) shows the with-grain ( $\theta = 90^\circ$ ) with strength to be lower than the across-grain ( $\theta = 0^\circ$ ) strength, and the off-axis strengths to be about the same as the with-grain strength. The anticipated (Section 3.2) minimum in strength at  $\theta = 45^\circ$  was not observed. The trend of strengths seems at odds with the inference drawn from the fracture plane orientations (Section 5.5.1) that the plane of maximum shear stress in a  $45^\circ$  test is the weakest plane in the material. No convincing argument has been formulated to explain the observed trend of compressive strengths; factors which may enter into such an explanation include:

- a) the stress gradients resulting from shear-coupling effects in the off-axis tests.
- a) the effect on the material of the relatively large axial strains measured near fracture.

The strain data (Figures 54 and 55) follow, qualitatively at least, the expected trend of increasing stiffness with increasing  $\theta$ . However, it should be noted that the compressive Young's moduli measured at all values of  $\theta$  other than zero degrees, are lower than those measured in tension (see Section 5.6). A similar discrepancy between compressive

TABLE XVII

## SUMMARY OF COMPRESSIVE FRACTURE DATA (OFF-AXIS STUDY)

Orientation Angle (1)	Specimen Number (2)	Ultimate Stress psi	Axial Strain at Failure (3)
0°	01C	14050	- (4)
	02C	14000	-
	03C	13800	-
45°	451C	13100	-
	452C	13100	.054
	453C	13000	.052
70°	701C	12900	-
	702C	12700	-
	703C	13200	-
90°	901C	13100	.042
	902C	13200	.048
	903C	13300	.046

- (1) Angle between load axis and parent billet axis
- (2) All specimens from ATJ-S billet 16K9-27
- (3) Tabulated strains are average of two strain gages mounted 180° apart at specimen mid-length.
- (4) Absence of strain data due to strain gage failure prior to specimen failure.

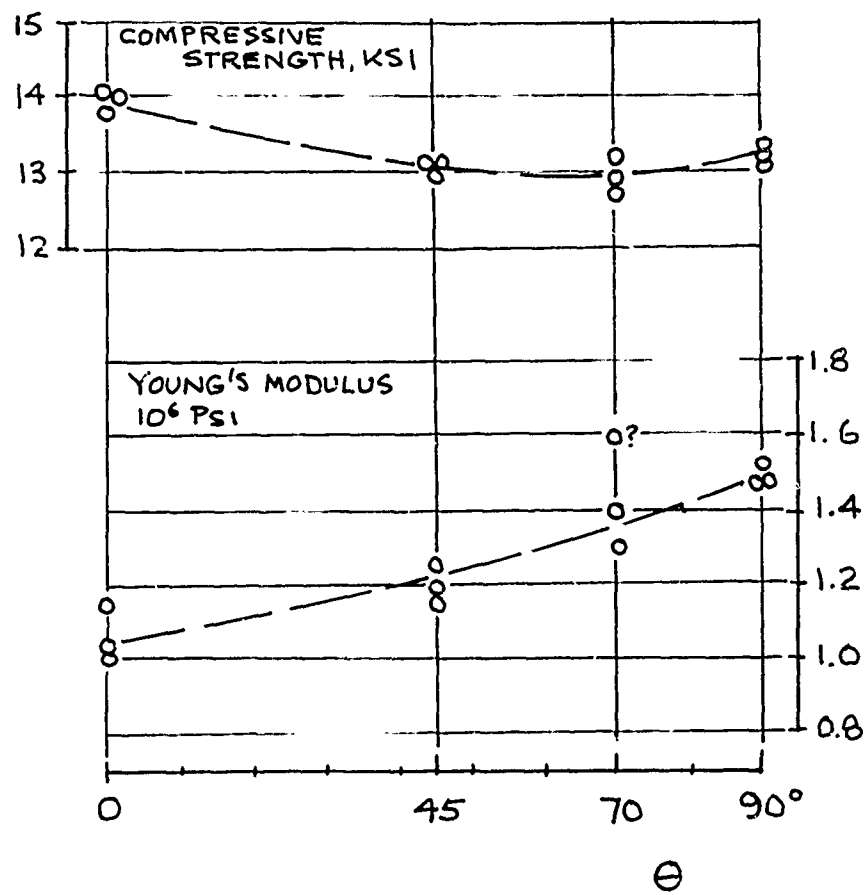


Figure 53. Compressive Strength and Modulus, Off-Axis Study

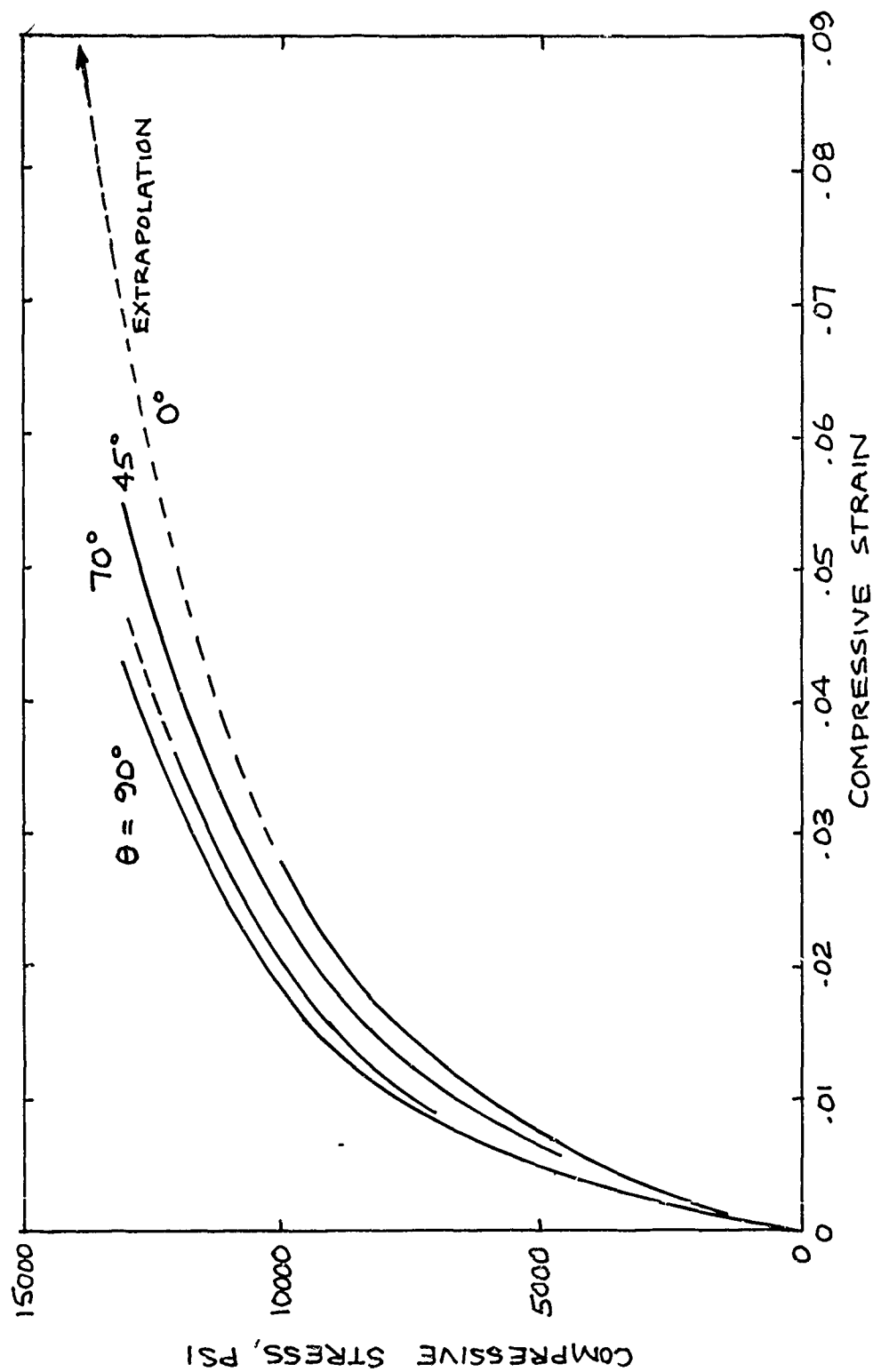


Figure 54. Axial Strain Curves in Compression, Off-Axis Study

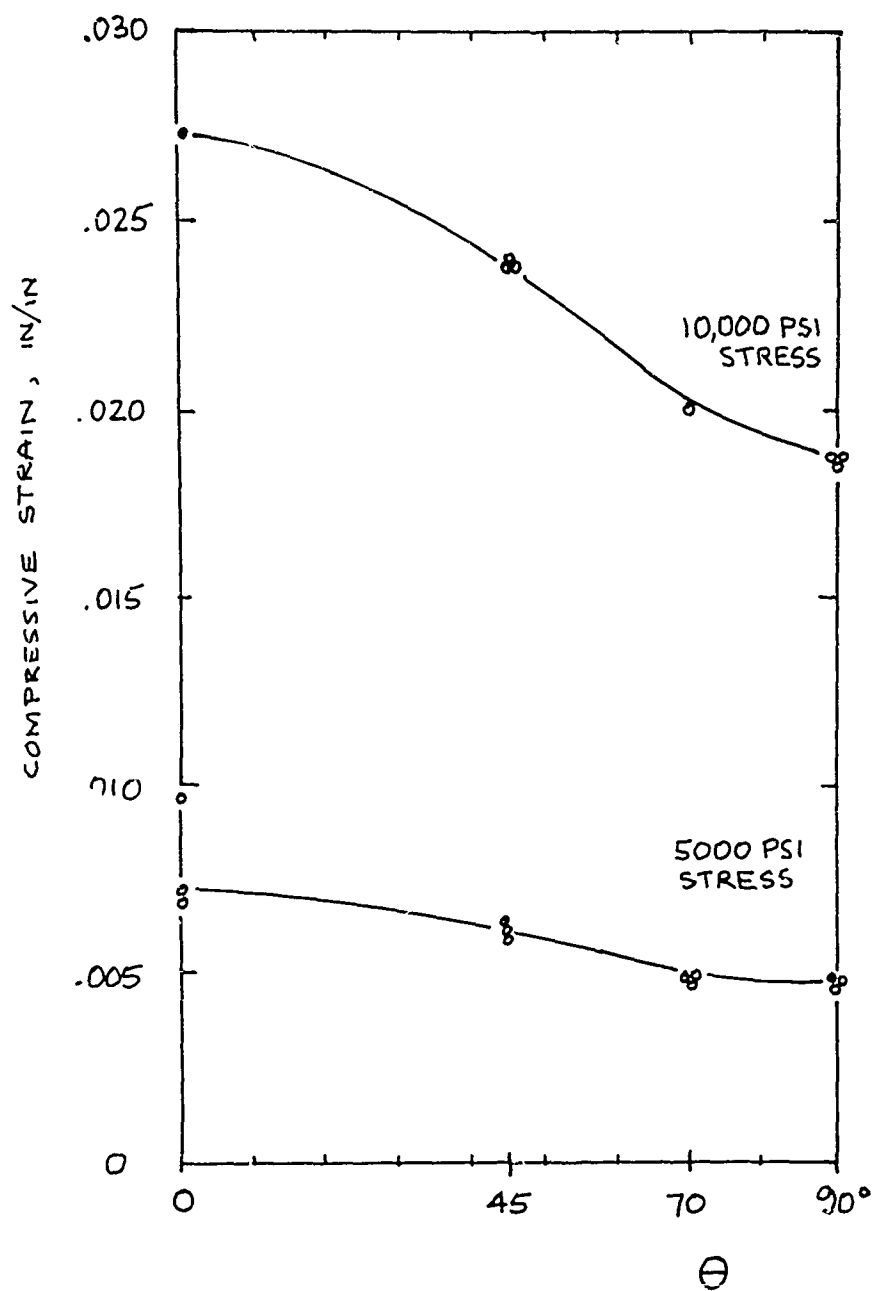


Figure 55. Axial Strain Response in Compression, Off-Axis Study



and tensile moduli has been reported for ATJ-S graphite in Reference 14. However, the discrepancy does not seem to be understood at this time.

## 5.6 Results in Tension

5.6.1 Fracture Orientations - Figures 56, 57, 58, and 59 show the fractured tensile specimens. In Figures 56 and 57, which show the  $0^\circ$  and  $90^\circ$  specimens, the fracture planes are at  $90^\circ$  (within  $1^\circ$ ) to the load axis as might be expected. In the case of the off-axis specimens, Figures 58 and 59, the fracture planes tend to be angled (between  $3^\circ$  and  $9^\circ$ ) to the plane that is normal to the load axis. When the fracture plane in the off axis tests is related to the billet geometry it is found in all cases that the angle is such that the fracture plane is closer to the a-b plane of the material (Figure 60).

Six out of the fourteen specimens tested failed at the tangent point between the gage section and the fillet. However, no obvious correlation between failure location and measured strength was observed.

5.6.2 Mechanical Data in Tension - The fracture results are summarized in Table XVIII and plotted as a function of angle  $\theta$  in Figure 61. Young's modulus, estimated as the quotient of stress and strain taken at 1000 psi stress, is also plotted in Figure 61. Figure 62 shows typical axial strain responses. The data show relatively little scatter and provide fairly smooth trends of properties as a function of angle. The transverse strain measurements and the axial strains measured at the tangent point were not analyzed in time for presentation here.

## 5.7 Comments on Off-Axis Biaxial Strength

Figure 4 in Section 3.2 showed schematically how off-axis tensile data might be used to infer an approximate failure envelope in the tension-tension quadrant. Also, in Section 3.2, the suggestion was made that failure in the highly compressive portion of the compression-tension

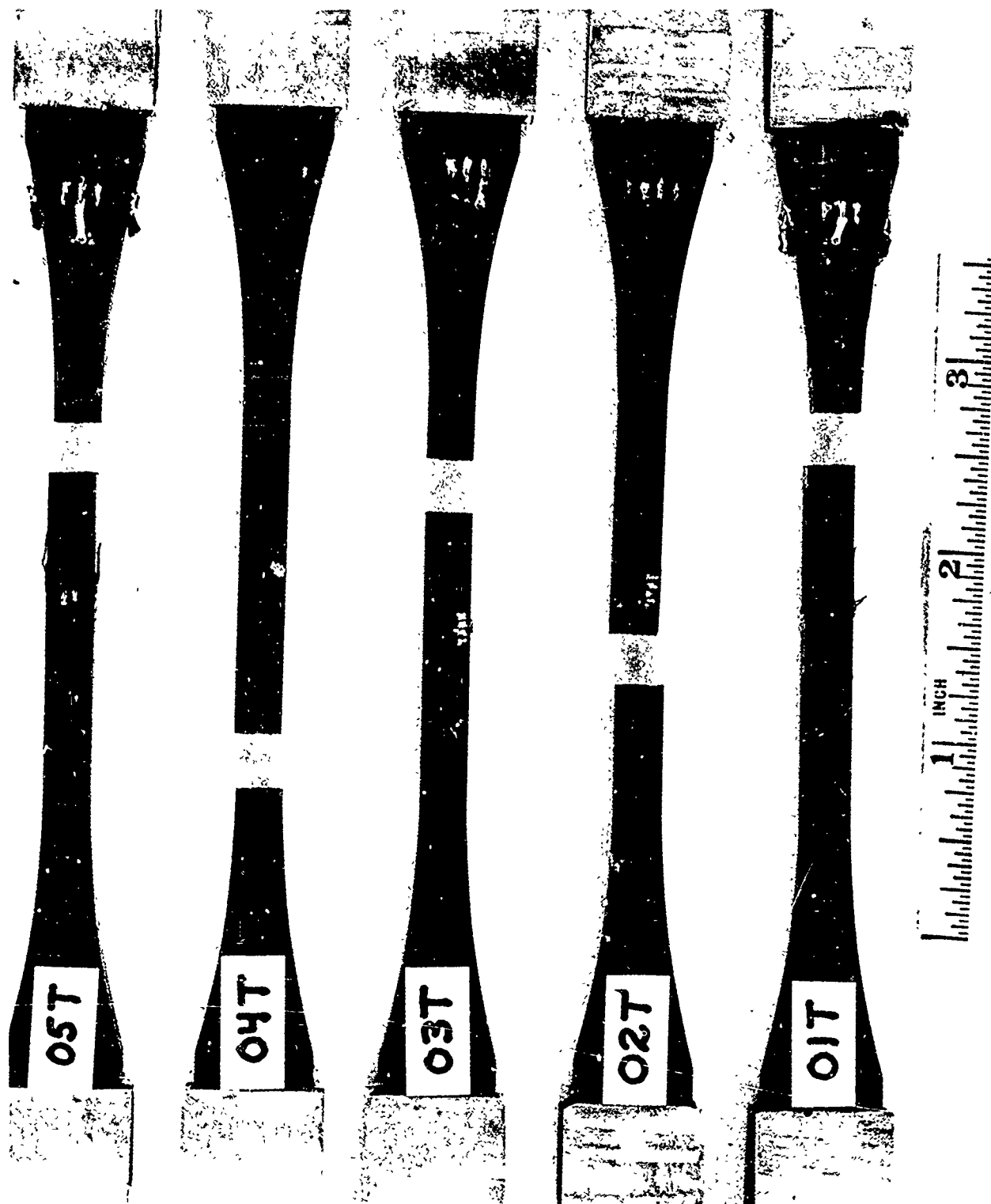


Figure 56. 0° Tensile Specimens After Test

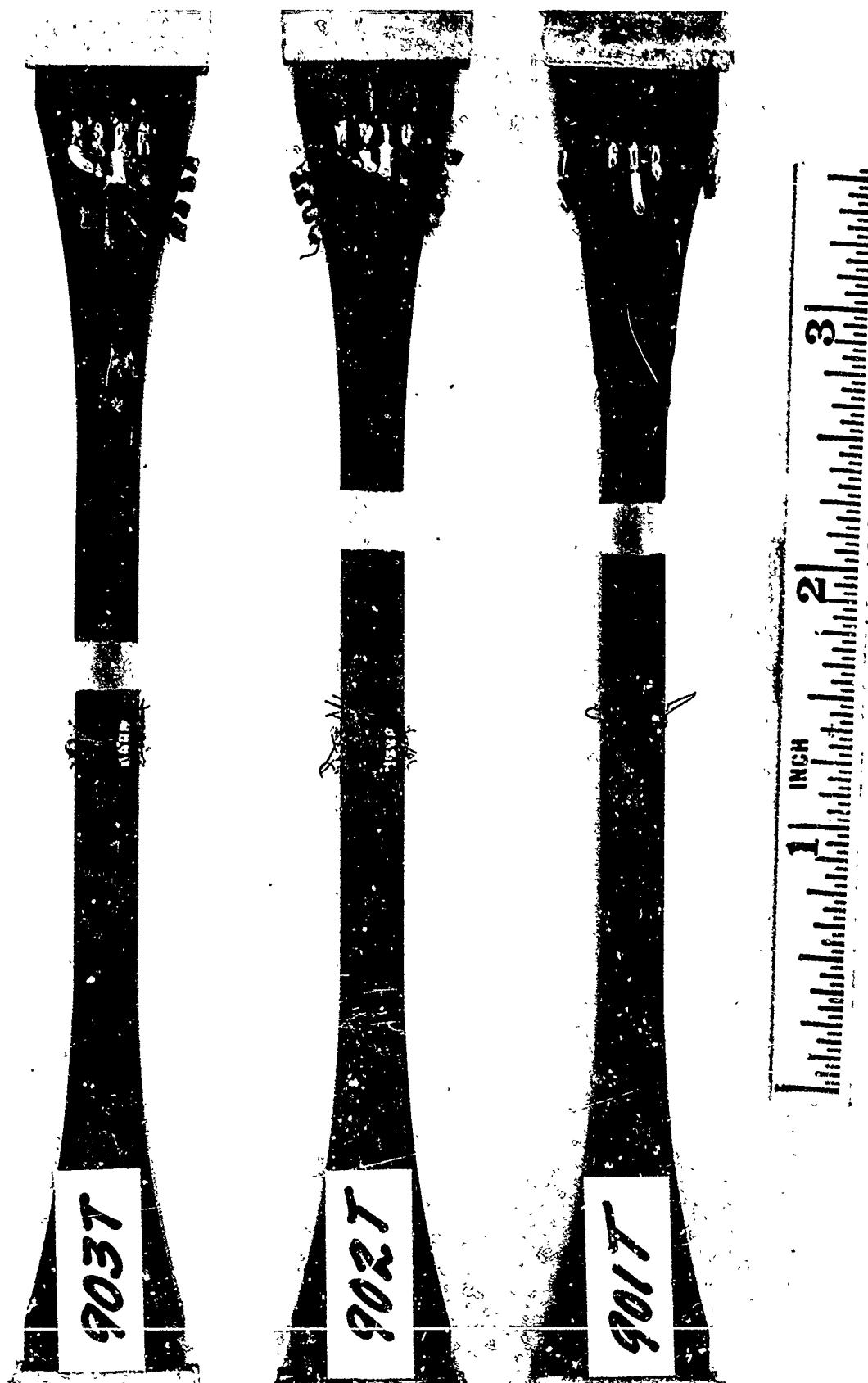


Figure 57. 90° Tensile Specimens After Test



Figure 58. 45° Tensile Specimens After Test



Figure 59. 70° Tensile Specimens After Test

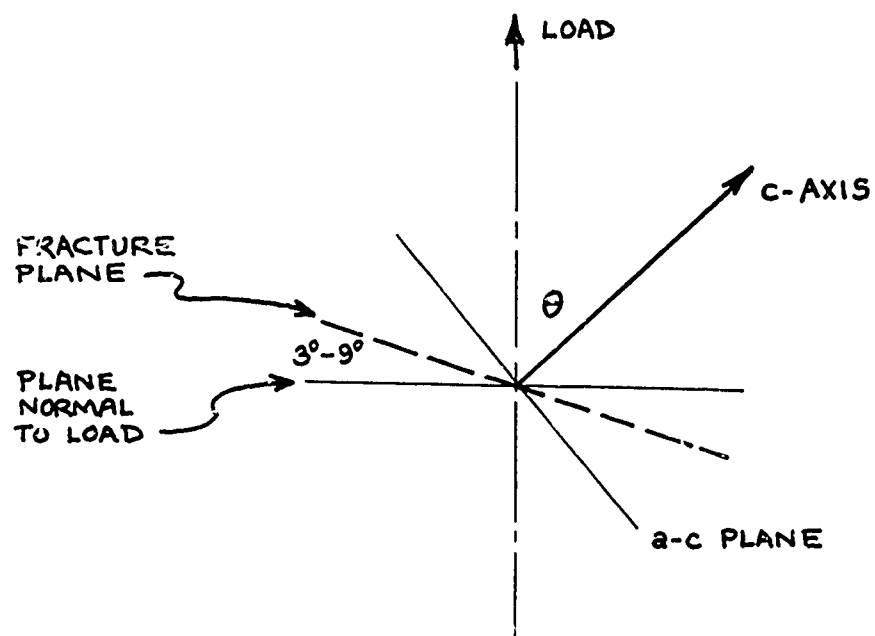


Figure 60. Fracture Plane Orientation in Off-Axis Tensile Tests

TABLE XVIII

## SUMMARY OF TENSILE FRACTURE DATA (OFF-AXIS STUDY)

Orientation Angle (1)	Specimen Number (2)	Ultimate Stress psi	Axial Strain at Failure (3)
0°	01T	4075	.0053
	02T	4200	.0057
	03T	4100	.0052
	04T	4290	- (4)
	05T	4540	.0058
45°	451T	4750	.0051
	452T	4650	.0049
	453T	4640	.0051
70°	701T	5100	.0046
	702T	5050	.0046
	703T	5030	.0046
90°	901T	5400	.0047
	902T	4850	.0039
	903T	5350	.0045

- (1) Angle between load axis and parent billet axis.  
(2) All specimens from ATJ-S graphite billet 16K9-27.  
(3) Tabulated strain is average of two strain gages.  
(4) Specimen 04T was not strain-gaged.

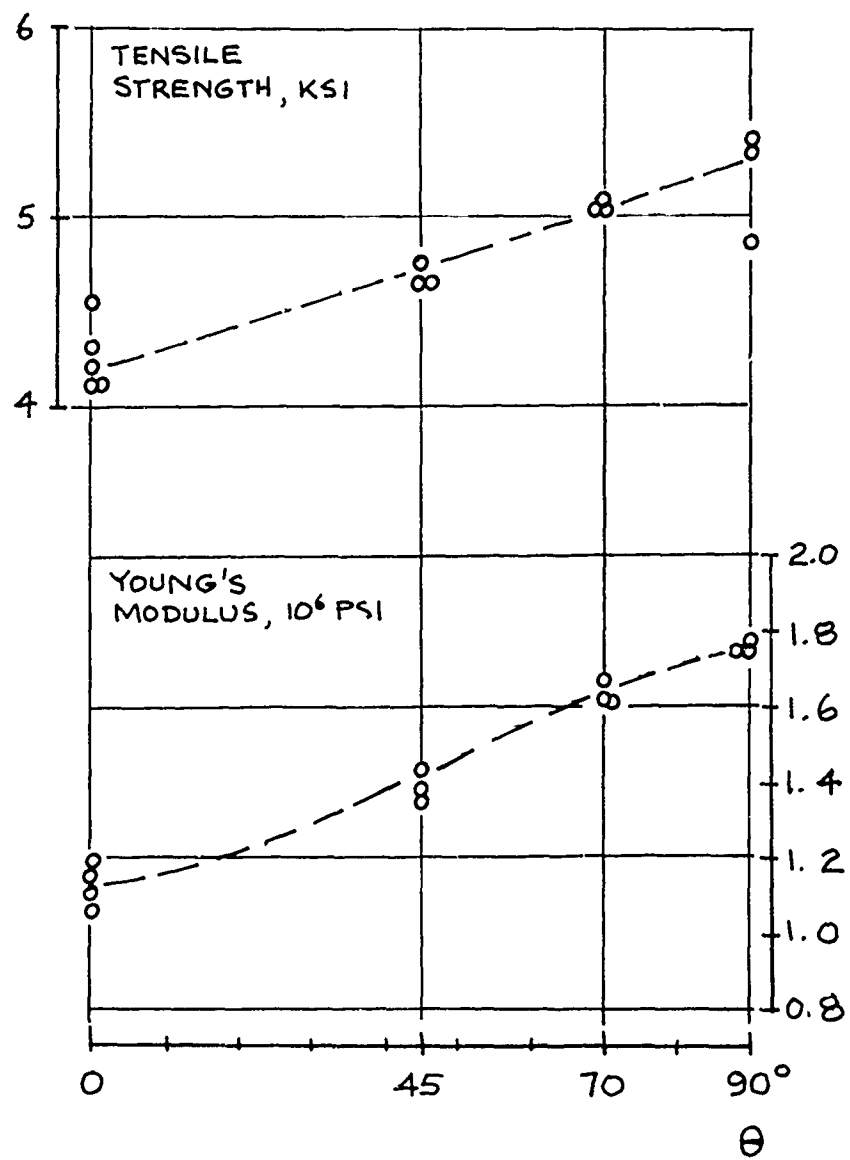


Figure 61. Tensile Strength and Modulus, Off-Axis Study



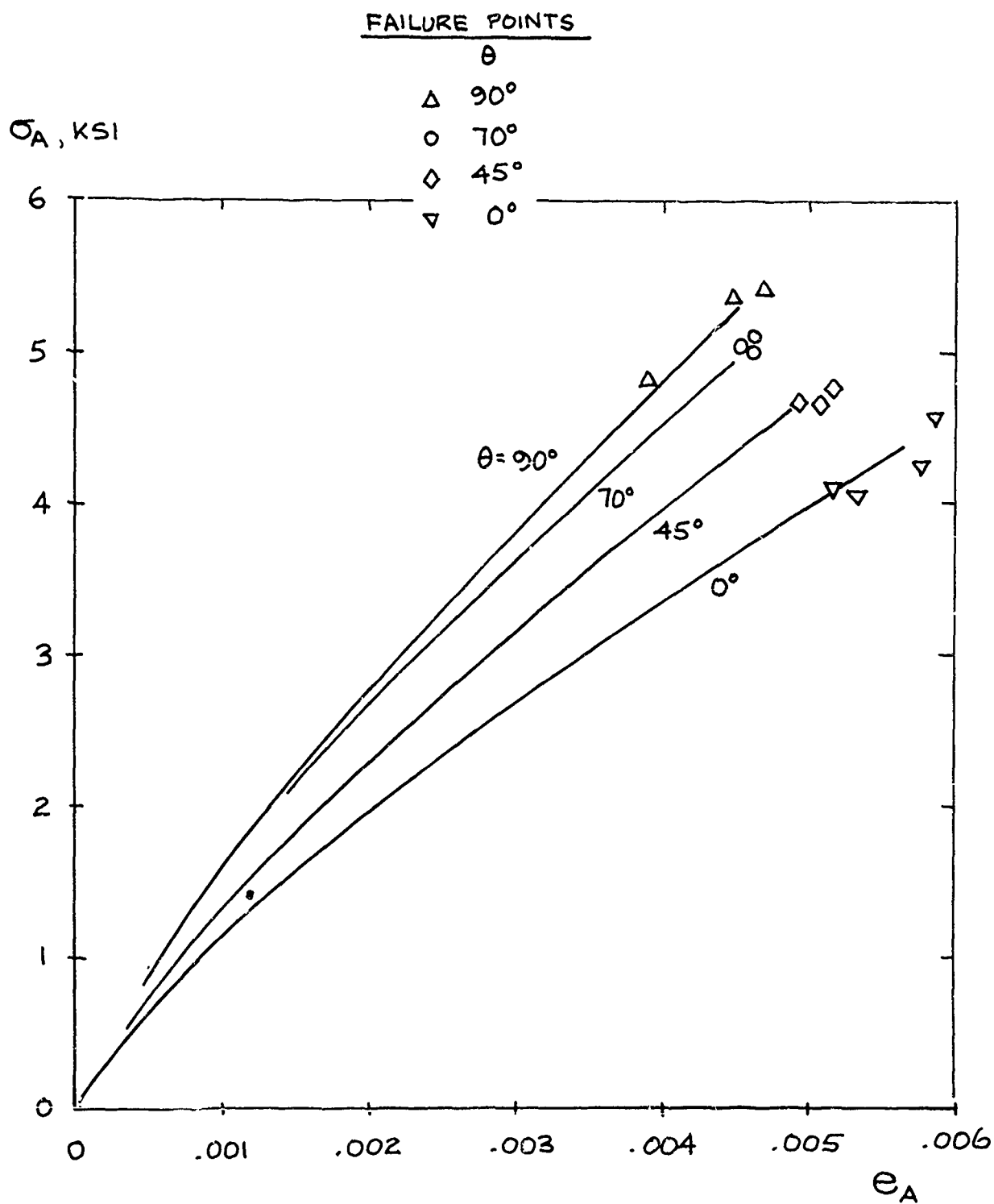


Figure 62. Axial Strain Curves in Tension, Off-Axis Study

quadrant occurs as a result of the maximum resolved shear stress. In Figure 63, the off-axis trends obtained in this study are superposed on the available biaxial data (Section 4.5) to provide an estimate of off-axis effects on the median biaxial failure envelope. In preparing Figure 63, only the data from billets 1C0-15 and 16K9-27 was used in estimating median strengths; however, the "lower bound" line includes all data obtained in this program and also from Reference 1. Since biaxial specimens typically give somewhat lower strength values in uniaxial tension than do uniaxial specimens, the uniaxial off-axis points plotted in Figure 63 have been normalized to the biaxial data.

Figure 63 shows that the potential effects of off-axis biaxial loading are small in comparison to the scatter in on-axis biaxial data. Furthermore, the lower bound strength envelope in biaxial tension appears to be more isotropic than does the median-strength envelope. Therefore, the sensitivity of the lower-bound biaxial tension envelope to off-axis loading might be rather small. In the compression-tension quadrant, in the absence of more compression-tension data, the dotted lines suggesting the median failure envelopes are, of course, speculative.

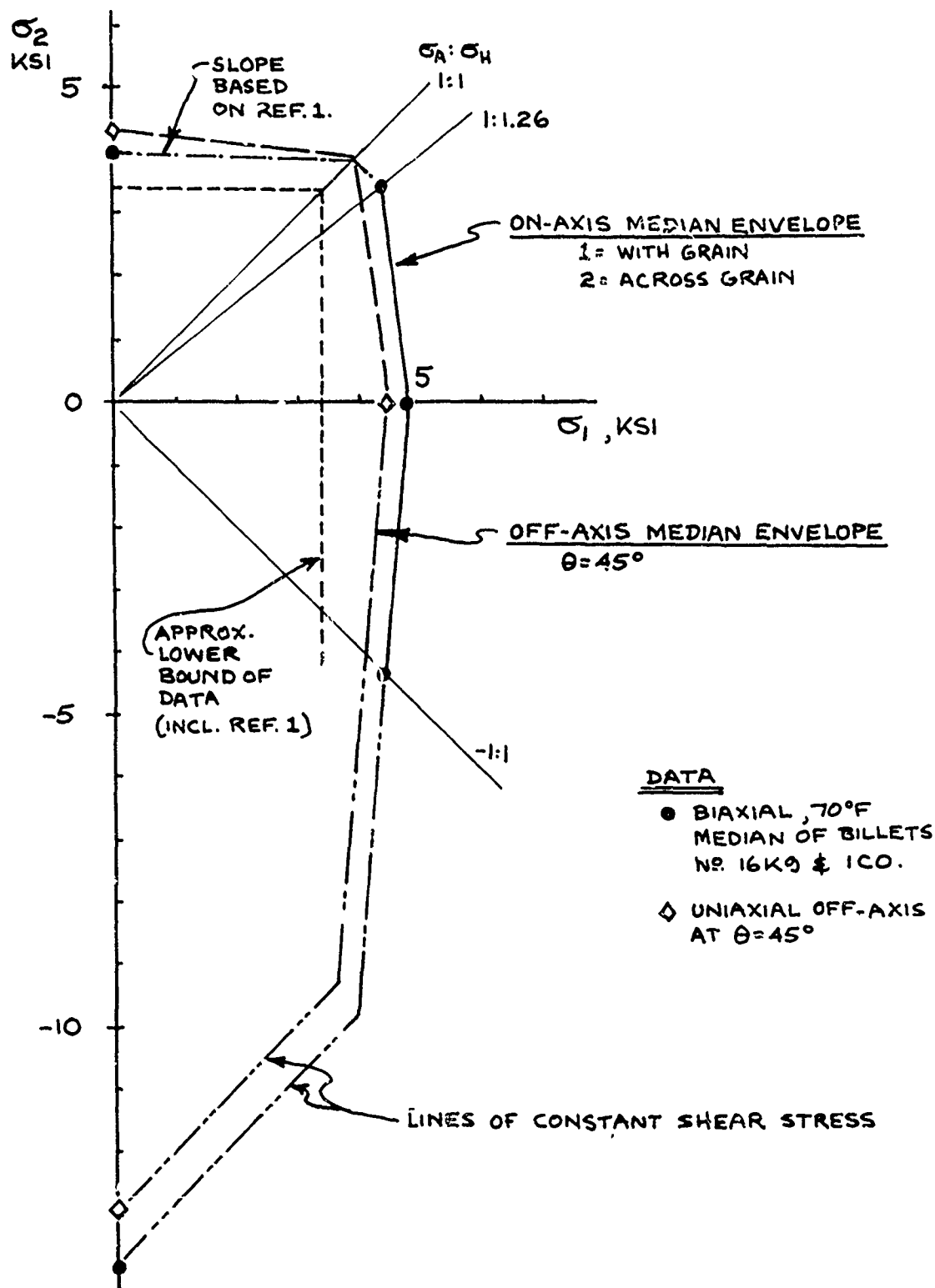


Figure 63. Estimated Effect of Off-Axis Loading on Biaxial Strength

## Section 6

### CONTINUING EFFORTS

This interim report is being published to disseminate a preliminary summary of available data as soon as possible. Analysis of the biaxial and off-axis data is continuing and the results are to be published in the next report. Among the continuing efforts are:

- 1) The biaxial fracture data obtained in this program and the previous effort (Reference 1) are being reviewed to assess the role of billet-to-billet variations. An attempt will be made to pool the data in a way which best reveals the behavioral trends of the material.
- 2) Biaxial stress-strain curves are being prepared. The specimen stress analyses will be reviewed to determine to what extent specimen configuration may be responsible for the biaxial "softening" described in Section 4.6. The results of Reference 3 are also being reviewed to determine whether similar effects were measured on AXF-5Q graphite.
- 3) Further analysis of the off-axis data is being conducted. Transverse strain curves are being prepared which, hopefully, will give further insight into the constitutive relations of ATJ-S graphite. The finite element stress analyses are being reviewed to provide estimates of shear-coupling effects on measured strains and on fracture plane orientations.

In addition, the development of triaxial test techniques is continuing and will be described in the next report.

Preceding page blank

## Section 7

### REFERENCES

1. J. Jortner, "Biaxial Mechanical Properties of ATJ-S Graphite, Final Report under AF Contract F04701-068-C-0288, Change Order 15, McDonnell Douglas Report No. MDC-G2072, December 1970.
2. R. D. Perkins, et al., Multiaxial Loading Behavior of Four Materials including ATJ-S Graphite and RAD-6300 Carbon Phenolic, SAMSO-TR-69-393, Volume 1, Material Response Studies (MARS II), August 1970.
3. J. Jortner, et al., "Biaxial Testing," Section 3.1.2 of SAMSO-TR-70-248, Volume II, Part A, Final Report-Hardening Composites, Refractories, and Transpiration Cooling (RESEP II), August 1970.
4. J. C. Halpin, et al., "Characterization of Anisotropic Composite Materials," ASTM STP 460, Composite Materials: Testing and Design, December 1969.
5. O. Ishai and R. E. Lavengood, "Characterizing Strength of Unidirectional Composites," ASTM STP 460, Composite Materials: Testing and Design, December 1969.
6. R. E. Ely, Strength Results for Ceramic Materials Under Multiaxial Stresses, U. S. Army Missile Command Report RR-TR-68-1, April 1968.
7. Anon., High Temperature Tensile Properties and Thermal Expansion of ATJ-S Graphite, Southern Research Institute Rept 9157-2096-1, July 1968.
8. S. J. Green and F. L. Schierloh, Uniaxial Stress Behavior of S-200 Beryllium, Isotropic Pyrolytic Boron Nitride, and ATJ-S Graphite at Strain Rates to  $10^3$ /sec and 700°F, General Motors MSL 68-11, March 1968.
9. A. Nadai, Theory of Flow and Fracture of Solids, McGraw-Hill Book Company, New York, 1950.

Preceding page blank

#### REFERENCES (Cont'd)

10. R. Sedlacek and F. A. Holden, Methods of Tensile Testing of Brittle Materials, Review of Scientific Instruments, Vol. 3, No. 3, pp 289-300, 1962.
11. L. W. Hu, "Development of a Triaxial Stress Testing Machine and Triaxial Stress Experiments," Proceedings of Spring Meeting of Society for Experimental Stress Analysis, Cleveland, Ohio, May 1958.
12. R. M. Jones and J. G. Crose, SAASII-Finite Element Analysis of Axisymmetric Solids, Air Force Report No. SAMS0-TR-68-455, September 1968.
13. D. R. Schryer, Crystallite Orientation in Molded Graphites, NASA Technical Note D-6200, April 1971.
14. C. D. Pears, "Thermal and Mechanical Characterization of Advanced Graphite Materials", Section V of Part I (see Table 5), Graphitic Materials for Advanced Reentry Vehicles, edited by D. M. Forney, Jr., AFML-TR-70-133, August 1970.
15. N. J. Pagano and J. C. Halpin, Influence of End Constraint in the Testing of Anisotropic Bodies, J. Composite Materials, Vol. 2, No. 1 (January 1968) p. 18.
16. Brisbane, J. J., Finite-Element Stress Analysis of Anisotropic Bodies, Rohm and Haas Company Technical Report S-143, August 1968.